

**New Models for
Telomerase Inhibition by Antisense 2'-O-Methyl-RNA
in Lung Cancer Therapy**

Dissertation
zur Erlangung des Grades
des Doktors der Naturwissenschaften
der Naturwissenschaftlich-Technischen Fakultät III
Chemie, Pharmazie, Bio- und Werkstoffwissenschaften
der Universität des Saarlandes

von

Meng Dong

Saarbrücken

2011

Tag des Kolloquiums: 08. April 2011

Dekan: Prof. Dr. Wilhelm F. Maier

Berichterstatter: Prof. Dr. Claus-Michael Lehr
Prof. Dr. Ulrich Klotz

Vorsitz: Prof. Dr. Alexandra K. Kiemer

Akad. Mitarbeiterin: Dr. Britta Diesel

This doctoral thesis was performed under the supervision of

Prof. Dr. Claus-Michael Lehr

Department of Biopharmaceutics
and Pharmaceutical Technology,
Saarland University

Prof. Dr. Ulrich Klotz

Dr. Margarete Fischer- Bosch- Institute
of Clinical Pharmacology, Stuttgart and
University of Tübingen

My sincere gratitude to them for providing me with the opportunity to perform my doctoral studies and their valuable scientific guidance and suggestions.

*My deeply grateful to **Dr. Thomas E. Mürdter** from the Dr. Margarete Fischer-Bosch-Institute of Clinical Pharmacology, Stuttgart and University of Tübingen for directing the detailed research work throughout my studies.*

Table of Contents

Abstract	VII
Kurzzusammenfassung	VIII
Chapter 1: General Introduction and Aim of the Thesis	1
1.1 Lung.....	2
1.1.1 Lung cancer.....	3
1.1.2 Lung cancer therapy.....	5
1.1.3 Inhalation therapy	8
1.2 Telomere and Telomerase.....	9
1.2.1 Telomerase as a target for cancer therapy.....	11
1.3 Nanoparticles	14
1.3.1 Nanoparticles as drug delivery systems	15
1.3.2 Nanoparticles as delivery system for telomerase inhibitors.....	16
1.4 Aim of the thesis	18
Chapter 2: Optimization of Methods for Measurements of Telomerase Activity and Telomere Length.....	19
2.1 Abstract.....	20
2.2 Introduction.....	21
2.3 Part 1: Telomerase activity measurement.....	22
2.3.1 Materials and methods	22
2.3.1.1 Preparation of cell extracts.....	22
2.3.1.2 Preparation of tumor tissue extracts.....	22
2.3.1.3 Protein concentration determination	22
2.3.1.4 Telomerase activity assay using capillary electrophoresis.....	23
2.3.1.5 Telomerase activity assay using real-time quantitative PCR	24
2.3.1.6 Statistical analysis.....	25
2.3.2 Results and discussion	25
2.3.2.1 Capillary electrophoresis based TRAP assay for telomerase measurement.....	25
2.3.2.2 Real-time quantitative PCR based TRAP assay for telomerase measurement.....	27
2.3.2.3 Comparison of telomerase assays	29
2.4 Part 2: Telomere measurement	30
2.4.1 Materials and methods	30

Table of Contents

2.4.1.1 Preparation of genomic DNA	30
2.4.1.2 Telomere measurement by terminal restriction fragment length determination	30
2.4.1.3 Telomere measurement by real-time quantitative PCR	31
2.4.2 Results and discussion.....	33
2.4.2.1 Telomere measurement by terminal restriction fragment length determination	33
2.4.2.2 Telomere measurement by real-time quantitative PCR	33
2.4.2.3 Comparison of telomere assays	34
2.5 Conclusion	36
Chapter 3: Telomerase Inhibition by Liposomal Delivery of 2'-O-Methyl- RNA in Human Non-Small Cell Lung Cancer Cells	37
3.1 Abstract.....	38
3.2 Introduction.....	39
3.3 Material and methods.....	40
3.3.1 Cell culture	40
3.3.2 Oligonucleotides.....	40
3.3.3 Preparation of oligonucleotide transfection.....	40
3.3.4 Confocal laser scanning microscopy analysis	43
3.3.5 Telomerase activity assay using capillary electrophoresis	43
3.3.6 Statistical analysis	44
3.4 Results.....	44
3.4.1 Evaluation of transfection efficiency by confocal laser scanning microscopy.....	44
3.4.2 Evaluation of telomerase inhibition by capillary electrophoresis.....	47
3.5 Discussion.....	48
3.6 Conclusion	50
Chapter 4: Telomerase Inhibition and Telomere Shortening by Nanoparticles Delivery of 2'-O-Methyl-RNA in Human Lung Cancer Cells.....	51
4.1 Abstract.....	52
4.2 Introduction.....	53
4.3 Material and methods.....	54
4.3.1 Cell culture	54
4.3.2 Oligonucleotides.....	54

Table of Contents

4.3.3 Chitosan-coated PLGA nanoparticles preparation and characterization.....	55
4.3.4 Preparation of oligonucleotide-nanoparticle-complexes (nanoplexes) transfection	55
4.3.5 Fluorescence-activated cell sorting (FACS) analysis	56
4.3.6 Confocal laser scanning microscopy.....	56
4.3.7 Quantification of oligonucleotides uptake	56
4.3.8 Cytotoxicity assay	57
4.3.9 Telomerase activity assay using real-time quantitative PCR.....	57
4.3.10 Telomere measurement by real-time quantitative PCR	58
4.3.11 Statistical analysis.....	58
4.4 Results.....	58
4.4.1 Characterization of chitosan-PLGA nanoparticles as a delivery system	58
4.4.2 Inhibition of telomerase activity by 2'-O-methyl-RNA-nanoparticle complexes	59
4.4.3 Nanoparticle mediated uptake of 2'-O-methyl-RNA into human lung cancer cells.....	59
4.4.4 Cytotoxicity of 2'-O-methyl-RNA-nanoparticle-complexes on cells.....	63
4.4.5 Telomerase inhibition by 2'-O-methyl-RNA-nanoparticle complexes.....	65
4.4.6 Long-term treatment with 2'-O-methyl-RNA-nanoparticle complexes resulting in progressive telomere shortening	65
4.5 Discussion.....	67
4.6 Conclusions.....	70
Chapter 5: Tissue Slice Model of Human Lung Cancer to Investigate Telomerase Inhibition by Nanoparticle Delivery of Antisense 2'-O-Methyl-RNA.....	71
5.1 Abstract.....	72
5.2 Introduction.....	73
5.3 Material and methods	74
5.3.1 Lung tumor materials.....	74
5.3.2 Primary cells isolation, cultivation and characterization	74
5.3.3 Tissue slice preparation and cultivation.....	75
5.3.4 Oligonucleotides	75
5.3.5 Preparation and characterization of chitosan-coated PLGA nanoparticles.....	76
5.3.6 Preparation of oligonucleotide-nanoparticle-complexes (nanoplexes) for transfection.....	76
5.3.7 Fluorescence-activated cell sorting (FACS) analysis	77
5.3.8 Confocal laser scanning microscopy analysis.....	77
5.3.9 Telomerase activity assay using real-time quantitative PCR.....	78

Table of Contents

5.3.10 Immunohistochemical staining.....	78
5.3.11 Statistical analysis	79
5.4 Results.....	79
5.4.1 Cultivation and characterization of primary cells.....	79
5.4.2 Preparation and cultivation of tissue slices	79
5.4.3 Nanoparticle delivery of 2'-O-methyl-RNA in primary lung cancer cells and tissue slices	81
5.4.4 Cytotoxicity of nanoparticles delivery of 2'-O-methyl-RNA	83
5.4.5 Impact of 2'-O-methyl-RNA-nanoparticle-complexes on cell proliferation and telomerase expression in tissue slices.....	84
5.4.6 Inhibition of telomerase activity by 2'-O-methyl-RNA-nanoparticle-complexes in primary lung cancer cells and tissue slices	85
5.5 Discussion.....	86
5.6 Conclusion	89
Chapter 6: Inhalation of Nanoplexes for the Delivery of 2'-O-Methyl-RNA in An Isolated Perfused Rat Lung Model	91
6.1 Abstract.....	92
6.2 Introduction.....	93
6.3 Material and methods.....	93
6.3.1 Animals	93
6.3.2 Isolated perfused rat lung (IPL) preparation.....	94
6.3.3 Inhalation of nanoplexes.....	94
6.3.4 Immunohistochemical staining.....	95
6.4 Results and discussion	95
6.5 Conclusion	98
Chapter 7: Proliferation Marker KI67, Human Telomerase Reverse Transcriptase (hTERT), Stem Cell Marker CD133 Expression and Telomerase Activity in Non-Small Cell Lung Cancers.....	99
7.1 Abstract.....	100
7.2 Introduction.....	101
7.3 Material and methods.....	102
7.3.1 Tissues collection	102

Table of Contents

7.3.2 Telomerase activity measurement of lung cancer tissues	102
7.3.3 Immunohistochemical staining	103
7.3.4 Scoring methods.....	103
7.3.5 Statistical analysis.....	103
7.4 Results.....	103
7.4.1 Telomerase activity and histopathology of lung tumors	103
7.4.2 Relationships between telomerase activity and expressions of KI67, hTERT and CD133	104
7.5 Discussion.....	107
7.6 Conclusion	109
Chapter 8: Summary and Outlook	111
Chapter 9: Zusammenfassung und Ausblick	113
Abbreviations	115
References	117
Acknowledgements	129
Curriculum Vitae	131

Abstract

Telomerase activity can be detected in about 80% of non-small cell lung cancers (NSCLC). Inhibition of telomerase is a specific approach for treatment of NSCLC. The oligonucleotide 2'-O-methyl-RNA (OMR) binding to the RNA component of telomerase acts as a selective telomerase inhibitor. Chitosan-coated poly(lactide-co-glycolide) (PLGA) nanoparticles which are capable to form nanoplexes with OMR are one promising carrier system for OMR delivery. This thesis is mainly focused on the therapeutic potential of OMR based on different *in vitro* and *ex vivo* models. In cell culture models, delivery of OMR by nanoparticles exhibited 50%-70% telomerase inhibition 72h after treatment. In A549 cells telomerase activity was continuously reduced by 80% and the telomere length shortened about 50% during a treatment for 102 days with nanoplexes. In a new tissue slice model, nanoplexes can penetrate into tumor tissue slices, deliver OMR and subsequently inhibit telomerase activity by about 40% without changing tissue architecture. An isolated perfused rat lung model was successfully applied to investigate the inhalative delivery of nanoplexes to the lung without altering lung physiology. In 40 NSCLC tumor samples, stem cell marker CD133 positive tumor cells tend to have a lower telomerase activity. These experiments provide evidence that telomerase inhibitors delivered by nanoparticles have a great potential for *in vivo* application to render a more selective anticancer therapy.

Kurzzusammenfassung

Etwa 80% aller nicht-kleinzelligen Lungentumoren (NSCLC) weisen Telomerase-Aktivität auf. Hemmung der Telomerase wäre eine spezifische Tumorthherapie. Das Oligonukleotid 2'-O-Methyl-RNA (OMR) bindet an die RNA Komponente der Telomerase und ist ein selektiver Telomerase-Inhibitor. Chitosan beschichtete Polylaktat-coglykolat (PLGA)-Nanopartikel, die mit OMR Nanoplexe bilden, sind ein vielversprechendes Trägersystem. Diese Arbeit setzt verschiedene *in vitro* Modelle ein, um das therapeutische Potenzial von OMR zu untersuchen. Eine Nanopartikel-vermittelte Aufnahme von OMR in NSCLC Zelllinien und primäre humane Lungenkarzinomzellen führte nach 72 Stunden zu einer 50% bis 70%igen Hemmung der Telomerase. Eine 102-tägige Behandlung von A549 Zellen mit Nanoplexen reduzierte die Telomerase-Aktivität kontinuierlich um 80% und verkürzte die Telomere auf etwa 50%. Nanoplexe drangen in *ex vivo* kultiviertes Tumorgewebe ein. Die so eingeschleuste OMR hemmte die Telomerase-Aktivität um etwa 40%, ohne die Gewebe-Struktur zu verändern. Im Modell der isoliert perfundierten Rattenlunge wurden Nanoplexe inhalativ verabreicht, ohne die Lungenphysiologie zu verändert. OMR konnte in diesen Lungen nachgewiesen werden. In 40 NSCLC Proben zeigten die Tumorzellen mit positiver Expression des Stammzell-Markers CD133 eine Tendenz zu einer geringeren Telomerase-Aktivität. Diese Experimente zeigen, dass die Nanoplexe ein großes Potenzial für die *in vivo* Anwendung und eine selektivere Krebstherapie haben.

Chapter 1

General Introduction and Aim of the Thesis

Parts of this chapter have been published as an editorial commentary in *European Journal of Clinical Pharmacology*:

Dong M, Mürdter TE, Klotz U.

Telomeres and telomerase as novel drug targets: reflections on the 2009 Nobel Prize in Physiology or Medicine. *Eur J Clin Pharmacol*. 2010 Jan;66(1):1-3.

1.1 Lung

The lung is one of the largest organs in the human body where respiration takes place. It is divided into lobes by interlobular fissures. The left lung consists of two lobes (upper and lower lobes). The right lung consists of three lobes (upper, middle and lower lobes). They are separated into several bronchopulmonary segments and further into many lobules. In humans, the trachea splits into two main bronchi that enter the lungs. The bronchi continue to divide within the lung and give rise to bronchioles. At the level of terminal bronchioles, the alveolar sacs are made up of clusters of alveoli (Fig.1). The individual alveoli are tightly wrapped in blood vessels where gas exchange occurs [http://www.theodora.com/anatomy/the_lungs.html]. Each lobe is supplied by a secondary bronchus. Each segment is supported by a tertiary bronchus that is a branch of the secondary bronchus. Each lobule has a lymphatic vessel, an arteriole, a venule, and a branch from terminal bronchioles (Fig.1). Terminal bronchioles are subdivided into tiny branches called respiratory bronchioles and further into several (2 to 11) alveolar ducts.

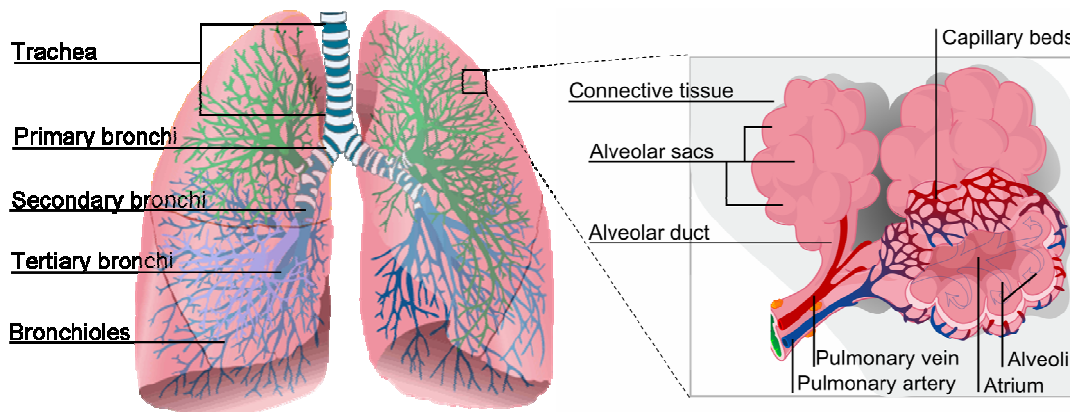


Fig. 1: The structure of lung

(Modified from [http://commons.wikimedia.org/wiki/File:Lungs_\(animated\).gif](http://commons.wikimedia.org/wiki/File:Lungs_(animated).gif); http://en.wikipedia.org/wiki/File:Alveolus_diagram.svg, accessed 23rd Nov. 2010)

The substance of the lung is a light, porous, spongy texture. The normal human lungs weigh about 1kg containing 40% to 50% blood. Nearly 50 distinct types of cells have been identified in the lungs, at least 12 types of cells can be found in the airways. The lung composes of about 300 million alveoli providing a surface area of 90m^2 [Effros, 2006]. An adult alveolus has a mean diameter of 200 to 300 μm . The alveoli consist of an epithelial layer and extracellular matrix surrounded by capillaries. Three major alveolar cell types in the alveolar wall are shown in Fig.2. The first cell type is alveolar type I cells also called squamous alveolar cells. They are very flat and thin (about $0.2\mu\text{m}$ in width) cells making up 97% of the alveolar surfaces. The second cell type is alveolar type II cells are also called great alveolar

cells. They cover the remaining 3% of the alveolar surface and are interspersed among the type I cells. The type II cells are more round shaped and secrete pulmonary surfactant by exocytosis to reduce surface tension. These cells can maintain alveolar integrity by dividing and differentiating into type I cells [Crapo *et al.*, 1982]. It is possible to isolate primary human type II cells for *in vitro* studies but it is not possible to isolate primary type I cells [Kemp *et al.*, 2008]. The third cell type, alveolar macrophages are important in removing any debris that escapes the mucus and cilia in the conducting portion of the system. They are also responsible for destroying pathogens such as bacteria.

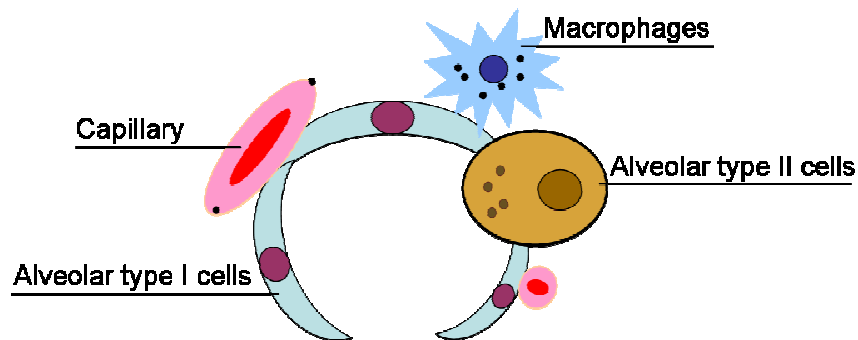


Fig. 2: The structure of an alveolar

1.1.1 Lung cancer

Lung cancer is the second most frequently diagnosed cancer in both men and women, and the leading cause of cancer-related death worldwide [Jemal *et al.*, 2010]. Symptoms suggesting lung cancer include cough, chest discomfort or pain, dyspnea, wheezing and hemoptysis. However, no cancer specific symptoms can be found at the early stage of the disease. Most patients present the symptoms with advanced disease. The main causes of lung cancer include smoking, genetic factors, radon gas, asbestos, viruses and air pollution [Gorlova *et al.*, 2007; Kabir *et al.*, 2007]. Smoking is still the major risk factor for this type of cancer [Collins *et al.*, 2007].

According to histological findings lung cancers can be classified as small cell lung cancer (SCLC) and non-small cell lung cancer (NSCLC). NSCLC is most prevalent and constitutes about 80% of all lung cancers. SCLC is less common and accounts for about 15%. NSCLC can be further differentiated into adenocarcinoma, squamous cell carcinoma and large cell carcinoma to facilitate treatment [Collins *et al.*, 2007]. The histological images of these subtypes of NSCLC can be seen in Chapter 7: Fig.2. The details of the histologic classification of lung cancer are summarized in Table 1.

Table 1: Histological type and frequency of lung cancer according to the World Health Organization (Information from Collins *et al.*, 2007; Mountain 1997; Brambilla *et al.*, 2001)

Histological type	Histological sub-type	Frequency
Non-small cell lung cancer	Adenocarcinoma	40%
	Squamous cell carcinoma	25%
	Large cell carcinoma	10%
	Adenosquamous carcinoma	< 5%
		80%
Small cell lung cancer		15%
Carcinoid		< 5%
Sarcomatoid		
Salivary-gland carcinoma		
Unclassified carcinoma		

Adenocarcinoma is the predominant histological subtype of NSCLC and accounts for 40% of lung cancers [Travis, 2002]. It is the most common type of lung cancer in "never smokers". They are histologically heterogeneous peripheral masses that metastasize early and usually originate in peripheral lung tissue [Collins *et al.*, 2007]. The subclassification of adenocarcinoma is not easy because it is highly heterogeneous. The subtypes show a mixed pattern of acinar, papillary, bronchioloalveolar, and solid adenocarcinoma with mucin formation [Brambilla *et al.*, 2001].

Squamous cell carcinomas are centrally located endobronchial masses and generally metastasize late in the course of the disease [Collins *et al.*, 2007]. Hemoptysis, postobstructive pneumonia, or lobar collapse may be present at the same time. They are closely correlated with a history of smoking and more common in men than in women.

Large cell carcinomas are poorly differentiated large peripheral masses associated with early metastases [Collins *et al.*, 2007]. It is actually a "diagnosis of exclusion" for tumor cells that lack light microscopic characteristics which classify the neoplasm as other lung cancer types.

SCLC arising mostly in the larger airways (primary and secondary bronchi), grow rapidly and aggressively [Collins *et al.*, 2007]. Smoking is a significant etiological factor for SCLC, which is more metastatic than NSCLC and often has a poor prognosis [Barbone *et al.*, 1997].

The diagnosis of lung cancer includes tissue diagnosis, a staging process including metastases and a functional patient evaluation. Histological diagnosis can be performed with sputum cytology, accessible lymph node biopsy, thoracentesis, bronchoscopy, transthoracic needle aspiration, thoracotomy [Collins *et al.*, 2007]. The metastasis evaluation relies on patient history, physical examination, laboratory tests and clinical presentation. The functional evaluation is the last step before discussing treatment options [Collins *et al.*, 2007].

In lung cancer therapy staging is an important issue to determine prognosis and potential treatment. Lung cancer staging is the assessment of the degree to which a lung cancer has spread from its original source. The international tumor node metastasis (TNM) system is used for staging NSCLC [Mountain, 2000]. In this system T stands for the extent of the primary tumor (T0-T4), N describes the involved regional lymph nodes (N0-N3) and M indicates the absence (M0) or presence (M1) of distant metastasis. The numerals I, II, III, and IV (plus 0) are used to describe the progression of cancer. Using this system, NSCLC is classified into five stages from 0 to IV. Stage 0 refers to carcinoma in situ, stages I, II and III are further subdivided into A and B according to different situations [Collins *et al.*, 2007; Mountain, 1997; Mountain, 2000]. Normally, the higher the stage, the poorer the prognosis. The staging for SCLC is different from NSCLC; it is divided into limited and extensive disease according to the spread of the tumor to distant sites. Limited stage tumors are confined to the ipsilateral hemithorax, extensive stage tumors are associated with metastases and are located beyond the ipsilateral hemithorax.

1.1.2 Lung cancer therapy

The most common treatments for lung cancer include surgery, chemotherapy, radiotherapy or a combination of these options. Treatment varies according to the cell type, the stage of the lung cancer and functional evaluation of the patient [Collins *et al.*, 2007]. Adjuvant therapy is given after the primary treatment to lower the risk of cancer relapse. It may include chemotherapy, radiation therapy, hormone therapy, targeted therapy, or biological therapy. Table 2 shows an overview of the treatment for different stages of NSCLC. SCLC is more sensitive to chemotherapy and radiation therapy.

Table 2: Treatment strategies for NSCLC

(Information from Collins *et al.*, 2007; Merck Manual Professional)

NSCLC stage	Treatment
I and II	Surgery with or without adjuvant chemotherapy or radiotherapy
IIIA (resectable)	Surgery with or without preoperative chemotherapy, adjuvant chemotherapy with or without radiotherapy
IIIA (unresectable)	Chemotherapy or subsequent radiotherapy without adjuvant
IIIB	Radiotherapy with or without chemotherapy
IV	Chemotherapy with or without palliative radiation therapy or resection of primary brain metastasis and primary T1 tumor

The overall five-year survival rate for all patients diagnosed with lung cancer is about 15% and it decreases by cancer stage [Spiro *et al.*, 2010]. About 40 to 70% of patients at stage I

and II survive more than 5 years from the time of diagnosis but for patients of stage IV with metastasis, the five-year survival rate is less than 1% [Collins *et al.*, 2007].

Table 3: Adverse effects and modes of action of drugs used currently in lung cancer chemotherapy

The adverse effects mentioned are the most common occurring in more than 30% of patients. (Information from Eldridge 2010, Taetz 2008, <http://www.chemocare.com/> Chemotherapy Drugs)

Drug	Adverse effects	Mechanism
Cisplatin	Low blood cell count, nausea, vomiting, renal toxicity, blood test abnormalities	Platinum-based, interacts with DNA, causes cell apoptosis.
Carboplatin	Similar to Cisplatin	
Docetaxel	Low blood cell count, nausea, hair loss, diarrhea, swelling, infection, nail changes	Anti-mitotic medication interferes with cell division.
Paclitaxel	Low blood cell count, nausea, vomiting, hair loss, diarrhea, arthralgias, myalgias, mouth sores, fever, chills, skin rash	
Vinorelbine	Low blood cell count, nausea, vomiting, muscle weakness, constipation	
Vinblastine	Low blood cell count, reactions at injection site, fatigue, weakness	Folate antimetabolites
Gemcitabine	Low blood cell count, nausea, vomiting, flu-like symptoms, fever, fatigue, skin rash	
Pemetrexed	Low blood cell counts, nausea, vomiting, diarrhea, fatigue, skin rash, constipation	
Mitomycin C	Low blood cell counts, fatigue, poor appetite, mouth sores	Antitumor antibiotics, incorporated into cell DNA strand and stops cell growing
Doxorubicin	Low blood cell count, nausea, vomiting, hair loss, mouth sores	
Ifosfamide	Low white blood count, low platelet count, hair loss, nausea, vomiting, blood in urine	Alkylating agent, effective in the resting phase of the cell.
Etoposide	Low white blood cell count, nausea, vomiting, hair loss, loss of fertility	Topoisomerase inhibitor, unwinds DNA and causes DNA strands to break.
Irinotecan	Low blood cell count, nausea, vomiting, hair loss, diarrhea, fever, weight loss	
Topotecan	Low blood count, nausea, vomiting, hair loss, diarrhea	

Chemotherapy mainly works by killing rapidly dividing cells. Most of the used medications are given intravenously, some are also given as tablets. Chemotherapy can cause adverse effects. Table 3 summarizes the currently administered drugs, their common adverse events

and their mode of action. In clinical practice, two or more drugs are often given at the same time to improve therapeutic efficiency.

Targeted therapy as a newer form of cancer treatment is used in combination with chemotherapy or when other options fail. This therapy applies a drug which attacks more specifically cancer cells, resulting in less damage to normal cells. So far only few drugs are approved for advanced NSCLS treatment. Most of the agents are still under clinical investigation to characterize their safety and effectiveness. In Table 4 some targeted drugs are listed which are tested in clinical trials.

Table 4: Targeted drugs and their mode of action

* Still in clinical trials for NSCLC therapy. (Information from Sun *et al.*, 2007; <http://www.chemocare.com/> Chemotherapy Drugs, <http://clinicaltrials.gov/> Clinical trails)

Drug	Mode of action	
Gefitinib	Epidermal growth factor receptor (EGFR) tyrosine kinase inhibitor	Inhibitors of EGFR pathway
Erlotinib		
Cetuximab	Anti-EGFR monoclonal antibody	
Panitumumab *		
Bevacizumab	Vascular endothelial growth factor (VEGF) inhibitor	
Tipifarnib *	Inhibitors of Ras pathway	
Lonafarnib *		
p53 adenovirus *	Tumor suppressor gene	
Bortezomib *	Proteasome inhibitor	
GRN163L *	Telomerase inhibitor	

Recent evidence has suggested that cancers may arise from a rare subpopulation of stem cell-like tumor cells [Reya *et al.*, 2001]. Like normal stem cells, these cancer stem cells have several properties: self-renewal, extensive proliferation, differentiation to other malignant cells, active telomerase activity, activation of antiapoptotic pathways, increased membrane transporter activity and the ability to migrate and to metastasize [Wicha *et al.*, 2006]. Several stem cell markers have been used to isolate cancer stem cells from lung cancer [Eramo *et al.*, 2008; Wicha *et al.*, 2006; Sun *et al.*, 2007]. As the same markers were found in the developed tumors and the lung stem cells a strong link between stem cells and carcinogenesis in the lung was assumed [Sun *et al.*, 2007]. The small subpopulation of cancer stem cells may be resistant

to the cytotoxic effects of the presently used drugs. The failure of current cancer therapies may be due to the inefficacy of drugs on cancer stem cells [Dean *et al.*, 2005]. Several selective therapies targeting cancer stem cells are under development. Stem cell self-renewal pathways such as Hedgehog, Notch, and Wnt signalling pathways can be used as potential targets [Sun *et al.*, 2007]. Applying immunotherapy-based vaccines against antigens present on cancer stem cells offers another option. Furthermore, inducing cancer stem cells differentiation with soluble factors, inhibiting DNA repair enzymes or inhibiting telomerase activity of cancer stem cells represent modern targeting tools [Sun *et al.*, 2007]. As given in Table 4, one telomerase inhibitor GRN163L is currently in phase II trials. Thus, telomerase inhibition is a promising strategy in treating lung cancer more selectively.

1.1.3 Inhalation therapy

The human lung has a large absorptive surface area (up to 100m²), extremely thin (0.1µm – 0.2µm) alveolar capillary membranes and a very good blood supply. Due to this unique structure and its transport function between the external environment and systemic circulation, the pulmonary route has the potential for the systemic delivery of therapeutic agents. Drug administration by inhalation has been used commonly for the treatment of asthma, chronic obstructive pulmonary disease and cystic fibrosis [Anabousi, 2006]. There is also an expanding role of aerosols in systemic drug delivery such as insulin for diabetes [Laube, 2005]. Nowadays increasing attention was also attributed to the potential of inhalative administration for lung cancer treatment.

Pulmonary administration of drugs can be achieved by aerosol which is generated either from a liquid drug solution in a nebuliser, a dry powder inhaler, or a pressurised metered dose aerosol [Vidgren *et al.*, 1988]. Inhaled particles have different distribution patterns in the lung depending on their sizes and deposited regions. Large particles (~20µm) impacting in the throat are swallowed soon after inspiration. Smaller particles (0.2-2.0µm) are the respirable fractions and can finally enter the respiratory bronchioles and alveoli. The medium-sized particles can deposit within the tracheal-bronchial tree and might be swept out of the lung by mucociliary clearance [McCalden, 1990]. It is not easy to deposit aerosols in high yield into the alveoli. From a pressurised metered dose aerosol, only about 10% of the administered materials are able to reach the terminal airways. All the rest is deposited into the upper airways [Vidgren *et al.*, 1988]. Thus a better pharmacokinetic distribution to the targeted area should be achieved in inhalation therapy.

Direct drug administration by inhalation for cancer treatment offers several theoretical advantages. The drug can be delivered topically to the tumor area thus increasing the local drug concentration and limiting systemic drug exposure with fewer systemic side effects. Problems with poor oral bioavailability and intestinal/hepatic first-pass metabolism of the drug would be avoided by the pulmonary application and the use of a noninvasive needle-free delivery system [Gagnadoux *et al.*, 2008; Anabousi, 2006]. On the other hand, this method also has some disadvantages. Patients might have difficulties by administering a drug via inhaler, which could directly influence the applied drug quantity. Only a small portion of the inhaled drugs can reach the intended target in the lower respiratory system [Anabousi, 2006]. Local administration of high doses of a cytotoxic drug by inhalation may increase the risk of drug-induced lung disorders. Several chemotherapeutic agents such as doxorubicin, gemcitabine and paclitaxel have been studied in animal models for their safety, pharmacokinetic advantages and antitumor effects [Gagnadoux *et al.*, 2008]. However, inhalation therapy is not yet a clinical standard treatment of lung cancers. Efficiency of drug delivery, pulmonary and systemic toxicity need to be further evaluated.

1.2 Telomere and Telomerase

The 2009 Nobel Prize in Physiology or Medicine was awarded to Elizabeth H. Blackburn, Carol W. Greider, and Jack W. Szostak for their discovery of “how chromosomes are protected by telomeres and the enzyme telomerase” which solved a major problem in biology: how chromosomes can be properly copied during cell division and how they are protected from degradation by a highly conserved telomeric DNA sequence synthesized through a unique reverse transcriptase called telomerase.

Telomeres are DNA-protein complexes that contain repeating nucleotide sequences and cap the end of linear chromosomes of most eukaryotic organisms. It can protect the chromosomes from recombination, degradation and fusion with other chromosomes [Zimmermann *et al.*, 2007]. Human telomeric DNA consists of a 2-15kb duplex repeats of TTAGGG/AATCCC sequences ending with a 100-200 nucleotides single-stranded G-rich 3' overhang. Several proteins bind specifically to telomeric DNA, and these recruit other proteins to the chromosome end as shown in Fig.3. The human telomere length shortens at a rate of 50 to 200bp during each cell cycle because of the end replication problem [Zimmermann *et al.*, 2007; Blackburn, 1991]. Most somatic cells stop dividing when their telomeres reach a certain point, and eventually the cells die. The maintenance of functional telomeres is crucial for cell

proliferation. Almost all eukaryotic cells use the reverse transcriptase telomerase for telomere elongation.

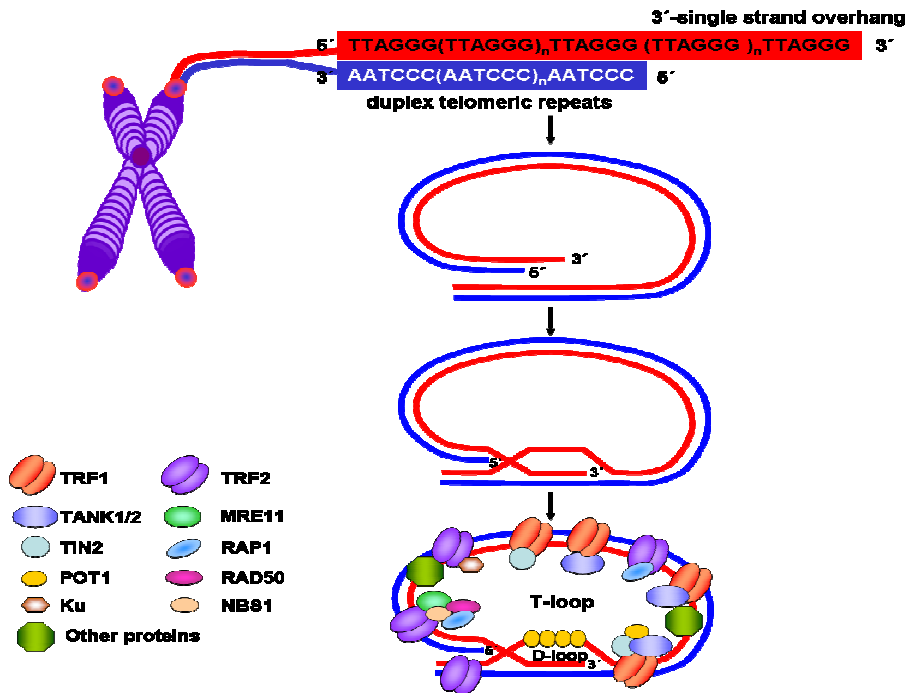


Fig. 3: Proposed schematic structure of the human telomere

Telomeres are shown as red points at the end of chromosome. The telomere DNA can turn back on itself forming the so called telomere loop (T-loop). The 3' overhang can invade and anneal with part of the duplex telomeric repeats forming a displacement loop (D-loop). The protecting protein of telomeres-1 (POT1) binds to the single-stranded DNA. Two double-stranded telomeric repeat binding factors (TRF1 and TRF2) are associated with the duplex repeats. TRF1 and TRF2 may also form multiple complexes and recruit other proteins, such as the tankyrases 1/2 (TANK1/2); double-strand break repair protein complexes consisting of MRE11; RAD50 and NBS1; TRF1-interacting factor-2 (TIN2); Ras-proximate-1 (RAP1); Protein Ku that binds to DNA double-strand break ends. Some other proteins are also involved in the telomeric complexes which are shown as other proteins in the figure (Information from Neumann *et al.*, 2002; Griffith *et al.*, 1999; de Lange, 2004).

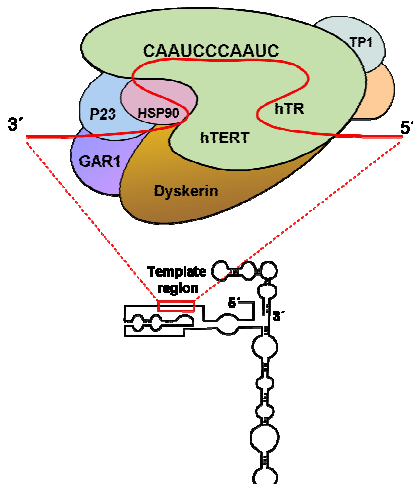


Fig.4: Telomerase components

Human telomerase is comprised of the template telomerase RNA (hTR), the telomerase reverse transcriptase catalytic subunit (hTERT), and some associated proteins. The sequence of the template region on hTR is 3'-CAAUCCCAAUC-5'. (Information from Keith *et al.*, 2002; Shay *et al.*, 2006).

Telomerase is a ribonucleoprotein complex that synthesizes telomeric DNA. As illustrated in Fig.4 human telomerase contains two major components: human telomerase RNA (hTR) which serves as a template for production of telomeric repeats to the telomere DNA and human telomerase reverse transcriptase (hTERT) that works as the catalytic protein subunit [Nakamura *et al.*, 1997; Feng *et al.*, 1995; Meyerson *et al.*, 1997]. The mode of action of telomerase on telomeric DNA synthesis is illustrated in Fig.5.

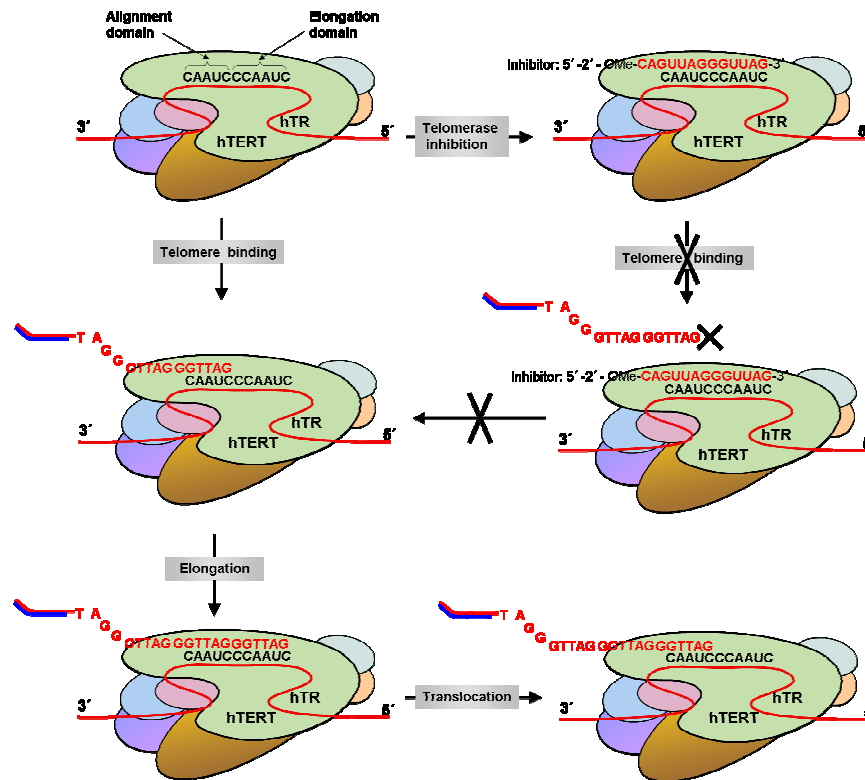


Fig. 5 : The mechanism of telomerase on telomeric DNA synthesis

The RNA template on hTR contains two domains. The alignment domain hybridised to the 3' end of the telomere. The telomere is subsequently extended by reverse transcription of the elongation domain. Three steps are involved in telomere synthesis: (1) telomere binding, in which the 3' end of telomeric single strand binds to the alignment domain of the template; (2) elongation, in which nucleotides are sequentially added to the telomere; (3) translocation, in which the telomere shifts 6 nucleotides and moves to the alignment domain for next round of elongation. Oligonucleotides with sequence complementary to the template region of hTR can act as a telomerase inhibitor and hybridise with RNA template, block telomere binding and prevent telomere elongation. (Information from Gavory *et al.*, 2002; Harley, 2008).

1.2.1 Telomerase as a target for cancer therapy

In most human cells telomerase activity is down-regulated during embryogenesis, which leads to successive telomere shortening. When the telomere length erodes to a critical length (~5kbp) cells reach mortality stage 1 or senescence stage (Fig. 6) and cell proliferation is arrested. However this can be bypassed by inactivation of tumor suppressor genes or

mutations [Shay *et al.*, 1991]. By escaping senescence, cells continue to proliferate leading to critically telomere shortening. They reach mortality stage 2 or crisis stage with massive cell death. Very rare cells can escape this stage by developing a mechanism to maintain the telomeres becoming immortal cancer cells (Fig. 6). Generally, tumor cells can survive from crisis by reactivation of telomerase [Kim *et al.*, 1994].

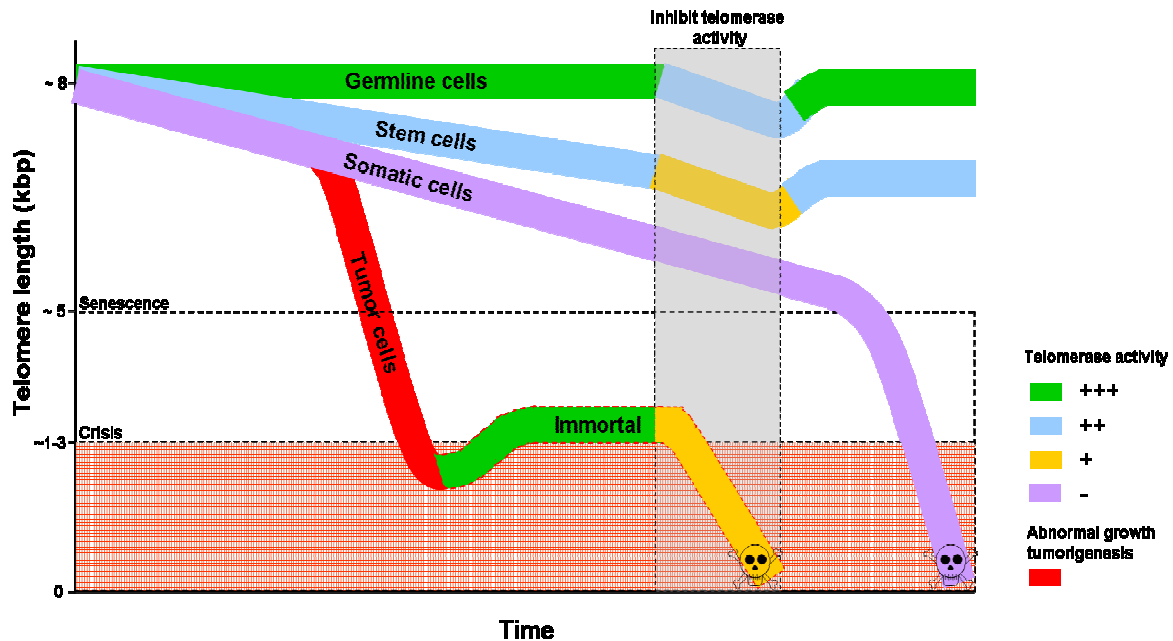


Fig. 6 : Telomere and telomerase activity dynamics and telomerase inhibition function

Germline cells show high telomerase activity maintaining long and stable telomere length. Telomerase is down-regulated during embryonic development, which leads to telomere shortening with cell divisions in most somatic cells. When the telomere length is reduced to lower than 3 kbp, massive genomic instability is triggered and eventually cells die. Adult stem cells have relatively higher telomerase activity, but they still undergo slowly telomere shortening. Bypassing the crisis barriers and reactivating high telomerase activity, about 90% of tumor cells get immortal. Inhibition of telomerase activity for a certain period of time (grey area) can cause telomere shortening on all telomerase positive cells. As germline cells and adult stem cells have longer telomere length and lower proliferation rates, the effects on these cells are moderate. Their telomeres are extended after the treatment when telomerase activity is recovered. Tumor cells will be selectively killed because of their predominantly shorter telomere length and their fast proliferation rate (Information from Zimmermann *et al.* 2007; Harley *et al.* 2008).

In contrast to normal somatic cells, the vast majority of tumor cells exhibit short telomere length and high telomerase activity. This makes telomerase an attractive drug target for cancer therapy. The major advantage of targeting telomerase is its specificity for cancer cells, including the putative cancer stem cells which are considered to be responsible for the current failure of anticancer therapy [Harley, 2008].

Different strategies have been employed to inhibit telomerase in all kinds of tumor cells [Rankin *et al.*, 2008; Kleideiter *et al.*, 2007; Chen *et al.*, 2009]. A large-scale screen of a chemical library has been performed to identify highly selective isothiazolone-derived telomerase inhibitors. The nonnucleosidic compounds (e.g. BIBR 1532 [Pascolo *et al.*, 2002] or TELIN [Kakiuchi *et al.*, 2004]) can bind directly to hTERT; the G-quadruplex-interactive compounds (e.g. BRACO19) can fix the single-stranded telomeric end as a G-quadruplex structure [Taetz *et al.*, 2008]. Unfortunately, the development of nonnucleosidic telomerase inhibitors has not yet generated compounds which can induce significant telomerase inhibition *in vivo* over a longer time period [Zimmermann *et al.*, 2007]. However, the oligonucleotide-based therapeutic agents have reached clinical trials [Harley, 2008].

Table 5: Approaches and mechanisms of telomerase-based anticancer therapy (Information from Zimmermann *et al.*, 2007; Harley, 2008)

Approach	Mode of action	Features
Telomerase inhibition	Direct enzyme inhibition	
Targeting hTERT	<ul style="list-style-type: none"> • Target hTERT mRNA expression • Mutant hTERT • hTERT phosphorylation inhibitors • Repress hTERT transcription 	<p>The products may not be subject to common drug-resistance mechanisms. A lag phase is noted between the initiation of telomerase inhibition and the effect on tumor cell growth. Long treatment duration might be necessary.</p>
Targeting hTR	<ul style="list-style-type: none"> • Antisense oligonucleotides target hTR template • Small interfering RNAs (si RNAs) target hTR • Ribozymes • Mutant hTR template 	
Targeting additional telomerase components	<ul style="list-style-type: none"> • Targeting telomerase-associated protein 1 • Blocking the interaction of hTERT with chaperones 	
Telomerase immunotherapy	Stimulating immune system to attack cancer cells that express hTERT. The antigen-presenting cells are exposed to relatively high levels of TERT peptides, mRNA, plasmid or viral DNA.	Life-long effects with periodic boosting possible. Many patients may have weak TERT response.
Suicide gene therapy	Telomerase promoter is placed upstream of a toxic gene or gene that triggers a toxic downstream event. Cells will be killed when the products are expressed.	Rapid killing of telomerase positive tumor cells. Effective delivery to the tumor area is changing.
Telomere-disrupting agents	Alter the structure of the telomere leading to inability of telomerase to access the telomere.	Rapid induction of cell death. Assumed toxicity to normal cells and tissue.
Targeting telomere-associated proteins	Target the telomere-associated proteins (e.g. HSP90, TRF1, TRF2) and influence the stability and function of telomere	Rapid function on telomeres. Possibility of influencing the normal cell telomere function.

Several strategies have been employed in oligonucleotide-based inhibition of telomerase activity. They are summarized in Table 5. Either hTERT or hTR can be targeted by different

molecules. Stabilized antisense oligonucleotides directed against hTR, such as peptide nucleic acids (PNAs) or RNA oligomers with methyl-substituted ribose sugar rings (2'-O-methyl-RNA) prevent telomere elongation by hybridizing to hTR [Dong *et al.*, 2009].

Agents being in clinical trials are mainly focusing on telomerase enzyme inhibitors and active immunotherapy. GRN163L is an hTR template antagonist with covalent lipid(L) modification. *In vivo* it shows sufficient cellular uptake and biodistribution at very low concentrations and has moved to phase II clinical trials [Harley, 2008]. Furthermore, GV-1001 is a biological telomerase peptide vaccine which is undergoing phase III clinical trials [Harley, 2008].

Inhibition of telomerase activity will induce progressive telomere shortening resulting in reduced proliferation and apoptosis after a certain time delay. Therefore, telomerase inhibitor-based therapy will be a long-term treatment. This requires high demands on the profile of drug safety [Dong *et al.*, 2009]. In addition, tumor cells have variable telomere length. It is necessary to identify telomere length and telomerase activity before treating the patients with telomerase inhibitors. Patients with short telomeres in their tumors may benefit more from this kind of therapy.

A major obstacle with all potential oligonucleotide-based anticancer agents is their safe and efficient delivery to the tumor cells and their uptake at the site of action. Whereas a covalently bound lipid residue will enhance the cellular uptake of the antisense oligonucleotide GRN163L, biodegradable nanoparticles might also serve as an efficient carrier system for intracellular delivery of the various oligonucleotide-based telomerase inhibitors [Herbert *et al.*, 2005; Beisner *et al.*, 2010].

1.3 Nanoparticles

Nanoparticles are microscopic particles normally measured in nanometers (nm). In nanotechnology, particles are defined as fine and ultrafine particles according to their sizes. The diameter of fine particles cover the range between 100 and 2500 nm, while the ultrafine particles have diameters between 1 and 100 nm. The up to date definition of nanoparticles is similar to ultrafine particles having a maximum feature size of 100nm. Nanoparticles may exhibit some size-related physical properties that differ from those of bulk materials when their sizes do not reach a limiting value. However, such size thresholds vary with the material types and may not be the only determinant for nanoparticle classification. An accepted definition extends this upper size limit to 1 micron, the sub-micron range being classified as nano [Buzea *et al.*, 2007].

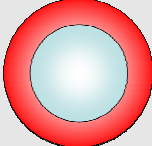
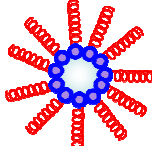
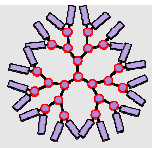
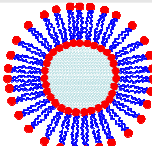
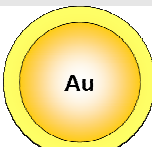
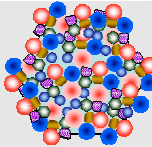
1.3.1 Nanoparticles as drug delivery systems

Two important aspects have to be considered when developing a new drug delivery system for cancer therapy. First, the delivery system must be able to carry the drug to the tumor tissue with minimal loss of the active agent. Second, the drug can target and kill the tumor cells with a controlled release mechanism of the active form [Cho *et al.*, 2008]. Nanoparticles can be used as a drug delivery system to meet these two requirements. They can use both active and passive targeting strategies to concentrate drugs in cancer cells [Maeda, 2001] and they can bypass P-glycoprotein mediated drug efflux which is an important mechanism of drug resistance [Larsen *et al.*, 2000]. Table 6 illustrates the types of nanoparticles used as carrier system for drug delivery.

Size and surface characteristics are important factors to determine the application of nanoparticles. Uptake of nanoparticles into cells is size dependent. Smaller nanoparticles have significantly higher uptake efficiency than larger nanoparticles [Prabha *et al.*, 2002]. For a suitable drug delivery system, the size of nanoparticles must be large enough to prevent rapid leakage into blood capillaries but small enough to avoid rapid filtration by the spleen and to pass through the fenestra of the Kuffer cells in the liver ranging between 150 to 200nm [Wisse *et al.*, 1996]. The gap junction between endothelial cells of the leaky tumor vasculature has a range between 100 to 600nm [Yuan *et al.*, 1995]. Therefore the perfect size of nanoparticles should be greater than 100nm allowing an efficient delivery of drugs to tumor tissues.

Surface characteristic is another important factor to influence nanoparticles drug delivery. Nanoparticles coated with hydrophilic polymers (e.g. PEG) can escape macrophage capture and they have prolonged half-lives [Moghimi *et al.*, 2003]. Nanoparticles with hydrophobic surfaces are more easily taken up by liver, spleen and lung [Brigger *et al.*, 2002]. The surface charge of nanoparticles is a crucial property for drug delivery and cytotoxicity [Nafee, 2008]. Positively charged nanoparticles are often used in oligonucleotides delivery. Since DNA and RNA are negatively charged, a positive charge of the nanoparticle can provide better interaction with oligonucleotides. The charge of nanoparticles can be modified with different materials. Poly(lactide-co-glycolide) (PLGA) nanoparticles are negatively charged and therefore interaction with negatively charged oligonucleotides is restricted. Chitosan has a strong affinity for DNA and it is against the degradation by DNase [Nafee, 2008]. Thus, chitosan coated PLGA nanoparticles can exhibit a positive charge and will efficiently bind to the negatively charged oligonucleotides representing a promising drug delivery system.

Table 6: Classification of different nanocarriers for drug delivery(Information from Cho *et al.*, 2007 ; Gradishar *et al.*, 2005 ; Sabbatini *et al.*, 2004 ; Maik *et al.*, 1999).

Type	Structure	Nanoparticle -drug interaction	Raw materials	Characteristics
Polymeric nanoparticles		Conjugation or encapsulation	<ul style="list-style-type: none"> Natural polymers: albumin, chitosan, alginate; Synthetic polymers: Poly(lactide-co-glycolide) (PLGA), <i>N</i>-(2-hydroxypropyl) methacrylamide copolymer (HPMA); polyethylene glycol (PEG); poly-<i>L</i>-glutamic acid (PGA). 	<ul style="list-style-type: none"> Biodegradable Surface modification Specific targeting the cancer cells Selective accumulation and retention in tumor tissue
Polymeric micelles		Encapsulation or covalent attachment	Amphiphilic block copolymers: PEG-poly(D,L-lactide)-paclitaxel	<ul style="list-style-type: none"> Hydrophilic shell stabilizes hydrophobic core and makes the polymers water-soluble Biocompatible and biodegradable Self-assembling structure
Dendrimers		Encapsulation or covalent attachment or ionic interaction	Polyamidoamine (PAMAM)	<ul style="list-style-type: none"> Monodispersity Water solubility Functionalizable peripheral groups Multifunctionality
Liposomes		Encapsulation	Lipid bilayers	<ul style="list-style-type: none"> Self-assembling structures composed of lipid bilayers Amphiphilic, biocompatible Easy to be modified
Carbon nanotubes		Covalent attachment	Carbon	<ul style="list-style-type: none"> Water solubility and biocompatible by chemical modification Toxicity problems Multifunctionality
Metal nanoparticles		Electrostatic forces	Gold (iron, silver, platinum, titanium)	<ul style="list-style-type: none"> Gold has high chemical stability Optical properties Low toxicity
Viral-based nanoparticles		Gene expression or protein conjugation	Viruses: cowpea mosaic virus, bacteriophages, adenovirus, lentivirus	<ul style="list-style-type: none"> Surface modification Biological compatibility Specific tumor targeting Multifunctionality

1.3.2 Nanoparticles as delivery system for telomerase inhibitors

The antisense oligonucleotide 2'-O-methyl-RNA (OMR) with a phosphorothioate backbone has been reported as a potent and sequence-selective telomerase inhibitor [Pitts *et al.*, 1998;

Herbert *et al.*, 2006]. However, the poor cellular uptake of oligonucleotides limits a successful application of OMR [Loke *et al.*, 1989]. Chitosan-coated PLGA nanoparticles have been shown to be an efficient drug delivery system [Kumar *et al.*, 2004]. Fig.7 demonstrates the principle of the chitosan-coated nanoparticles delivery of the telomerase inhibitor OMR into cells.

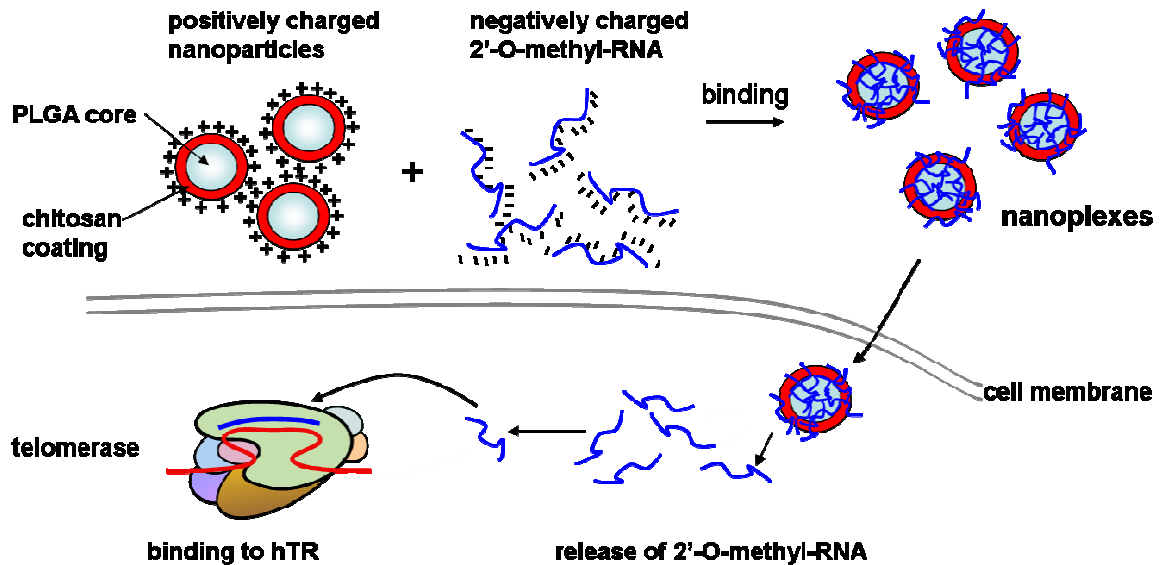


Fig. 7 : Schematic representation of chitosan-coated PLGA nanoparticles delivery of the telomerase inhibitor 2'-O-methyl-RNA(OMR) into cells

Positively charged nanoparticles bind to negatively charged OMR to form nanoplexes that pass through the cell membranes and enter cells. In the cells telomerase inhibitors are released and specifically block telomerase RNA template region (Information from Kumar *et al.*, 2004).

Delivery of OMR with chitosan-coated PLGA nanoparticles induced efficient telomerase inhibition and telomere shortening in human NSCLC [Beisner *et al.*, 2009]. Therefore they offer a new therapeutic option for lung cancer treatment. The special anatomy and transport function of the lung would suggest that inhalation could accomplish an optimal approach for nanoparticle- based drug delivery. The chitosan-coated PLGA nanoparticles and OMR formed nanoplexes can be inhaled in form of an aerosol by a nebuliser device and the tumor cells in the lung would be directly targeted. Inhalation therapy for lung cancer patients has several advantages. The administration of anticancer drugs by inhalation of nebulised aerosols has been reported to be highly effective with low systemic drug distribution [Tatsumura *et al.*, 1993]. Concerning nanoparticles for lung cancer inhalation therapy, particle size, drug-particle ratio, appropriate dosage and consequently the median aerodynamic diameter of the aerosols should be considered. Therefore, there is still a long way to go before this promising approach will enter clinical trials for lung cancer therapy.

1.4 Aim of the thesis

The aim of the thesis was to evaluate the potential of a telomerase inhibitor, the antisense oligonucleotide 2'-O-methyl-RNA (OMR), for non-small cell lung cancers (NSCLC) therapy based on *in vitro* and *ex vivo* models. Biodegradable and chitosan-coated poly(lactide-co-glycolide) (PLGA) nanoparticles which can form nanoplexes with OMR were intensively studied as OMR carrier system. The thesis can be divided in the following parts:

- **Assays for telomerase activity and telomere length:** Methods optimization to provide quantitative data for various biological specimens.
- ***in vitro* cell culture model:** Telomerase inhibition and telomere shortening induced by OMR and delivered by different carrier systems were assessed in human NSCLC cell lines and primary lung cancer cells to prove especially the potential of nanoparticles as OMR delivery system for lung cancer treatment.
- ***ex vivo* tissue slice model:** Using 0.2 mm thick tissue slices from freshly excised tumor samples of NSCLC patients to investigate whether nanoplexes formed from nanoparticles and OMR can penetrate into tumor tissue, efficiently deliver OMR to the tumor cells and subsequently inhibit telomerase. Relationships between telomerase expression and activity, cell proliferation and cancer stem cells population were evaluated.
- ***ex vivo* isolated perfused rat lung model:** An inhalation system for the delivery of nanoplexes to the lung was established by an isolated perfused rat lung model. The pulmonary transport and distribution of the inhaled nanoplexes and their influence on the physiological function of the lung was assessed.

The experiments were performed in cooperation with several groups and financially supported by the German Cancer Aid (Grant no. 107541) and the Robert Bosch Foundation (Stuttgart, Germany). The chitosan-coated PLGA nanoparticles were produced and supplied by the group of Professor Dr. Claus-Michael Lehr from the Department of Biopharmaceutics and Pharmaceutical Technology, Saarland University, Saarbrücken. The lung tumor tissue specimens were provided as surgical waste by Prof. Dr. Godehard Friedel from the Department of Thoracic Surgery, Schillerhöhe Hospital, Gerlingen. The inhalation experiments of the isolated perfused rat lung model were done in cooperation with PD Dr. Susanne Ammon-Treiber from the Department of Clinical Pharmacology University Hospital Tübingen, Tübingen.

Chapter 2

Optimization of Methods for Measurements of Telomerase Activity and Telomere Length

2.1 Abstract

Background: Telomerase is present in 80-90% of all human cancers. It adds special telomeric repeats (TTAGGG in vertebrates) to the end of linear eukaryotic chromosomes. Telomeres are protective structures located at the end of linear chromosomes. Telomerase activity and telomere shortening are considered as important factors in some human diseases. The most widely used methods to measure these two factors are the telomeric repeat amplification protocol (TRAP) for telomerase activity and the Southern blot of mean terminal restriction fragment (TRF) length measurement for telomere length. However both methods are time-consuming and do not provide precise quantitative analysis. In the present study we compared different assays and optimized the methods for telomerase activity and telomere measurements with quantitative real-time PCR.

Methods: We compared the real-time quantitative TRAP (Q-TRAP) assay with the capillary electrophoresis-based TRAP (TRAP-CE) assay with lung carcinoma cell lines and primary lung cancer tissues. The Q-TRAP assay was optimized in 384-well plate with 7900HT Fast Real-Time PCR System. For telomere length measurement, we compared the real-time quantitative PCR (Q-PCR) method with traditional Southern blot of TRF measurement with different lung carcinoma cells.

Results: Compared to TRAP-CE, Q-TRAP analyzes the exponential amplification phase of the PCR reaction avoiding plateau-related events. It is specific, highly sensitive, permits rapid analysis with lower costs and less contamination potentials. For the telomere length measurement, the Southern blot of TRF measurement is time-consuming and requires large amounts of DNA. In contrast, the Q-PCR method is a rapid, simple, and accurate measurement for large sample sets.

Conclusion: Our data suggest that both real-time quantitative PCR based assays for telomerase activity and telomere length measurements are simple and specific. The rapid and reliable quantifications can be used in a large range of applications.

2.2 Introduction

Telomerase adds special telomeric repeats to the end of linear eukaryotic chromosomes. The enzyme activity is present in 80-90% of all human cancers [Harley, 2008]. In recent years telomerase has been considered as a new marker for cancer diagnosis and a promising drug target for anti-cancer therapy [Hiyama *et al.*, 2002; Harley, 2008; Shay *et al.*, 2006]. Evaluation of telomerase activity is essential to better understand telomerase biology and its clinical impact. A standard method, termed telomeric repeat amplification protocol (TRAP) was established for determining telomerase activity [Kim *et al.*, 1994]. This PCR-based method was widely used for measurement of telomerase activity and was further modified to improve quantification and to simplify the post-PCR steps. These modified TRAP assays include gel-based TRAP assay [Kim *et al.*, 1997; Piotrowska K *et al.*, 2005], ELISA-based TRAP assay [Wu *et al.*, 2000], capillary electrophoresis-based TRAP assay [Atha *et al.*, 2003] and several other methods. Some of the assays are also available as commercial kits. However, these methods are based on the end-point PCR product which provides insufficient quantitative information and allows only a relatively low throughput. The post-PCR process is time-consuming and more susceptible to contaminations. Recently, a real-time quantitative TRAP assay has been developed to overcome these problems [Hou *et al.*, 2001; Herbert *et al.*, 2006]. This method using the PCR reaction with SYBR Green PCR master mix kit allows a rapid and reliable quantification of telomerase activity. In our experiments we compared capillary electrophoresis-based TRAP assay (TRAP-CE) with the real-time quantitative TRAP assay (Q-TRAP) for the measurement of telomerase activity and optimized a simplified Q-TRAP assay for an accurate measurement of telomerase activity with large sample sets and low costs.

Telomere is a protective element, which contains repeating nucleotide sequences (TTAGGG in vertebrates), located at the end of linear chromosomes of most eukaryotic organisms. Human telomeres shorten naturally at a rate of 50 to 200bp during each cell cycle [Blackburn, 1991]. A correlation has been reported between telomere shortening and age-related diseases and cancers [Blasco, 2005]. There are several techniques to measure telomere length in eukaryotic cells such as fluorescence in situ hybridization (FISH) and flow cytometry [Hultdin *et al.*, 1998]. The most widely used method of measuring telomere length in genomic DNA analyzes the mean terminal restriction fragment (TRF) length by Southern blot [Allshire *et al.*, 1989]. This method involves hybridization of a labeled telomere specific oligonucleotide probe to digested genomic DNA which was fractionated by electrophoresis and transferred to a membrane, and further exposed to X-ray film for analyzing. It needs large

amounts of DNA (about 5µg) and is very time-consuming (3 to 5 days). The results can vary depending on different restriction enzymes and the blot has a large variability. A real-time quantitative PCR based method (Q-PCR) for telomere measurement has been established [Cawthon *et al.*, 2002]. This Q-PCR method is a fluorescence - based assay which needs less DNA amount without enzyme digestion. It is a rapid and high throughput method. In this study, we compared the traditional Southern blot with the Q-PCR method for the measurement of telomere length and proved that the Q-PCR method is a powerful tool for investigating telomere biology in a large range of applications.

2.3 Part 1: Telomerase activity measurement

2.3.1 Materials and methods

2.3.1.1 Preparation of cell extracts

Human lung carcinoma cell lines A549, NCI-H23 (H23), NCI-H460 (H460) and primary lung carcinoma cells 5705 were used for telomerase extraction. Cultured cells were harvested, counted and 10^6 cells were pelleted and washed with PBS. The cell pellets were either stored at -80°C or immediately resuspended in 200µl ice-cold 3-[(3-cholamidopropyl) dimethylammonio]-1-propanesulfonate (CHAPS) lysis buffer and incubated on ice for 30min. The lysates were centrifuged at $12\ 000\times g$ for 20min at 4°C and the supernatants were aliquoted, snap-frozen and stored at -80°C .

2.3.1.2 Preparation of tumor tissue extracts

Tumor tissues (50-100mg) were isolated by FastPrep methods. 300µl CHAPS buffer with 200U recombinant RNase inhibitor (RNaseOUT™, Invitrogen, Carlsbad, CA) were added into a Lysing Matrix D tube with spheres (MP Biomedical, Solon, OH). The frozen tissues were minced into slices and transferred into the tube. Slices in the buffer were homogenized using a FastPrep® FP120 cell disrupter (Thermo Savant Bio101, Cedex, France) for 20sec at speed setting of 6.0 at 4°C . After short centrifugation the tubes were left on ice for 30min. The upper phase was transferred to new tubes and centrifuged at $12\ 000\times g$ for 20min at 4°C . The supernatants were aliquoted, snap-frozen and stored at -80°C .

2.3.1.3 Protein concentration determination

The amount of cellular protein in the lysates was determined with bicinchoninic acid (BCA) assay which is based on reduction of the cupric (Cu^{2+}) ion to cuprous (Cu^{1+}) ion by protein [Smith *et al.*, 1985]. The BCA assay was performed using a Sigma Protein Assay kit (Sigma-Aldrich Chemie, Steinheim, Germany). CHAPS buffer was used as dilution buffer and blank

for the measurement. 1mg/ml bovine serum albumin (BSA) was used as standard solution and a serial dilution (0, 200, 400, 600, 800, 1000 μ g/ml) was used for the calibration curve. Protein lysates were diluted to concentrations between 200 to 1000 μ g/ml. Bicinchoninic acid and copper (II) sulphate were mixed in a ratio of 50 to 1 and formed the mixed reaction solution. 200 μ l of mixed reaction solution and 10 μ l test solution were added into 96-well plates and incubated at 37°C for 1h. The plate was measured in a microtiter plate reader (Victor Multilabel Counter 1420, Wallac-PerkinElmer, Waltham, MA, USA) at 562nm. The concentration of protein in the lysates was determined from the calibration curve. All measurements were performed in triplicates.

2.3.1.4 Telomerase activity assay using capillary electrophoresis

Telomerase activity was measured using a modified protocol of the TRAP_{EZE}[®] Telomerase Detection Kit (Chemicon International, Hampshire, UK). The manufacturer's protocol was modified as follows: TS primer labeled with 6-carboxy-fluorescein (FAM) (TS Primer, MWG-Biotech AG) and CX primer (CX Primer, MWG-Biotech AG) were used instead of unlabeled TS primer and TRAP primer mix provided in the TRAP_{EZE}[®] kit. TRAP reaction was performed in a final reaction volume of 50 μ l containing 2 μ l cell extract (0.05 μ g protein), 100nM of labeled TS primer and CX primer, 50 μ M of each deoxynucleotide triphosphate (dATP, dCTP, dGTP and dTTP), 2U Taq polymerase (Qiagen, Hilden, Germany), 10 μ l of solution Q (Qiagen, Hilden, Germany), 10fg internal telomerase assay standard (ITAS) and TRAP reaction buffer (20mM Tris-HCl (pH 8.3), 1.5mM MgCl₂, 63mM KCl, 0.05% Tween 20, 1mM EGTA) as shown in Table 1. Solution Q was added to achieve a better amplification. ITAS represents a 150bp fragment of the rat myogenin cDNA that is amplified using TS and CX primer. Thermal cycling conditions were as follows: 30°C for 30min for the telomerase mediated extension reaction (if present), 95°C for 5min followed by 35 cycles of 95°C for 30sec, 57°C for 30sec with a final extension step at 57°C for 30sec. TSR8, which is an oligonucleotide with a sequence identical to telomere primers, was used as positive control. CHAPS-buffer was used as negative control. After cycling was finished the PCR products were immediately frozen. Fluorescence capillary electrophoresis (ABI PRISM 310 Genetic Analyzer) was used for separating PCR products. 2 μ l of the amplified PCR products were added to 11 μ l of highly deionized formamide and 0.5 μ l GeneScan-500 ROX size standard (Applied Biosystems, Foster City, CA, USA). Samples were denatured for 5min at 95°C and chilled on ice. Denatured PCR fragments were separated on the genetic analyzer using Applied Biosystems GeneScan[™] capillary and POP6 polymer system. Fragment sizes were determined using the internal size standard GeneScan-500 ROX and collected data were

analyzed with GeneScan Analysis software ABI Prism™ and GeneScan™ Version 3.1. The quantity of extension product was calculated for each sample as the total integral (area under the curve) of FAM-labeled peaks corresponding to the extension products in relation to the area of the ITAS peak. TA= Peak area_{total} / Peak area_{ITAS}.

Table 1: Primers, sequences and 1× PCR reaction components of TRAP-CE

Primer	Sequence
TS-FAM	5'-FAM-AATCCGTCGAGCAGAGTT-3'
CX	5'-CCCTTACCCTTACCCTTACCCTAA-3'

Component	volume [μl]
RNase/DNase-free H ₂ O	29.6
50 × dNTP mix	1
10 × TRAP buffer	5
TS-FAM primer (10μM)	0.5
CX primer (10μM)	0.5
5 × Solution Q	10
Taq Polymerase (2U)	0.4
ITAS 10fg/μl	1
Sample	2
Total volume	50

2.3.1.5 Telomerase activity assay using real-time quantitative PCR

Telomerase activity was measured using a modified real-time quantitative PCR based telomeric repeat amplification protocol (Q-TRAP) as previously described [Herbert *et al.*, 2006]. Q-TRAP reaction was performed in 384-well clear optical reaction plate (MicroAmp®, Applied Biosystems, USA) with a final reaction volume of 12μl containing 2μl cell extract (0.1μg protein), 50ng of telomerase primer TS, 50ng of anchored return primer ACX and SYBR Green PCR Master Mix (QuantiTect®, QIAGEN, Germany) as shown in Table 2. SYBR Green is a dye which binds to the double-stranded DNA and gives signal during real-time PCR reaction. Using the 7900HT Fast Real-Time PCR System (Applied Biosystems, USA), samples were incubated for 30min at 30°C for telomerase mediated extension reaction (if present), 95°C for 15min followed by 40 cycles of 94°C for 15sec, 60°C for 60sec. The threshold cycle value (C_t) of each sample was determined from amplification log plots (the change in fluorescent signal was plotted against cycle number) and compared to standard curves. The standard curve was generated from serial dilutions of telomerase-positive human

lung cancer cell line A549 cell extracts with 1.0, 0.2, 0.1, 0.05, 0.01 and 0.002 μ g protein respectively. The C_t values of standard control were plotted against log [protein] to calculate the linear equation. Inactivated samples were created by heating at 85°C for 10min. Telomerase activity of each sample was converted into relative telomerase activity (RTA) compared to A549 cells (telomerase activity of 1 μ g protein of A549 cell extracts was defined as 1). Standards, inactivated samples and lysis-buffer controls were assayed on each Q-TRAP assay plate. Lysis-buffer and heat-inactivated samples were used as negative controls to check for contaminations. TS and ACX primers were synthesized by Biomers (Ulm, Germany). The sequences are shown in Table 2. All measurements were performed in triplicates.

Table 2: Primers sequences and PCR component with 1 \times reaction of Q-TRAP

Primer	Sequence
TS	5'-AATCCGTCGAGCAGAGTT-3'
ACX	5'-GCGCGGCTTACCCTTACCCTTACCCTAACC-3'

Component	Volume [μ l]
RNase/DNase-free H ₂ O	1.5
SYBR Green Master Mix	6.25
EGTA (10mM)	1.25
ACX primer (100ng/ μ l)	0.5
TS primer (100ng/ μ l)	0.5
Sample	2
Total volume	12

2.3.1.6 Statistical analysis

Spearman test was used to determine statistical correlations between different methods. $p < 0.05$ (two-sided) was considered as statistically significant. Data were analyzed using Graphpad Prism version 4.0 (GraphPad Software Incorp., San Diego, CA).

2.3.2 Results and discussion

2.3.2.1 Capillary electrophoresis based TRAP assay for telomerase measurement

The capillary electrophoresis based TRAP assay was performed with fluorescence labeled TS primer and analyzed with GeneScan Analysis software. Fig. 1A displays the electropherograms of decreasing concentrations of A549 cell lysates. The extension products are in the range of 50bp to 140bp with 6bp intervals as shown in blue. The internal size standards are shown in red.

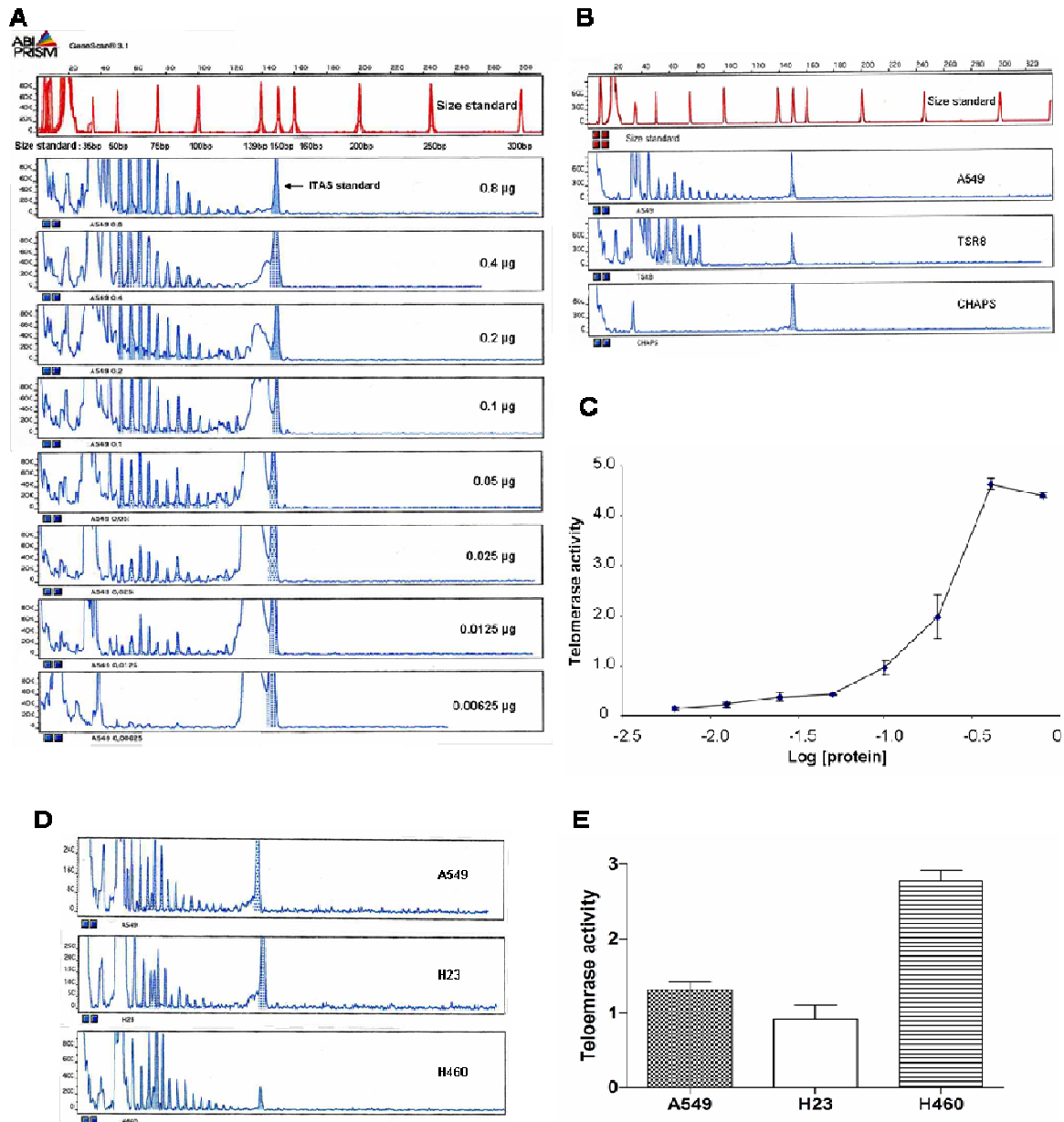


Fig. 1: TRAP-CE measurement of telomerase activity

(A) Electropherograms of diluted A549 lung carcinoma cell lysates (0.8, 0.4, 0.2, 0.1, 0.05, 0.025, 0.0125 and 0.00625µg protein, respectively). PCR products were separated by fluorescence capillary electrophoresis and collected data were analyzed with GeneScan Analysis software. Internal size standards GeneScan-500 ROX (35, 50, 75, 100, 139, 150, 160, 200, 250 and 300bp) are shown as red. Extension products, ranging from about 50 bp to 140bp with 6bp repeats, are shown in blue. The ITAS standard appears at 150bp. (B) Electropherograms of the positive control TSR8 and negative control CHAPS buffer. (C) The titration curve was generated with quantified values from electropherograms of (A). Fragment sizes were determined using the internal size standard. The quantity of extension product was calculated for each sample as the total integral (area under the curve) of FAM-labeled peaks corresponding to the extension products in relation to the area of ITAS peak. The TA can be calculated according to the equation $TA = \text{Peak area}_{\text{total}} / \text{Peak area}_{\text{ITAS}}$. TA values of different A549 concentrations were plotted as a function of log [protein]. (D) Electropherograms of lung carcinoma cell lines A549, H23 and H460 extracts with same protein content. (E) Samples were quantified according to the electropherograms of Fig.D. Data present the mean +SD of 3 independent experiments.

A plot of the calculated TA values against the log[protein] of A549 cells used in the TRAP assay is shown in Fig. 1C. Each point is the result of an individual CE separation corresponding to the Fig. 1A. When the protein content was lower than 0.4 μ g, increased protein content showed elevated telomerase activity. Telomerase activity reached a plateau phase when the protein content was higher than 0.4 μ g and subsequently the tested telomerase activity declined. The telomerase activities of the diluted A549 cells did not give a linear regression line (Fig. 1C). Therefore, the protein content used in measurements might influence the final results and a pre-test is needed to adjust the proper protein content. Fig. 1B shows the electropherograms of different samples with size standards. A549 represents a cell line with positive telomerase activity. Negative control CHAPS-buffer did not show extension products except the ITAS peak (150bp) and the primer-dimer peak (~30bp).

A549 cells with 0.00625 μ g protein content (Fig. 1A) shows similar electropherograms as negative CHAPS-buffer control (Fig. 1B) indicating that ~0.00625 μ g is the lower limit of TRAP-CE measurement. Fig. 1D illustrates the TRAP-CE measurement of different cell lines. All samples had the same protein content (0.1 μ g) in the PCR reaction. The telomerase activity after calculation is given in Fig. 1E. H460 had highest telomerase activity compared to the other two cell lines. The results of these three cell lines were comparable to the Q-TRAP measurement (Fig. 2D).

2.3.2.2 Real-time quantitative PCR based TRAP assay for telomerase measurement

The amount of cellular protein in A549 lung carcinoma cell lysates was determined and then analyzed for telomerase activity using Q-TRAP assay. The dilution series for A549 cell line is illustrated in Fig.2A.

The green line represents the threshold in the amplification plot. The threshold cycle (C_t) of each sample was determined according to this green line. From curve 1 to 6, with decreasing protein concentration, the C_t values of the samples increased. If the amount of protein lysates is greater than 1 μ g, it can interfere with the PCR reaction and will increase C_t values [Herbert *et al.*, 2006]. Therefore in our experiments the standard curve started from 1 μ g. Fig. 2B shows the relative standard curve calculated according to the data from Fig. 2A. C_t values of the samples were plotted against log [protein] to calculate the liner equation. The r^2 , which should be greater than 0.9, was 0.9919 in this experiment indicating a good correlation between C_t and log [protein]. The Y-intercept (as c in the equation $y = bx + c$) and the slope (as b in the equation $y = bx + c$) of the regression line were used to calculate the relative

telomerase activity (RTA) of unknown samples. Using this relative standard curve method, different samples assayed in the same experiment can be compared.

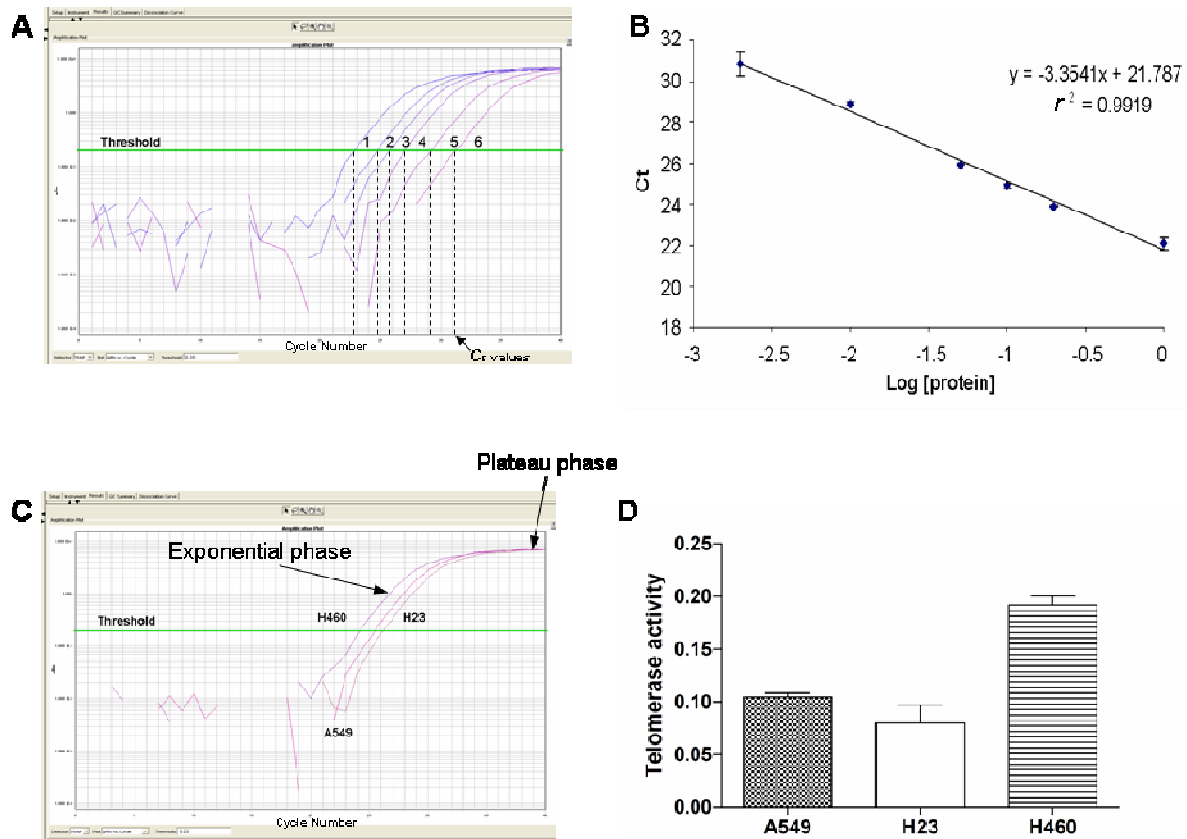


Fig. 2: Real-time quantitative PCR based TRAP assay (Q-TRAP) measurement of telomerase activity

(A) Real-time amplification plot of diluted A549 lung carcinoma cell lysates (1, 0.2, 0.1, 0.05, 0.01 and 0.002 μ g protein corresponding to curve 1 to 6 respectively). The change in SYBR Green fluorescent signal was plotted against cycle number. The threshold cycle value (C_t) represents the cycle where fluorescence is first detected above the baseline signal plus 10 standard deviations (SD) (10 SD=10 to the power 1). The dilutions of cell lysates result in increased C_t values. (B) The standard curve was generated from the amplification plot of (A). The C_t values of standard control were plotted against log [protein] to calculate the linear equation ($y = -3.3541x + 21.787$). According to the linear equation the RTA of unknown samples were calculated as $RTA_{unknown} = 10^{[(Ct_{sample} - 21.787)/(-3.3541)]}$. (C) Real-time amplification plot of lung carcinoma cell lines A549, H23 and H460 cell extracts with same protein content (0.1 μ g). (D) Samples were quantified according to the amplification plot in (C) and the standard curve in (B). Data present the mean + SD of 3 different measurements.

Telomerase activity of various samples also revealed individual curves as shown in Fig. 2C (the standard curves were not shown in this figure). The relative telomerase activities of these samples were quantified by the standard curve run in the same experiment and calculated as described above (Fig. 2D). H460 cells showed higher telomerase activity and smaller C_t values compared to the other two cell lines. H23 cells showed lowest telomerase activity and

had the greatest C_t value. The results are only valid when all the negative controls show no significant amplification signals.

In this study, we analysed samples of known protein concentrations (0.1 μ g protein was used for each sample), the calibration curve showed a very good correlation ($r^2 > 0.95$) and reproducibility between different experiments. It is easy and reliable to compare unknown samples within one experiment. The results between different PCR reactions can also be compared if the telomerase activity of the sample is normalized to a positive control (e.g. A549 cells) and expressed as a percentage of telomerase activity of the positive control.

2.3.2.3 Comparison of telomerase assays

To compare the TRAP-CE and Q-TRAP, telomerase activity was measured in primary lung cancer tissues which were obtained as surgical waste from patients. The two TRAP assays revealed a strong ($r=0.7182$) and significant ($p=0.0168$) correlation (Fig. 3).

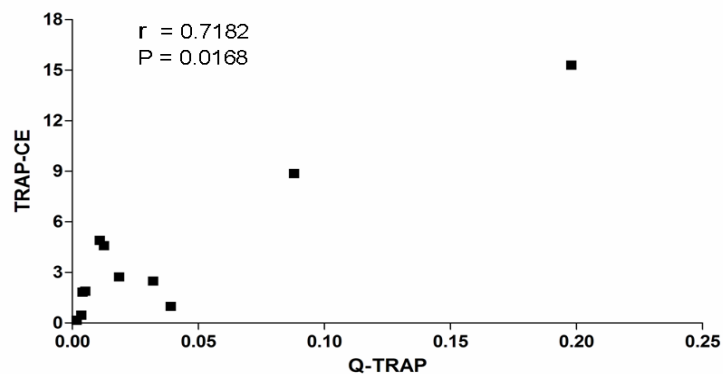


Fig. 3: Correlation between TRAP-CE and Q-TRAP assays for measurement of telomerase activity in primary lung cancer tissues

Eleven primary lung cancer tissues were analyzed for telomerase activity by TRAP-CE and Q-TRAP.

Compared to TRAP-CE, Q-TRAP has several advantages: it is specific and highly sensitive; it can provide linear telomerase detection down to low protein content; it can permit rapid analysis within less than 6h including protein isolation and determination. The real-time PCR reaction does not need post-PCR steps and the carryover contamination is reduced. One of the major advantages of the Q-TRAP assay is that it is not an end-point PCR as the results are generated during the exponential amplification phase which can avoid disturbing plateau-related events (Fig. 2A and C). In the Q-TRAP the anchored return primer ACX was used to reduce primer-dimer interference and to prevent 3' elongation of telomerase products [Kim *et al.*, 1997]. We modified the reaction in a 384-well plate using the 7900HT Fast Real-Time PCR System, so more samples can be run in one set and the costs for each sample were also less. TRAP-CE as an end-point PCR reaction is time consuming, laborious and has a

relatively low throughput. It was reported that a several-fold difference in telomerase activity can not be easily discriminated by the conventional TRAP method [Hou *et al.*, 2001]. In our experiments Q-TRAP can distinguish a two-fold difference in telomerase activity in A549 cells (Fig. 2A). It was also reported that Q-TRAP can overestimate the telomerase activity in samples of very low-activity [Herbert *et al.*, 2006]. Q-TRAP showed good linearity down to 0.002 μ g protein (Fig. 2B), but attention is needed if samples with very weak telomerase activity (lower than 0.2% of A549 cells) are analyzed. The ideal protein content in the PCR reaction has to be evaluated at the beginning of the Q-TRAP assay.

Because telomerase is a heat sensitive enzyme, samples have to be prepared at 4°C, snap-frozen with liquid nitrogen and stored at -80°C. Frequent thawing and freezing of the samples should be avoided. The protein extracts can be stored at -80°C for 10 years while the telomerase activity can be completely lost within 2 months when samples are stored at -20°C [Piatyszek *et al.*, 1995]. The Q-TRAP assay can be used as a powerful tool for measurement of telomerase activity in various specimens.

2.4 Part 2: Telomere measurement

2.4.1 Materials and methods

2.4.1.1 Preparation of genomic DNA

Genomic DNA was isolated from cells using the QIAamp[®] DNA Mini Kit (QIAGEN, Hilden, Germany). Cultured cells were harvested, counted and washed with PBS. Up to 5 \times 10⁶ cells were resuspended in 200 μ l PBS and added into a 1.5ml microcentrifuge tube which contained 20 μ l Proteinase K and 40 μ l RNase A (10 mg/ml). After 200 μ l buffer AL (from kit) was added, the sample was incubated at 56°C for 10min. The following steps were done according to the QIAamp[®] DNA Mini Kit protocol. The final DNA was eluted in Buffer AE (from kit) and stored at -20°C. DNA was quantified using a NanoDrop spectrophotometer (PEQLAB, Erlangen, Germany). For terminal restriction fragment length determination by Southern blot, 5 μ g of genomic DNA were digested with 10U (2U/ μ g DNA) of the restriction enzyme Hinf I.

2.4.1.2 Telomere measurement by terminal restriction fragment length determination

Telomere length was determined by measurement of mean terminal-restriction fragment (TRF) lengths with southern blotting. Restriction enzyme Hinf I digested DNA was fractionated by electrophoresis on a 0.8% agarose gel and transferred to a positively charged nylon membrane. DNA was fixed on the membrane by UV-crosslinking. The membrane was pre-hybridized with pre-hybridization mix at 42°C for 30min and subsequently hybridized with digoxigenin -

labeled 5'-(TTAGGG)₇ telomere-specific probe overnight at 42°C. The membrane was washed twice with 2× sodium chloride-sodium citrate buffer (SSC)/0.1% sodium dodecyl sulfate buffer (SDS) for 15min at 42°C and further washed with 2×SSC for 5min at room temperature. Blocking solution was added to the membrane to prevent unspecific binding. The membrane was incubated with anti-DIG-alkaline phosphatase for 45 min. Finally, the immobilized telomere probe was visualized by a highly sensitive chemiluminescent substrate for alkaline phosphatase (CDP-star, Roche, Mannheim, Germany). The membrane was exposed to an X-ray film (Hyperfilm; GE Healthcare Bio-Sciences, Piscataway, NJ, USA) which was densitometrically scanned. TRF length analysis was performed on the scanned image with AIDA image analyzer software (Raytest, Straubenhardt, Germany). The mean TRF length was calculated by quantification of the signal intensities at each point above background integrated over the entire distribution of fragments. The average telomere length in each sample was calculated as weighted mean of the peak with the highest optical density compared to a standard molecular weight marker (Roche, Mannheim, Germany).

2.4.1.3 Telomere measurement by real-time quantitative PCR

Telomere measurement was performed by a quantitative real-time PCR described previously (Cawthon RM 2002). All samples were measured on the 7500 Real-Time PCR System with the SDS Version 1.2.3 software (Applied Biosystems, Foster City, USA). Endogenous control 36B4 is a single copy gene which encodes the acidic ribosomal phosphoprotein P0 (Cawthon RM 2002). For 36B4 PCR reaction, the final volume of 20µl contains 35ng DNA, 300nM 36B4u primer, 500nM 36B4d primer and 10µl SYBR Green PCR Master Mix (QuantiTect[®], QIAGEN, Germany).

For telomere content PCR reactions, the final volume of 20µl contains 35ng DNA, 270nM telomere forward primer, 900nM telomere reverse primer, 1mM MgCl₂ and 10µl SYBR Green PCR Master Mix. The cycling conditions for both telomere and 36B4 PCR reaction were: 95°C for 15min followed by 40 cycles of 94°C for 15sec, 54°C for 60sec. The threshold cycle value (C_t) of each sample was determined from amplification log plots (the change in fluorescent signal was plotted against cycle number). The relative telomere length of the sample was calculated by the delta-delta C_t method ($\Delta\Delta C_t$). The relative quantities of telomere content and the single copy gene 36B4 were expressed as the level of dilution of the reference DNA sample. This will make the experimental and reference samples equivalent with regard to the number of cycles of PCR needed to generate a given amount of telomere PCR or single copy gene PCR product during the exponential phase of the PCR (Cawthon

RM 2002). The relative telomere (T) to single copy gene(S) ratio (T/S) is the ratio of the dilution factors in this experiment. H23 cells were used as reference DNA sample and its T/S ratio was set as 1. The relative telomere length of each sample was determined by dividing the T/S ratio of the sample to the T/S ratio of H23 cells. A sample of cord blood from a newborn baby was used as long telomere control in each run. Primers were all synthesized by Biomers (Ulm, Germany) and the sequences are shown in Table 3. All measurements were performed in triplicates.

Table 3: Primers, sequences and 1x PCR reaction components for telomere measurement by real-time quantitative PCR

Primer	Sequence
Telomere forward	5'-GGTTTTTGAGGGTGAGGGTGAGGGTGAGGGTGAGGGT-3'
Telomere reverse	5'-TCCCGACTATCCCTATCCCTATCCCTATCCCTATCCCTATCCCTA-3'
36B4u	5'-CAGCAAGTGGGAAGGTGTAATCC-3'
36B4d	5'-CCCATTCTATCATCAACGGGTACAA-3'

Telomere content PCR:

Component	volume [μ l]
RNase/DNase-free H ₂ O	1.66
Telomere forward primer (26.4 μ M)	0.21
Telomere reverse primer (54.5 μ M)	0.33
SYBR Green Master mix	10
MgCl ₂ (25mM)	0.8
Sample	7
Total volume	20

Endogenous control PCR:

Component	volume [μ l]
RNase/DNase-free H ₂ O	2.47
36B4u forward primer (30.8 μ M)	0.20
36B4u reverse primer (30 μ M)	0.33
SYBR Green Master mix	10
Sample	7
Total volume	20

2.4.2 Results and discussion

2.4.2.1 Telomere measurement by terminal restriction fragment length determination

Fig. 4A exhibits the telomere length determined by the mean telomere TRF using Southern blot. The mean TRF length was calculated by quantifying on the blot the signal intensities of each sample. The white line on each sample shows the maximum of the optical detected peak density. A standard molecular weight marker (λ -Hind III) was used to calculate the average TRF by comparing the weighted mean of the peak signal with the highest optical density to the weight marker. Fig. 4B illustrates the quantification results calculated from Fig. 4A. The cord blood has the longest telomere length (~15kb) and the H23 cell has the shortest telomere length (~3.6kb) in the tested samples.

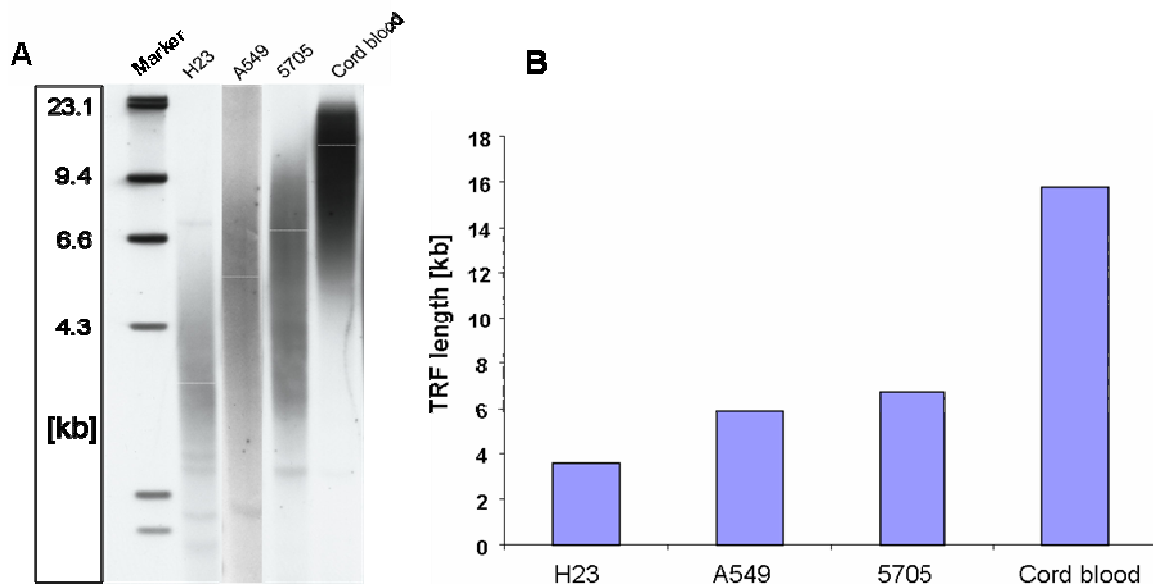


Fig. 4: Telomere length determined by measurement of mean TRF lengths with Southern blot

(A) Southern blot of lung carcinoma cells and a cord blood sample. (B) Quantitative analysis of the TRF from the Southern blot of (A).

2.4.2.2 Telomere measurement by real-time quantitative PCR

Fig. 5A shows the real-time amplification plot of the Q-PCR. In each sample the T/S was used to normalize the telomere signal to a single copy gene in each sample to avoid the interindividual variation between different samples. In this study we chose single copy gene 36B4 as the basis to normalize the quantitative telomere PCR signal [Cawthon *et al.*, 2002; Boulay *et al.*, 1999].

We assumed that the PCR reaction was quite efficient, so the amount of the PCR product was considered to be doubled in each PCR cycle. The T/S ratio can be calculated as $2^{-\Delta Ct}$ while

$\Delta C_t = C_t(\text{telomerase}) - C_t(36B4)$. The other samples were normalized to H23 to get the relative T/S ratios. The relative T/S ratio of each sample is $2^{-\Delta\Delta C_t}$ while $\Delta\Delta C_t = \Delta C_t(\text{sample}) - \Delta C_t(\text{H23})$. By using this $\Delta\Delta C_t$ method, a relative T/S ratio of each sample was calculated to indicate the relative telomere length. Fig.5B shows the results after the $\Delta\Delta C_t$ method calculation. The cord blood from a newborn baby has the longest relative telomere length. Lung carcinoma cell line A549 and primary lung cancer cells 5705 have shorter telomere length.

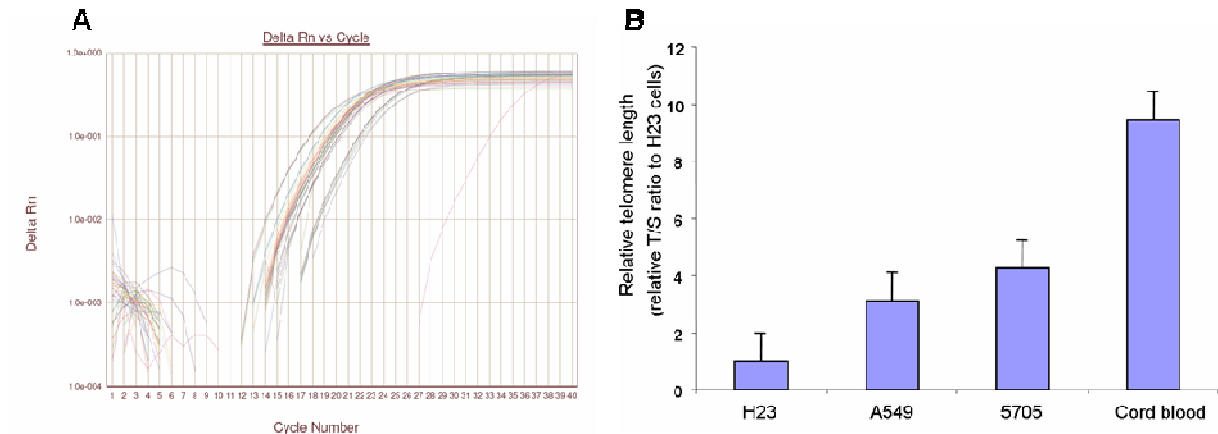


Fig. 5: Telomere length was determined by measurement of relative T/S ratios with Q-PCR

(A) Real-time amplification plot of samples by the Q-PCR method. (B) Quantitative analysis of relative T/S ratio from lung carcinoma cell lines and a human cord blood sample. Data present the mean + SD of 3 different measurements.

2.4.2.3 Comparison of telomere assays

As shown in Fig.6, in the tested 6 samples, relative T/S ratios determined by Q-PCR and relative TRF lengths measured by Southern blot exhibited a strong ($r=0.9856$) and significant ($p=0.0028$) correlation.

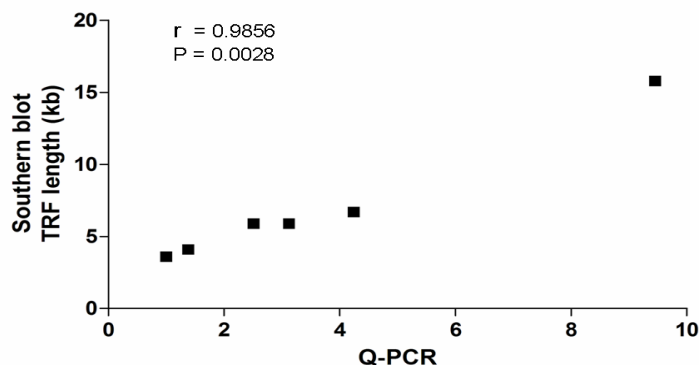


Fig. 6: Correlation between Southern blot and Q-PCR methods for measurement of telomere length in lung cancer cells

Six samples from lung cancer cell lines were analyzed for telomere length by Southern blot (TRF length) and Q-PCR (relative T/S ratio).

Cawthon RM *et al.* reported a correlation ($r^2=0.677$, $p < 0.01$) between these two methods in DNA analysis of blood samples from 95 individuals [Cawthon *et al.*, 2002]. This could be confirmed in our experiments with much stronger correlation. The stronger correlation of our experiment might be explained by a more homogenous samples or a small sample size. Fig. 7 gives the telomere lengths of A549 cells after 15 weeks of treatment with a telomerase inhibitor antisense 2'-O-methyl-RNA (OMR). Compared to the control, the group treated with the telomerase inhibitor exhibited a comparable telomere shortening by both measurements (Fig. 7B and C).

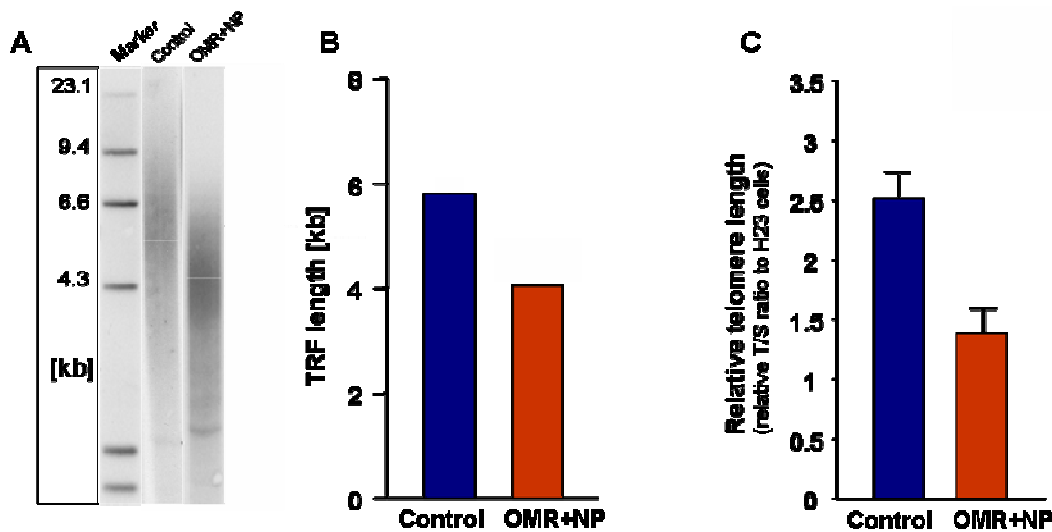


Fig. 7: Comparison of telomere length shortening of A549 cells measured by Southern blot and Q-PCR methods

Telomere length was determined by measurement of mean TRF lengths in Southern blotting and relative T/S ratios in Q-PCR. Untreated cells were used as control. A549 cells were treated with nanoparticles (NP) delivered telomerase inhibitor OMR for 15 weeks. (A) Southern blot of control and telomerase inhibitor (OMR+NP) treated A549 cells. (B) Quantitative analysis of the TRF from the Southern blot results of (A). (C) Quantitative analysis of the relative T/S ratio of control and telomerase inhibitor (OMR+NP) treated A549 cells by Q-PCR. Data present the mean +SD of triplicates. The T/S ratio of each sample was normalized to H23 cells.

Southern blot measurement of TRF requires about 5 μ g DNA for each sample and it is very time-consuming (about 3 days). The reproducibility of the blotting is low. The genomic DNA has to be digested before performing Southern blot. It was reported that the relative mean TRF lengths of the samples can be influenced by different restriction enzymes [Cawthon *et al.*, 2002]. This limits the application of this method. The measurement of telomere lengths by Q-PCR is a fluorescence based assay with closed tubes; it is a rapid (less than 2h for the real-time PCR reaction), simple and high throughput method. Recently, it has been published that the absolute telomere length can be measured with the Q-PCR method by introducing a 84-

mer oligonucleotide standard with known quantities [O'Callaghan *et al.*, 2008]. The absolute telomere measurement allows a better comparison of results between different experiments and laboratories. Since both methods can provide similar results and the absolute telomere length is not necessary in our experiments, we did not use O'Callaghan's method. The Q-PCR method we optimized can provide a rapid and useful tool for investigating telomere biology.

2.5 Conclusion

Our data suggest that both real-time quantitative PCR based assays for telomerase activity and telomere length measurements are simple and specific. Their rapid and reliable quantification can be used in a wide range of applications.

Chapter 3

Telomerase Inhibition by Liposomal Delivery of 2'-O-Methyl-RNA in Human Non-Small Cell Lung Cancer Cells

Parts of this chapter have been published as an original article in *Journal of Pharmaceutical Sciences*:

Beisner J, Dong M, Taetz S, Piotrowska K, Kleideiter E, Friedel G, Schaefer UF, Lehr CM, Klotz U, Mürdter TE.

Efficient telomerase inhibition in human non-small cell lung cancer cells by liposomal delivery of 2'-O-methyl-RNA. *J Pharm Sci.* 2009 May; 98(5):1765-74.

*The results presented in this chapter were obtained by Meng Dong.

3.1 Abstract

Background: A new promising approach for the treatment of non-small cell lung cancer (NSCLC) is based on the inhibition of telomerase in cancer cells. The antisense oligonucleotide 2'-O-methyl-RNA (OMR) targeting the RNA component of telomerase represents a selective telomerase inhibitor and a potential candidate for anticancer therapy. The poor cellular uptake and rapid nuclease-mediated degradation of oligonucleotides limit the application of OMR. To improve the cellular uptake and subsequent antitumoral efficiency of OMR in human lung cancer cells, we have compared five different transfection reagents.

Methods: In NSCLC A549 cells the transfection reagents DOTAP, MegaFectin 60, SuperFect, FuGENE 6 and MATra-A were tested for cellular uptake of OMR and the impact to mediate telomerase inhibition. A FAM-labeled OMR was applied to assess the intracellular distribution of the OMR by confocal laser scanning microscopy (CLSM). Telomerase activity was measured by a modified telomeric repeat amplification protocol using capillary electrophoresis (TRAP-CE) at 24h, 48h and 72h after transfection.

Results: In NSCLC A549 cells all five transfection reagents enhanced cellular uptake of OMR. Cationic liposomal transfection reagents DOTAP and MegaFectin 60 were most efficient in the delivery of OMR resulting in telomerase inhibition. DOTAP exhibited the lowest cytotoxicity and a strong induction of telomerase inhibition.

Conclusion: Our data show that in human NSCLC cells DOTAP is the most suitable transfection reagent for OMR delivery, displaying relatively high transfection efficiency, low cytotoxicity and strong telomerase inhibition. Effective delivery of OMR offers a potent therapeutic option for the treatment of lung cancer based on telomerase inhibition.

3.2 Introduction

In recent years telomerase has been considered as a promising drug target for anti-cancer therapy. Telomerase is an enzyme which adds telomeric repeats to the end of linear eukaryotic chromosomes. Telomerase activity is present in 80-90% of all human cancers including lung cancer which is the leading cause of cancer-related mortality [Jemal *et al.*, 2007; Harley, 2008]. Telomerase activity is detected in about 80% of non-small cell lung cancer (NSCLC) which is one of the main types of lung cancers [Taga *et al.*, 1999]. Inhibition of telomerase activity is a novel therapeutic strategy for NSCLC treatment.

Human telomerase contains two major components, the catalytic protein subunit human telomerase reverse transcriptase (hTERT) and the RNA template human telomerase RNA (hTR) [Feng *et al.*, 1995; Nakamura *et al.*, 1997]. Apparently, hTR is an ideal target for telomerase inhibition. The antisense oligonucleotide 2'-O-methyl-RNA (OMR) can directly bind to hTR and consequently could serve as a specific telomerase inhibitor [Pitts *et al.*, 1998]. After screening different classes of telomerase inhibitors, it has been reported that OMR demonstrated a high potential for telomerase inhibition in A549 lung cancer cells [Pitrowska *et al.*, 2005].

However poor cellular uptake and rapid nuclease-mediated degradation of oligonucleotides limit the application of antisense OMR. Specific delivery systems are required to enhance uptake of OMR and subsequent biological effects. In NSCLC A549 cells we have tested five different transfection reagents for their delivery of OMR, analyzed cellular uptake, toxicity and the impact to mediate telomerase inhibition. The cationic lipid reagents DOTAP and MegaFectin 60 were compared with two nonliposomal transfection reagents FuGENE 6 and SuperFect and with magnet assisted transfection (MATra-A) which uses magnetic force to deliver oligonucleotides into target cells. Cationic lipid reagents can enhance antisense oligonucleotide activity and can facilitate oligonucleotide cell internalization [Bennett *et al.*, 1992; Capaccioli *et al.*, 1993]. DOTAP is a liposome formulation of the monocationic lipid (N-1-2,3-Dioleoyloxy)-N,N,N-trimethylammonium propane methylsulfate and it is efficient in both *in vitro* and *in vivo* applications of oligonucleotides [Simberg *et al.*, 2004]. It has been reported that addition of cholesterol to the formulation of liposome can improve the transfection efficiency [Templeton *et al.*, 1997; Liu *et al.*, 1997]. In the presence of serum MegaFectin 60, a combination of DOTAP and cholesterol increase the delivery of DNA to cells [Crook *et al.*, 1998]. It has been used for gene transfer in *in vivo* experimental anticancer treatment [Anwer *et al.*, 2000]. SuperFect is based on a novel, activated-dendrimer technology which has been reported to be used in cellular delivery of antisense

oligonucleotides [Hollins *et al.*, 2004; Sato *et al.*, 2001; Bielinska *et al.*, 1996]. FuGENE 6 represents a multi-component formulation which has been applied as transfection reagent in many different cell lines [Jacobsen *et al.*, 2004]. We have compared these five different transfection reagents to identify a suitable reagent for efficient delivery of OMR into NSCLC A549 cells. Cationic lipids such as DOTAP and MegaFectin 60 were found to be more efficient in the delivery of OMR into NSCLC A549 cells. Furthermore, DOTAP is the most suitable transfection reagent for the delivery of OMR in human lung cancer cells.

3.3 Material and methods

3.3.1 Cell culture

Human non-small cell lung cancer (NSCLC) cells A549 were obtained from DSMZ (Braunschweig, Germany). They were cultivated in Roswell Park Memorial Institute (RPMI) 1640 medium (Biochrom, Berlin, Germany) supplemented with 10% heat inactivated fetal calf serum (FCS), 2mM L-glutamine (Biochrom), 50U/ml penicillin and 50 µg/ml streptomycin (Gibco BRL, Karlsruhe, Germany) in 5% CO₂ at 37°C. Cell viability was assessed by trypan blue exclusion test.

3.3.2 Oligonucleotides

An antisense 2'-O-methyl-RNA (OMR) with a phosphorothioate (ps) backbone 5'-2'-O-methyl [C(ps)A(ps)GUUAGGGUU(ps)A(ps)G]-3' was used as telomerase inhibitor in this study. 2'-O-methyl-RNA mismatch was 5'-2'-O-methyl [C(ps)A(ps)GUUAGAAUU(ps)A(ps)G]-3'. The fluorescence-labeled 2'-O-methyl-RNA (FAM-OMR) was 5'-FAM-2'-O-methyl [C(ps)A(ps)GUUAGGGUU(ps)A(ps)G]-3'. All oligonucleotides were synthesized by MWG-Biotech AG (Ebersberg, Germany). The oligonucleotides were dissolved in sterile water, aliquoted and stored at -20°C for further processing. To ensure the stability and biological activity of the oligonucleotides, small aliquots were tested in the cell-free TRAP assay prior to the use in the cell culture experiments.

3.3.3 Preparation of oligonucleotide transfection

A549 cells were selected to determine the biological effect of telomerase inhibitor OMR after transfection. A549 cells were seeded in 6-well plates before treatment. One day after seeding the cells reached approximately 60-80% confluency and they were transfected with 4µM OMR using five different transfection reagents according to the manufacturer's protocol. The ratio of oligonucleotide to transfection reagents is listed in Table 1.

The first transfection reagent was DOTAP (N-[1-(2,3-Dioleoyloxy) propyl]-N,N,N-trimethylammonium methyl-sulfate) (Roche, Penzberg, Germany). Oligonucleotides were

dissolved in HBS buffer (20mM HEPES, 150mM NaCl, pH 7.4) with a final concentration of 0.1µg/µl and 100µl DOTAP/HBS buffer (30µl DOTAP reagent was added in a sterile Eppendorf tube and filled up to 100µl with HBS buffer) was added. The mixture was mixed gently by pipetting to avoid foaming and incubated in the dark for 15min at room temperature. The mixture with certain amount of cell culture medium was applied to the cells and replaced by normal cell culture medium after 6h treatment.

The second transfection reagent was MegaFectin 60TM (Qbiogene, Illkirch, France). Following the kit protocol 153.8µl HEPES buffer was added to the lyophilized lipid and vortexed well until completely suspended to form the MegaFectin solution. Oligonucleotide was added to MegaFectin solution and incubated in the dark for 15min at room temperature. Certain amount of cell culture medium was added together with transfection mixture to the cells to make a final volume of 1.5ml for each well. Transfection mixture was replaced by cell culture medium 6h after treatment.

The third transfection reagent was SuperFect (Qiagen GmbH, Hilden, Germany). Oligonucleotides were first added to pure RPMI medium with supplements. SuperFect reagent was added to the oligonucleotide solution and mixed well. The mixture was incubated in the dark for 10min at room temperature to allow transfection-complex formation. The cells were washed with PBS once before applying the transfection mixture. Certain amount of cell culture medium with supplements was added to the cells and the transfection mixture was loaded to the cells. The final volume was 1.5ml for each well. Transfection mixture was removed 3h after treatment and the cells were continually cultured with cell culture medium.

The fourth transfection reagent was FuGENE6 (Roche, Penzberg, Germany). Certain amount of supplement-free RPMI medium was added into the Eppendorf tube, oligonucleotides were added together with FuGENE6 to the medium and mixed well. After 15min incubation in the dark at room temperature, the mix was applied to the cells and further replaced by cell culture medium after 6h treatment.

The fifth transfection device was magnet assisted transfection (MATra-A) (IBA GmbH, Göttingen, Germany). Oligonucleotides were added into supplement-free cell culture medium and mixed well. Certain amount of MATra-A reagent was added to the oligonucleotide solution and mixed well. The mixture was incubated for 20min at room temperature. During incubation, cell culture medium was changed; the bead-mixture was added to the cells and mixed immediately. The cell culture plate was placed on the suitable magnet plate and incubated for 15 min at 37°C. The magnet plate was removed and a medium change was performed once. Cells were continually cultured until analysis. Fig.1 provides an overview of

all the transfection procedures. Untreated A549 cells, A549 cells treated separately only with OMR, with transfection reagent or with a mismatch oligonucleotide were used as controls.

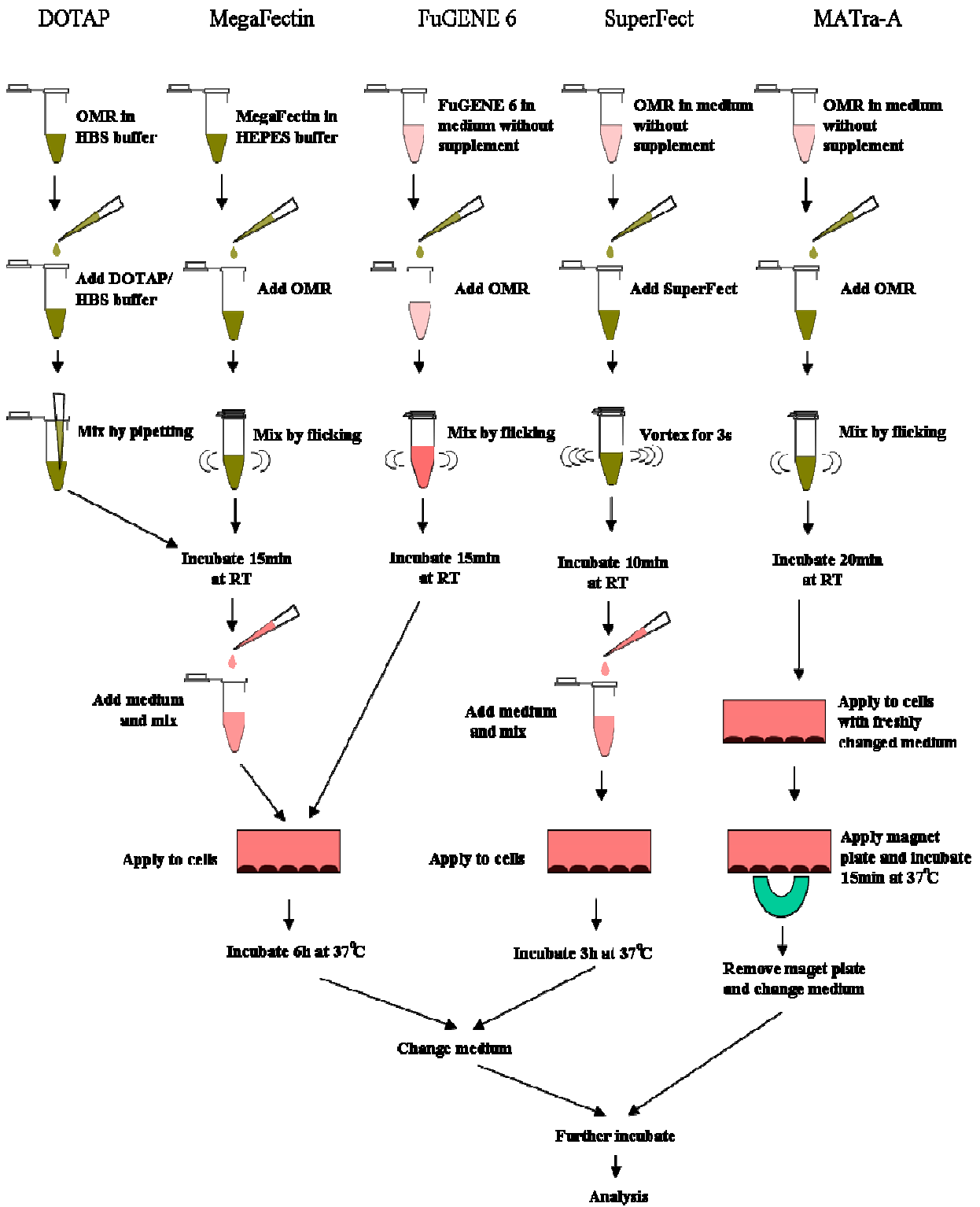


Fig. 1: Overview of the five transfection procedures (DOTAP, MegaFectin, FuGene6, SuperFect, MATra-A)

Table 1: Ratio of oligonucleotides to transfection reagents

	Transfection reagent (μ l)	OMR (μ g)
DOTAP	5	1
MegaFectin	5	1
SuperFect	2	1
FuGENE 6	1.5	1
MATra-A	1	1

3.3.4 Confocal laser scanning microscopy analysis

The transfection efficiency was analyzed by confocal laser scanning microscopy (CLSM). A549 cells were seeded in Lab-Tek[®] chamber slides (Nalge Nunc International, Naperville, USA) at a density of 65 000 cells per well one day before the transfection. 24h after seeding, cells were transfected as described above with the fluorescence labeled OMR (FAM-OMR). Cells were evaluated by confocal laser scanning microscopy 6h, 24h and 72h after treatment, respectively. After two times washing with PBS, cells were incubated with 25 μ g/ml rhodamine-labeled ricinus communis agglutinin I (RCA I, Vector Laboratories, Burlingame, CA, USA) for 15min at 37°C which enables detection of cell membranes by binding to oligosaccharides ending in galactose. The cells were washed twice with PBS and fixed with 100% ethanol at -20°C for 10min. The cell nuclei were stained with 1 μ M TO-PRO[®]-3 iodide (Molecular Probes Invitrogen, Eugene, OR, USA) in the dark for 10 min at room temperature. Cells were washed twice with PBS, the chamber and gasket were removed and slides were mounted with mounting medium (Vectashield[®] Mounting Medium, Vector Laboratories, Burlingame, CA) for analyzing by CLSM. Images were taken randomly from different areas. Cells which contained more than 5% FAM signal were considered as positive cells. For each image the uptake efficiency in percent was calculated by dividing the number of positive cells by the total cell number. A mean value of each sample was calculated from all 12 images. CLSM was performed with a Leica LCS (Leica Lasertechnik) instrument based on a Leica DM IRBE microscope equipped with argon and helium/neon lasers. The excitation (Ex.) and emission (Em.) wavelengths of the dyes were as follows: FAM (Ex. 488nm, Em. 500-540 nm); RCAI (Ex. 543nm, Em. 560-610 nm); TO-PRO[®]-3 (Ex. 563nm, Em. 650-700 nm).

3.3.5 Telomerase activity assay using capillary electrophoresis

A549 cells were harvested, counted 24h and 72h after transfection. 10⁶ cells were pelleted and washed with PBS. The cell pellets were either stored at -80°C or immediately resuspended in 200 μ l ice-cold 3-[(3-cholamidopropyl) dimethyl-ammonio]-1-propanesulfonate (CHAPS)

lysis buffer and incubated on ice for 30min. After the incubation, lysates were centrifuged at 12 000×g for 20 min at 4°C and supernatants were aliquoted, snap-frozen and stored at - 80°C. Telomerase activity was measured using a modified protocol of the TRAP_{EZE}[®] Telomerase Detection Kit (Chemicon International, Hampshire,UK). Detailed process is described in *Chapter 2: Part 1: Materials and methods: Telomerase activity assay using capillary electrophoresis*.

3.3.6 Statistical analysis

The Student's t-test was used to determine statistical differences between pairs of groups; $p < 0.05$ (two-sided) was considered as statistically significant. Data were analyzed using Graphpad Prism version 4.0 (GraphPad Software Incorp., San Diego, CA).

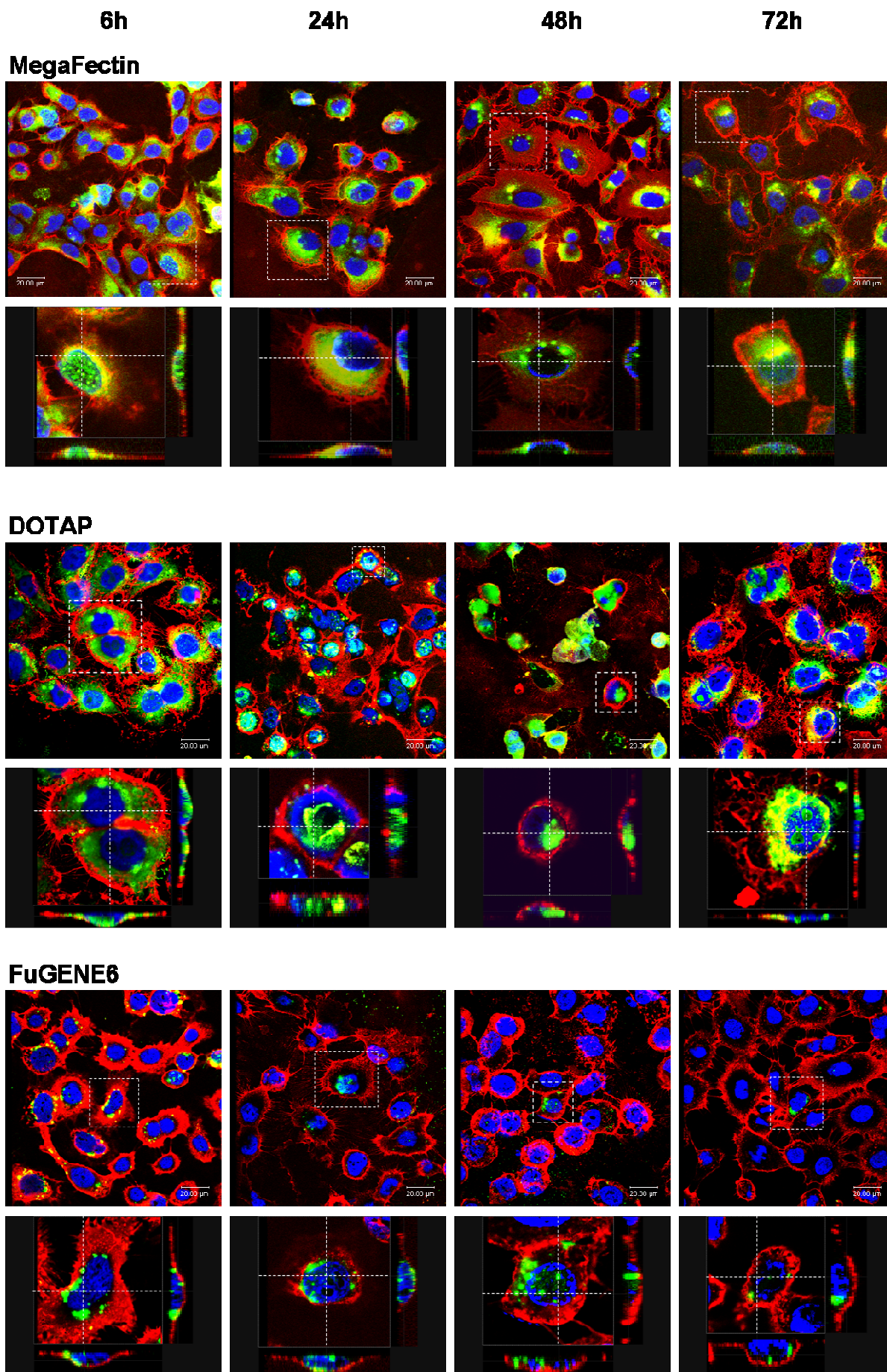
3.4 Results

3.4.1 Evaluation of transfection efficiency by confocal laser scanning microscopy

FAM-OMR was used to evaluate the uptake efficiency in A549 cells transfected with 5 different transfection reagents. CLSM images were taken 6h, 24h, 48h and 72h after transfection. DOTAP and MegaFectin 60 showed much higher transfection efficiencies than the other three reagents. FAM-OMR was present mainly in the cytoplasm of DOTAP transfected cells (Fig.2-DOTAP) and 6h after transfection the transfection efficiency reached about 74% (Table.2). The nuclear staining signal was found in about 25% of cells and the fluorescent signal increased to more than 50% 24h after transfection. The uptake efficiency remained stable and FAM-OMR was still present in about 70% of the cells 48h and 72h after transfection (Table.2).

CLSM images showed that about 68% of the cells contained the FAM-OMR 6h after transfection with MegaFectin (Table. 2). FAM-OMR was mainly localized in the perinuclear area of the cytoplasm and some nuclei exhibited a spotted staining (Fig.2-MegaFectin). The transfection efficiency was still around 60% at 72h and did not change significantly (Table. 2). Seventy-two hours after transfection high amount of FAM-OMR were still localized in the cytoplasm but no nuclear localization was obvious.

Transfection with FuGENE6 led to a poor uptake of FAM-OMR. Transfection efficiency was about 44% at 6h after transfection (Fig.2-FuGENE6). The transfection efficiency dramatically reduced at the following time points and reached only 12% at 72h after transfection (Table.2). The FAM-OMR was mainly found in the cytoplasm, a nuclear signal was only observed in very few cells.



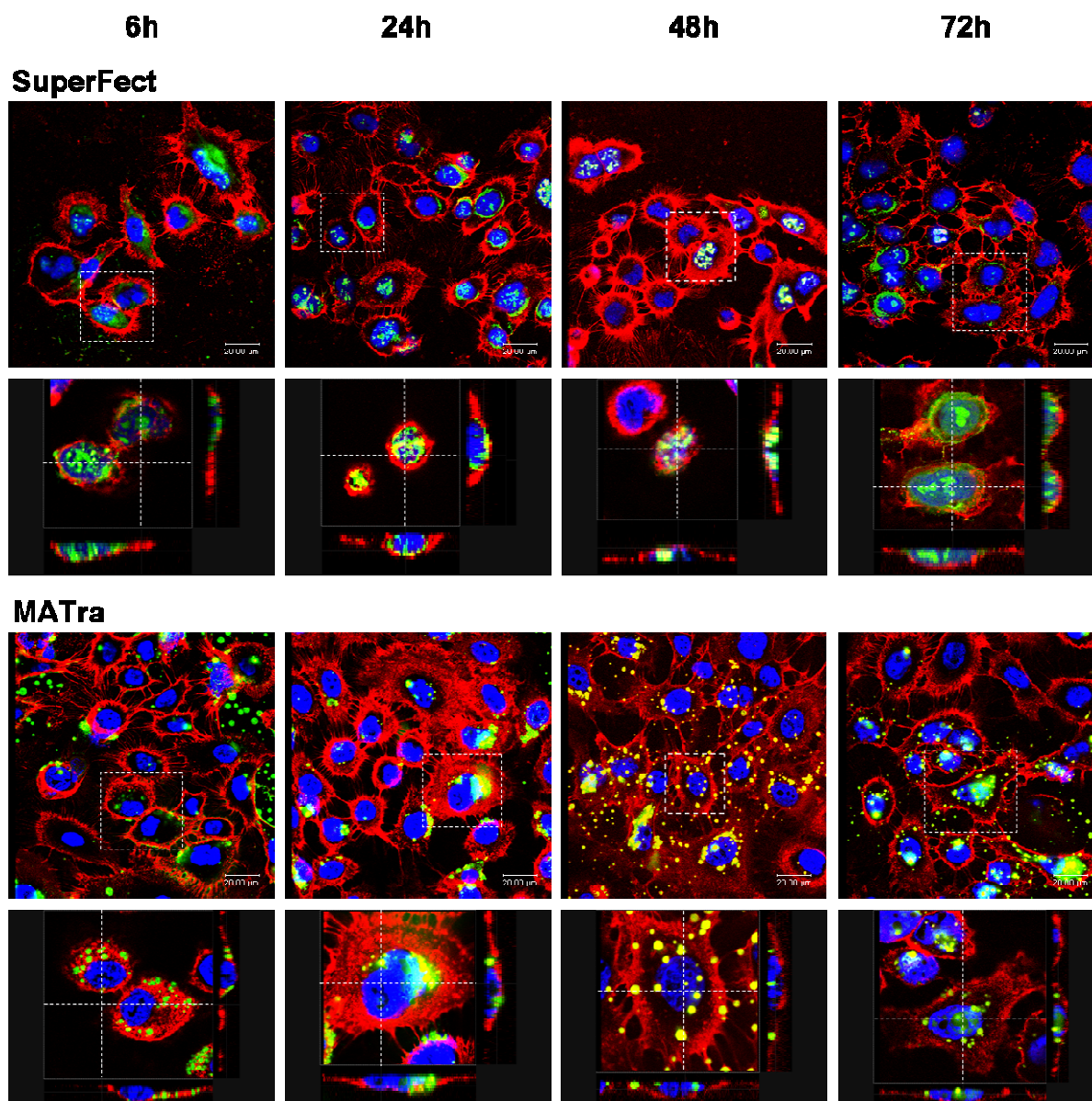


Fig. 2: Uptake of FAM-labeled OMR in A549 cells visualized by CLSM

A549 cells were transfected with 4 μ M FAM-OMR using MegaFectin 60, DOTAP, FuGENE6, Superfect and MATra-A. CLSM images were taken 6h, 24h, 48h and 72h after transfection. FAM-OMR has a fluorescence signal shown in green. Cells were counterstained with RCAI (membrane, red) and TOPRO-3 (nucleus, blue). The second row of each treatment shows the transverse (XZ axis) and vertical (YZ axis) cross sections of a single zoomed cell from corresponding upper image for each time point. Images were analyzed using a 63 \times objective. Scale bars represent 20 μ m.

SuperFect displayed lower transfection efficiency than DOTAP and MegaFectin. However, these differences did not reach statistical significance due to high variabilities. The FAM-OMR was present in only 59% of the cells 6h after transfection (Table.2). The majority of the FAM-OMR was localized in the cytoplasm but there were more cells showing fluorescent signal in the nuclei compared to the other transfections. The transfection efficiency remained

stable after 6h, but the nuclear localization increased with time and reached a plateau at 72h (Fig.2-SuperFect).

MATra uses magnetic nanoparticles delivering oligonucleotides into target cells by magnetic force. MATra was able to mediate delivery of FAM-OMR into A549 cells and resulted in a transfection efficiency of 53% 6h after transfection (Table.2). But the CLSM images also revealed that only low amounts of the OMR were present in the cytoplasm (Fig.2-MATra).The transfection efficiency of MATra increased slightly after 6h, and then stayed around 60% until 72h after transfection.

Table 2: Transfection efficiency of five transfection reagents

The efficiency is given as % positive cells of total number of cells (mean value \pm SD). Differences are compared to FuGENE6. * $p < 0.05$; ** $p < 0.01$.

Time after transfection (h) \ Transfection reagent	DOTAP	MegaFectin	SuperFect	MATra-A	FuGENE 6
6	74 \pm 18	68 \pm 13	59 \pm 12	53 \pm 17	44 \pm 20
24	76 \pm 15**	66 \pm 17*	51 \pm 19	60 \pm 17*	26 \pm 8
48	69 \pm 20**	65 \pm 20*	54 \pm 20*	56 \pm 14**	14 \pm 1
72	71 \pm 15**	60 \pm 29*	52 \pm 9 **	60 \pm 19**	12 \pm 2

3.4.2 Evaluation of telomerase inhibition by capillary electrophoresis

Transfection of mismatch-OMR using various transfection reagents did not demonstrate telomerase inhibition at all tested time points. As shown in Fig. 3, transfection of OMR with five different reagents exhibited different inhibitory effects. Twenty-four hours after transfection with DOTAP, MegaFectin and SuperFect an efficient and similar telomerase inhibition can be noted (at least 75%). Transfection with MATra-A and FuGENE6 resulted in weaker telomerase inhibition which was about 50% for MATra-A and 36% for FuGENE6 ($p < 0.05$ vs. DOTAP). Forty-eight hours after transfection, DOTAP and MegaFectin showed effective telomerase inhibition as after 24h. Cells transfected with SuperFect restored some telomerase activity. Compared to DOTAP, a weaker inhibition was observed for SuperFect, MATra-A and FuGENE6. Seventy-two hours after transfection, only DOTAP remained inhibitory and in the cells only about 16% of telomerase activity was left. The cells treated with the other transfection reagents demonstrated increased telomerase activity which was significantly different compared to DOTAP (Fig. 3). Transfection with MegaFectin resulted in 71% inhibition of telomerase 72h after transfection. Transfection of OMR with SuperFect reduced telomerase activity by 52%. MATra-A reduced telomerase activity 24h after

transfection by about 49% but this inhibition was not maintained up to 72h. In contrast, after transfection with FuGENE6 almost no telomerase inhibition could be observed.

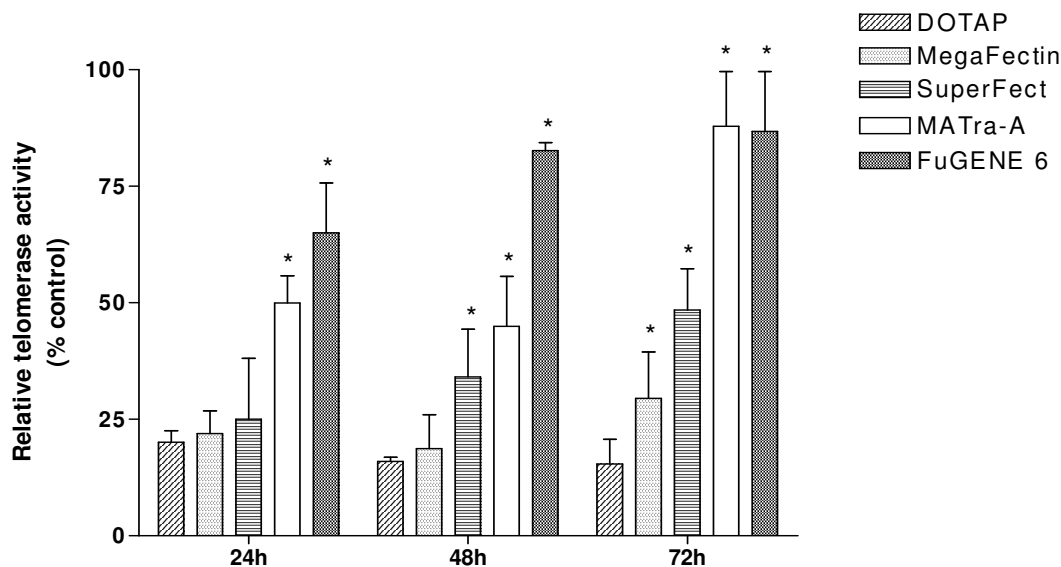


Fig. 3: Inhibition of the telomerase activity in A549 cells 24, 48 and 72h after transfection with 4µM OMR using DOTAP, MegaFectin 60, SuperFect, MATra-A and FuGENE6

Telomerase activity was determined by a modified TRAP-CE assay. Telomerase activity of cells treated with transfection reagents alone was set to 100%. Data represent the mean +SD from at least three independent experiments. * $p < 0.05$ compared to DOTAP at corresponding time point.

3.5 Discussion

The poor cellular uptake of oligonucleotides limits the application of the telomerase inhibitor OMR [Loke *et al.*, 1989]. We have compared five different transfection reagents to mediate the delivery of OMR to NSCLC A549 cells and monitored the cellular telomerase activity. Overall the liposomal transfection reagents showed better transfection efficiency of OMR and more effective telomerase inhibition than the other reagents.

It has been reported that 4µM OMR in combination with transfection reagents did not cause greater cytotoxicity compared to the transfection reagent alone [Beisner *et al.*, 2009]. FuGENE 6 had a significantly higher cytotoxicity compared to the other four transfection reagents; the cell viability was only about 50% 72h after transfection while the cells treated with other transfection reagents had about 70% to 80% of cell viability [Beisner *et al.*, 2009]. The liposomal transfection reagents DOTAP and MegaFectin demonstrated not only low cytotoxicity but also a relatively high binding efficiency with OMR.

The lipoplex size is a major factor which influences the lipofection efficiency *in vitro* [Ross *et al.*, 1999]. It has been shown that the cationic lipids DOTAP and MegaFectin have particle

sizes in the range of 600 and 800nm while those of SuperFect, FuGENE 6 and MATra-A are about 200nm. After combined with OMR, the particle size of FuGENE6 was almost doubled; the size of MegaFectin and DOTAP increased and reached more than 1 μ M [Beisner *et al.*, 2009]. OMR and DOTAP formed a complex of 1400nm which was found to be most efficient for uptake. The liposomal transfection reagents achieved better transfection efficiency than smaller complexes in the range from 10 to 300nm. Suspensions of the liposomal transfection reagents DOTAP and MegaFectin showed a very broad size distribution. After adding OMR, the size distribution changed significantly for DOTAP and FuGENE 6 but remained the same for MegaFectin [Beisner *et al.*, 2009]. All five transfection reagents had highly positive surface charges. After adding the negatively charged OMR, the zeta potential of the reagents decreased. This indicates an interaction of the OMR with the positively charged particle surface, especially with DOTAP whose zeta potential value was reduced below zero [Beisner *et al.*, 2009]. Because MegaFectin is a special DOTAP/cholesterol lipid formulation it was expected that MegaFectin could be more efficient than DOTAP alone. However, DOTAP showed better transfection efficiency, lower cytotoxicity and stronger telomerase inhibition and therefore represent the best compound among the tested transfection reagents for OMR.

SuperFect is an actived-dendrimer-based reagent which has potential cellular delivery of antisense oligonucleotides [Hollins *et al.*, 2004; Sato *et al.*, 2001; Bielinska *et al.*, 1996]. It has been also reported to be used in gene delivery *in vitro* [Tang *et al.*, 1996]. SuperFect had similar cytotoxicity as DOTAP, but the transfection efficiency and telomerase inhibition was lower than DOTAP.

FuGENE 6 has been used because of its low toxicity and high level of transfection in many different cell lines [Jacobsen *et al.*, 2004]. It can enhance the cellular uptake of oligonucleotides in cell cultures and the antisense phosphorothioate oligonucleotides complex with FuGENE 6 induced telomerase inhibition in HeLa cells [Tao *et al.*, 1999; Tamura *et al.*, 2000]. However, the transfection efficiency of FuGENE 6 was dramatically reduced 72h after transfection compared to other transfection reagents. In our experiments it also exhibited relatively high toxicity and low telomerase inhibition. This is probably due to the low binding efficiency between OMR and FuGENE 6. FuGENE 6 can not be regarded as the best choice for OMR delivery into A549 cells.

MATra-A is a magnetofection-based transfection technique which uses magnetic nanoparticles as delivery system. It has been described as a highly efficient tool for antisense oligonucleotide delivery *in vitro* and *in vivo* [Krötz *et al.*, 2003; Gersting *et al.*, 2004]. In our experiments we also observed low cytotoxicity of MATra. But the transfection efficiency was

low and it resulted in 51% inhibition of telomerase 24h after transfection, but 72h after transfection the telomerase inhibition was reduced to only 10%. The relatively weak inhibitory effect might be due to the strong interaction of OMR with the magnetic nanoparticles which probably prevents an effective action of OMR on telomerase inhibition [Beisner *et al.*, 2009].

Inhibition of telomerase inducing telomere shortening is a novel target in anticancer therapy. Because sufficient telomere shortening needs a lag period, a long-term treatment might be necessary and a sustained telomerase inhibition is required. The half life of telomerase is about 24h [Holt *et al.*, 1996]. For a long-term application cells have to be transfected every 3 or 4 days, so the telomerase inhibition should persist for more than 72h. From our data, only liposomal delivery of OMR can mediate efficient telomerase inhibition for 72h.

Imetelstat (GRN163L), a lipid modified 13-mer oligonucleotide that binds directly with high affinity to hTR resulting in direct, competitive inhibition of telomerase enzymatic activity, has entered phase I/II clinical trials. So far no direct toxicity could be observed in long-term studies. However it has been shown in a mouse model that GRN163L shows no difference in drug accumulation between healthy lung tissues and lung tumors [Dikmen *et al.*, 2005]. This might cause effects on normal cells and could limit its clinical application. More research has to be done to investigate the delivery and effects of OMR in anticancer therapy.

3.6 Conclusion

Our data show that the cationic lipid transfection reagent DOTAP is most suitable for OMR delivery because of its high transfection efficiency, low cytotoxicity and strong telomerase inhibition in human NSCLC cells. Therefore, DOTAP can be used for *in vivo* studies and hopefully also for anticancer therapy in patients with lung cancers.

Chapter 4

Telomerase Inhibition and Telomere Shortening by Nanoparticles Delivery of 2'-O-Methyl-RNA in Human Lung Cancer Cells

Parts of this chapter have been published as an original article in the journal *Lung Cancer*:

Beisner J, Dong M, Taetz S, Nafee N, Griese EU, Schaefer UF, Lehr CM, Klotz U, Mürdter TE.

Nanoparticle mediated delivery of 2'-O-methyl-RNA leads to efficient telomerase inhibition and telomere shortening in human lung cancer cells. *Lung Cancer*. 2010 Jun;68 (3):346-54.

*The results (except 4.4.1) presented in this chapter were obtained by Meng Dong.

4.1 Abstract

Background: Lung cancer is the leading cause of cancer-related mortality. Non-small cell lung cancer (NSCLC) accounts for more than 80% of all lung cancers and carries a very low 5-year survival rate. Telomerase activity is detected in 80% of NSCLC. Inhibition of telomerase in cancer cells is a promising approach for treatment of NSCLC. The antisense oligonucleotide 2'-O-methyl-RNA (OMR) binding to the RNA component of telomerase acts as a selective telomerase inhibitor. We analyzed the biological effects of chitosan-coated poly(lactide-co-glycolide) (PLGA) nanoparticle mediated delivery of telomerase inhibitor OMR in human lung cancer cells.

Methods: Antisense oligonucleotides OMR were complexed with chitosan-coated PLGA nanoparticles to form OMR-nanoparticle-complexes (OMR-nanoplexes) and loaded to human NSCLC cells (A549, Calu-3, NCI-H23 and NCI-H460) and primary lung fibroblasts. For long-term experiments, the A549 cells were treated every 3-4 days with OMR-nanoplexes over 100 days. The cellular uptake of OMR was investigated by FACS analysis and confocal laser scanning microscopy (CLSM). Cytotoxicity of the treatment was measured by the ATP test. Telomerase inhibition was measured by real time PCR based telomeric repeat amplification protocol (Q-TRAP). Telomere length shortening after the long-term treatment was measured by real-time PCR.

Results: Cellular uptake of OMR-nanoparticles was dramatically enhanced compared to the uptake of OMR alone as shown by FACS analysis. The internalization of OMR was further demonstrated by CLSM. OMR-nanoplexes treatment did not exhibit acute cytotoxicity in human lung cancer cells and nearly no influence in primary lung fibroblasts. Human NSCLC A549 cells did not show apoptosis 72h after treated with OMR-nanoplexes. Telomerase activity was continuously reduced by approximately 80% during a long-term experiment. Furthermore, in A549 cells the OMR-nanoplexes resulted in significant telomere shortening of about 50% in A549 cells.

Conclusion: In human lung cancer cells nanoparticle mediated delivery of OMR induced effective telomerase inhibition and telomere shortening. Therefore it represents a great *in vivo* potential for the treatment of lung cancer.

4.2 Introduction

Lung cancer is the leading cause of cancer-related mortality all over the world [Jemal *et al.*, 2007]. Small cell lung cancer and non-small cell lung cancer (NSCLC) are the two main types. NSCLC accounts for approximated 80% of all lung cancer cases. The treatment of NSCLC including surgery at early stages, chemotherapy combined with radiation for some advanced cancers provides minor improvement in survival as the 5-year survival rate is only about 15% [Molina *et al.*, 2008; Non-small Cell Lung Cancer Collaborative Group. 1995]. More efficient approaches are needed to target selectively the cancer cells.

Telomerase has become one of the promising drug targets for anti-cancer therapy. Telomerase is a ribonucleoprotein synthesizing telomeric repeats to the end of telomeres [Morin, 1989] which cap the end of linear eukaryotic chromosomes thus protecting the end of chromosomes from deterioration. Human telomerase contains two major components, the human telomerase RNA (hTR) which serves as a template for the addition of telomeric repeats to the telomere DNA [Nakamura *et al.*, 1997] and the human telomerase reverse transcriptase (hTERT) which works as the catalytic protein subunit [Feng *et al.*, 1995; Meyerson *et al.*, 1997]. Telomerase activity has been detected in human cancer cells as well as in germ line cells and stem cells, but not in most somatic cells [Kim *et al.*, 1994]. Telomerase is positively expressed in 80-90% of tumors [Harley, 2008]. It can prevent telomeres from shortening during each cell cycle and leads to immortalization of cancer cells. Telomerase activity has been detected in approximately 80% of NSCLC [Taga *et al.*, 1999; González-Quevedo *et al.*, 2002] and telomerase activity is associated with advanced stages and poor prognosis of NSCLC patients [Albanell *et al.*, 1997; Marchetti *et al.*, 1999]. Targeting telomerase is an attractive approach in NSCLC therapy. Compared to other anti-cancer methods, targeting telomerase is relative universal and specific for cancer cells as normal cells will not be affected [Harley, 2008].

Different strategies to inhibit telomerase have been developed and tested [Shay *et al.*, 2006]. The antisense oligonucleotide 2'-O-methyl-RNA (OMR) with a phosphorothioate backbone has been reported as a potent and sequence-selective telomerase inhibitor [Pitts *et al.*, 1998; Herbert *et al.*, 1999]. It binds to the complementary hTR template which is an ideal target for inhibition oligonucleotides and further influences the synthesis of telomeric repeats [Zimmermann *et al.*, 2007]. Previously we have shown that OMR can inhibit *in vitro* the telomerase activity in NSCLC A549 cells [Beisner *et al.*, 2009]. However, the poor cellular uptake of oligonucleotides limits the application of OMR [Loke *et al.*, 1989]. Biodegradable nanoparticles have been shown to be an efficient drug delivery system [Kumar *et al.*, 2004;

Nafee *et al.*, 2007]. In the present study, we developed positively charged chitosan-coated PLGA nanoparticles for the delivery of OMR and analyzed in human lung cancer cells the biological effects of nanoparticle mediated delivery of OMR.

4.3 Material and methods

4.3.1 Cell culture

Human NSCLC cell line A549 were obtained from DSMZ (Braunschweig, Germany), Calu-3 cells were from the American Type Culture Collection (ATCC, Rockville, MD, USA), NCI-H23 (ATCC Number: CRL-5800TM) cells were ordered from LGC Standards (Wesel, Germany), NCI-H460 (ATCC Number: HTB-177TM) cells were purchased from LGC Standards (Wesel, Germany). A549, NCI-H23 (H23) and NCI-H460 (H460) cells were cultivated in RPMI 1640 medium (Invitrogen, Carlsbad, CA, USA) supplemented with 10% heat inactivated fetal calf serum (FCS), 2mM L-glutamine, 50U/ml penicillin and 50µg/ml streptomycin. Calu-3 cells were cultivated in Minimum Essential Medium (MEM) with Earl's Salts and L-glutamine (Invitrogen, Carlsbad, CA, USA) supplemented with 10% heat inactivated FCS, 1% MEM non-essential amino acids (NEA, BioChromag, Berlin, Germany), 1mM sodium pyruvate, 50U/ml penicillin and 50µg/ml streptomycin. Cell viability was assessed by the trypan blue exclusion test.

4.3.2 Oligonucleotides

The telomerase inhibitor used in this study is an antisense 2'-O-methyl-RNA(OMR) with a phosphorothioate (ps) backbone 5'-2'-O-methyl [C(ps)A(ps)GUUAGGGUU(ps)A(ps)G]-3'. The mismatch OMR is 5'-2'-O-methyl [C(ps)A(ps)GUUAGAAUU(ps)A(ps)G]-3'. The fluorescence-labeled OMR (FAM-OMR) is 5'-FAM-2'-O-methyl [C(ps)A(ps)GUUAGGGUU(ps)A(ps)G]-3' and the digoxigenin-labeled OMR (Digo-OMR) is 5'-2'-O-methyl [C(ps)A(ps)GUUAGGGUU(ps)A(ps)G]-digoxigenin-3'. All the oligonucleotides were synthesized by Biomers (Ulm, Germany). Nuclease-free water (QIAGEN GmbH, Hilden, Germany) was used to dissolve the oligonucleotides and the oligonucleotides were aliquoted and stored at -20°C for further processing. To ensure stability and biological activity of the oligonucleotides, small aliquots were tested in the cell-free TRAP assay prior to the use in the cell culture experiments.

4.3.3 Chitosan-coated PLGA nanoparticles preparation and characterization

Chitosan-coated PLGA nanoparticles were prepared by an emulsion-diffusion-evaporation method described previously [Kumar *et al.*, 2004; Nafee *et al.* 2007]. In brief, 5ml of PLGA was dissolved in ethyl acetate (20mg/ml) and added dropwise under stirring to 5ml of an aqueous solution containing 2.5% (w/v) polyvinyl alcohol (PVA) and 0.3% (w/v) cationic polymer chitosan. The emulsion was stirred for 1h at room temperature and homogenized using an UltraTurrax T25 (Janke & Kunkel GmbH & Co-KG, Staufen, Germany) at 13,500 rpm for 10min. The homogenized emulsion was diluted with MilliQ-water to 50ml under constant stirring. Stirring was continued over night at room temperature to form the nanoparticle suspension which contained 3mg/ml of chitosan.

Nanoparticles were characterized directly after preparation in respect to size, polydispersity index (PDI) and surface charge. Photon correlation spectroscopy was used to determine average size and PDI. Surface charge was assessed as zeta potential in a ZetaSizer Nano ZS (Malvern Instruments Ltd., Worcestershire, UK). Samples were diluted in MilliQ-water for analyses. All measurements were performed in triplicates. Nanoparticle concentration was determined gravimetrically after lyophilization.

4.3.4 Preparation of oligonucleotide-nanoparticle-complexes (nanoplexes) transfection

The oligonucleotide was mixed with the nanoparticle solution in cell culture medium and vortexed thoroughly. The mixture was incubated for 15min at 37°C in a water bath to form oligonucleotide-nanoparticle-complexes (nanoplexes). The content ratio of nanoplexes is 1:100 ($\text{weight}_{\text{oligonucleotide}} / \text{weight}_{\text{nanoparticles}}$). Oligonucleotides were always used at a final concentration of 4 μ M in the nanoplexes. Six hours after treatment the nanoplexes were replaced by cell culture medium and cells were further cultured. Cells were loaded with OMR-nanoplexes, OMR or mismatch-OMR-nanoplexes; FAM-OMR or FAM-OMR-nanoplexes separately. Nanoparticles were labeled with the fluorescent dye DiI (1,1'-Diocadecyl-3,3,3',3'-tetramethylindocarbocyanine perchlorate) from Sigma-Aldrich Chemie GmbH, Taufkirchen, Germany. The DiI-labeled nanoparticles (DiI-NP) were also loaded with FAM-OMR to form nanoplexes. In short-term experiments, the cells were cultured for 6h, 24h, 48h or 72h before analyzing. In long-term experiments over 100 days, subsequently cells were seeded in 6-well plates at a density of 200,000 cells/well and treated every 3-4 days with OMR-nanoplexes. One day prior to transfection cells were trypsinized, collected and further seeded in 6-well plate at the same density 200,000 cells/well. The remaining cells were

collected and used for determination of telomerase activity and telomere length. Population doubling (PD) was calculated using the formula $PD = \lg(n_{\text{cells harvested}} / n_{\text{cells initially seeded}}) / \lg 2$.

4.3.5 Fluorescence-activated cell sorting (FACS) analysis

For uptake analysis, after treatment cells were collected and washed twice with PBS and resuspended in 500 μ l PBS. For apoptosis analysis, cells were incubated with 5 μ l Fluorescein-conjugated Annexin V (Annexin V-FITC) and 10 μ l of Propidium Iodide (PI) in 100 μ l binding buffer (FITC Annexin V, BD Pharmingen, Sandiego, CA) at room temperature for 15min in the dark and analyzed by FACScan fluorescence-activated cell sorter (Becton-Dickinson, Heidelberg, Germany). A minimum of 10,000 individual cells was analyzed per sample. The right population was gated from the dot plots, the fluorescence threshold was defined in reference to non-treated cells. The percentage of cell-associated fluorescence was analyzed by CellQuest software (Beckton-Dickinson, Heidelberg, Germany).

4.3.6 Confocal laser scanning microscopy

The cells were seeded in Lab-Tek[®] chamber slides (Nalge Nunc International, Naperville, USA) at a density of 65,000 cells per well one day before the treatment. Cells were loaded with either FAM-OMR alone or FAM-OMR-nanoplexes 24h after seeding. Then cells were evaluated by CLSM 6h, 24h and 72h after treatment, respectively. After two times washing with PBS, cells were incubated with 25 μ g/ml rhodamine-labeled ricinus communis agglutinin I (RCA I, Vector Laboratories, Burlingame, CA, USA) for 15min at 37 $^{\circ}$ C which enables detection of cell membranes by binding to oligosaccharides ending in galactose. Cells were washed twice with PBS and fixed with 100% ethanol at -20 $^{\circ}$ C for 10min. Cell nuclei were stained with 1 μ M TO-PRO[®]-3 iodide (Molecular Probes Invitrogen, Eugene, OR, USA) for 10min at room temperature in the dark. After two washing steps with PBS, the chamber and gasket were removed and slides were mounted with mounting medium (Vectashield[®] Mounting Medium, Vector Laboratories, Burlingame, CA) for analyzing by CLSM. CLSM was performed with a Leica LCS instrument (Leica Lasertechnik) based on a Leica DM IRBE microscope equipped with argon and helium/neon lasers. The emission (Em.) and excitation (Ex.) wavelengths of the dyes were as follows: FAM (Ex. 488nm, Em. 500-540 nm); RCA I and DiI (Ex. 543nm, Em. 560-610 nm); TO-PRO[®]-3 (Ex. 563nm, Em. 650-700 nm).

4.3.7 Quantification of oligonucleotides uptake

A549 cells were seeded in 24-well plates at a density of 50,000 cells / well. Cells were treated with FAM-OMR or FAM-OMR-nanoplexes. Six hours after treatment, the transfection

mixtures were collected and replaced by cell culture medium. Twenty-four hours after treatment, the cell culture medium was collected and the cells were trypsinized and kept as cell lysates. The original transfection mixes before loaded on cells, the transfection mixes at 6h, the cell culture medium at 24h and the cell lysates were serially diluted. 300µl per well of the dilution were loaded in a 96-well plate. The level of presented FAM was measured by a microtiter plate reader (Victor Multilabel Counter 1420, Wallac-PerkinElmer, Waltham, MA, USA). The FAM level of transfection mixes at 0h were set as 100%, the fluorescence of all the other groups were normalized to the results of transfection mixes at 0h. All measurements were performed in triplicates.

4.3.8 Cytotoxicity assay

A standardized ATP-based tumor chemosensitivity assay (ATP-TCA) was applied to determine cell viability (DCS Innovative Diagnostik Systeme, Hamburg, Germany). Cells were seeded at a density of 10^4 cells/well in 96-well plates and 24h later cells were treated with nanoplexes as described in 4.3.4. Seventy-two hours after transfection, cells were lysed by addition of 50µl/well of ATP cell extraction reagent. After 30min shaking at lowest speed, 50µl of the lysates from each well were transferred to a new well of a white 96 MicroWell™ plate (Nalgene Nunc International, Naperville, IL, USA) followed by addition of luciferin-luciferase reagent. Luminescence corresponding to the level of ATP present was measured by a microtiter plate reader (Victor Multilabel Counter 1420, Wallac-PerkinElmer, Waltham, MA, USA). Luminescence measurements are directly related to ATP levels and allow the measurement of the percentage of inhibition by reference to untreated control wells included in each plate. The absorbance of untreated cells was set as 100%. All measurements were performed in quadruplicates and each experiment was repeated at least three times. Cell death was also determined by Annexin V-FITC staining and analyzed by FACS as described in FACS analysis section.

4.3.9 Telomerase activity assay using real-time quantitative PCR

Cultured cells were harvested, counted and 10^6 cells were pelleted and washed with PBS. The cell pellets were either stored at -80°C or immediately resuspended in 200µl ice-cold 3-[(3-cholamidopropyl)dimethyl-ammonio]-1-propanesulfonate (CHAPS) lysis buffer and incubated on ice for 30min. The lysates were centrifuged at $12,000\times g$ for 20min at 4°C and the supernatants were aliquoted, snap-frozen and stored at -80°C .

Telomerase activity was measured using a modified real-time quantitative PCR based telomeric repeat amplification protocol (Q-TRAP) assay described previously [Herbert *et al.*,

2006]. We modified this method to reduce costs and to increase throughput using a 384-well reaction plate with a final reaction volume of 12 μ l. The detailed processes are described in *Chapter 2: Part 1: Materials and methods: Telomerase activity assay using real-time quantitative PCR*.

4.3.10 Telomere measurement by real-time quantitative PCR

Genomic DNA was isolated from cells using the QIAamp[®] DNA Mini Kit (QIAGEN, Hilden, Germany). Cultured cells were harvested, counted and washed with PBS. Up to 5 \times 10⁶ cells were resuspended in 200 μ l PBS and added into a 1.5ml microcentrifuge tube which contained 20 μ l Proteinase K and 40 μ l RNase A (10mg/ml). After 200 μ l Buffer AL was added, the sample was incubated at 56 $^{\circ}$ C for 10min. The following steps were done according to the QIAamp[®] DNA Mini Kit protocol. The final DNA was eluted in Buffer AE, stored at -20 $^{\circ}$ C. DNA was quantified using a NanoDrop spectrophotometer (PEQLAB, Erlangen, Germany). The telomere measurement was performed by quantitative real-time PCR described previously [Cawthon, 2002]. The details of the process are described in *Chapter 2: Part 2: Materials and methods: Telomere measurement by real-time quantitative PCR*.

4.3.11 Statistical analysis

Different groups were compared by Wilcoxon signed rank test or Wilcoxon matched pairs test. Results were considered statistically significant if $p < 0.05$. All data were analyzed by Graphpad Prism version 4.0 (GraphPad Software Incorp., San Diego, CA).

4.4 Results

4.4.1 Characterization of chitosan-PLGA nanoparticles as a delivery system

The diameter of nanoparticles was in the range of 150–170nm with a mean size of 160nm (\pm 5nm). The chitosan-coated PLGA nanoparticle suspension contained 3mg/ml of chitosan. Nanoparticles were characterized by a positive surface charge with a zeta potential of 37mV (\pm 5.9mV) and a polydispersity index (PdI) of 0.164 (\pm 0.054). The concentration of nanoparticles in the aqueous suspension was 4.6mg/ml (\pm 0.51mg/ml). The particles were spherical with a monomodal size distribution. The sizes of OMR-nanoplexes were comparable to those of the pure nanoparticle preparations. The surface of the nanoplexes decreased slightly with the addition of OMR indicating binding between oligonucleotide and cationic nanoparticles through electrostatic attraction [Nafee, 2008].

4.4.2 Inhibition of telomerase activity by 2'-O-methyl-RNA-nanoparticle complexes

Before the treatment the telomerase-inhibitory potential of OMR was first evaluated with the cell-free TRAP assay. Dilutions of OMR (10^{-12} to 10^{-5} M), mismatch-OMR (10^{-12} to 10^{-5} M) or nanoparticles (10^{-8} to 10^{-1} μ g/ μ l) were added to 0.1 μ g of telomerase-positive human lung cancer A549 lysates and the relative telomerase activity was measured.

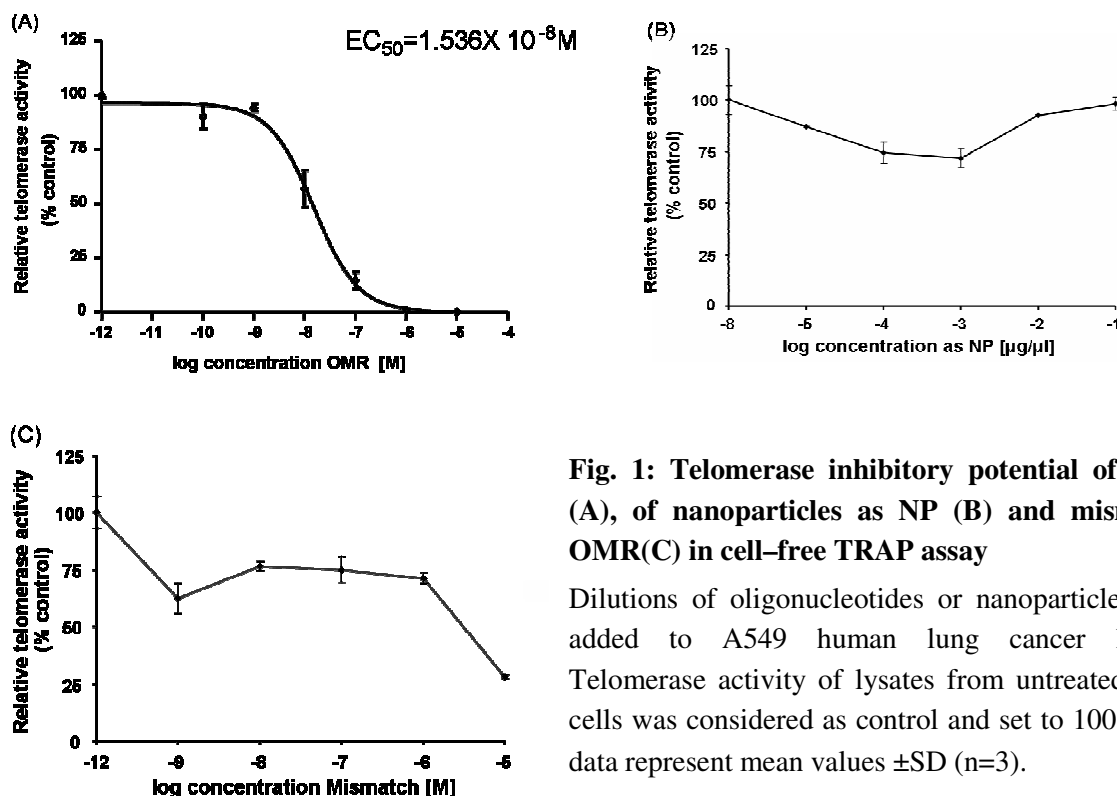


Fig. 1: Telomerase inhibitory potential of OMR (A), of nanoparticles as NP (B) and mismatch-OMR(C) in cell-free TRAP assay

Dilutions of oligonucleotides or nanoparticles were added to A549 human lung cancer lysates. Telomerase activity of lysates from untreated A549 cells was considered as control and set to 100%. The data represent mean values \pm SD (n=3).

As shown in Fig.1, in the cell-free TRAP assay, OMR showed an EC₅₀ value of 1.536×10^{-8} M (Fig.1A). Mismatch-OMR (2 mismatched bases) exhibited a slight inhibition (~25% to 38%) from 10^{-12} to 10^{-6} M; more than 70% inhibition was observed with 10^{-5} M (Fig.1C). Nanoparticles alone did not interfere with TRAP assay at all tested concentrations (Fig.1B).

4.4.3 Nanoparticle mediated uptake of 2'-O-methyl-RNA into human lung cancer cells

As shown in Fig. 2, uptake of FAM-OMR was strongly enhanced by nanoparticles mediated delivery. A549 and H23 cells treated with FAM-nanoplexes revealed a nearly complete shift in the fluorescence profile compared to the other treatments. Although Calu-3 cells exhibited less shift in the fluorescence profile, still more than 90% of the treated cells showed higher fluorescence intensities than the control population indicating an efficient delivery. FAM-OMR without nanoparticles delivery had only less than 5% uptake efficiency. Treatment with nanoparticles alone also did not have an obvious effect on the cell population. All three NSCLC cells lines illustrated similar results.

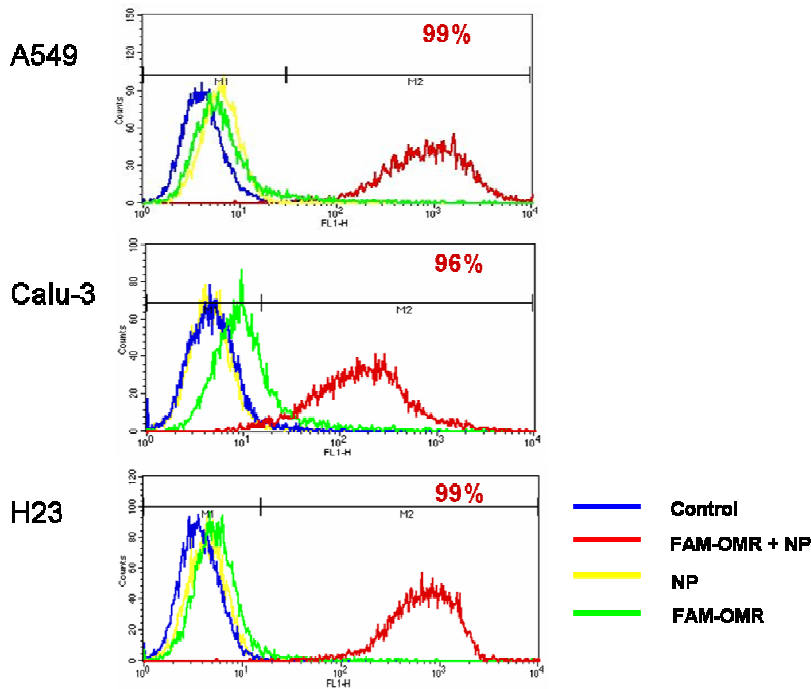
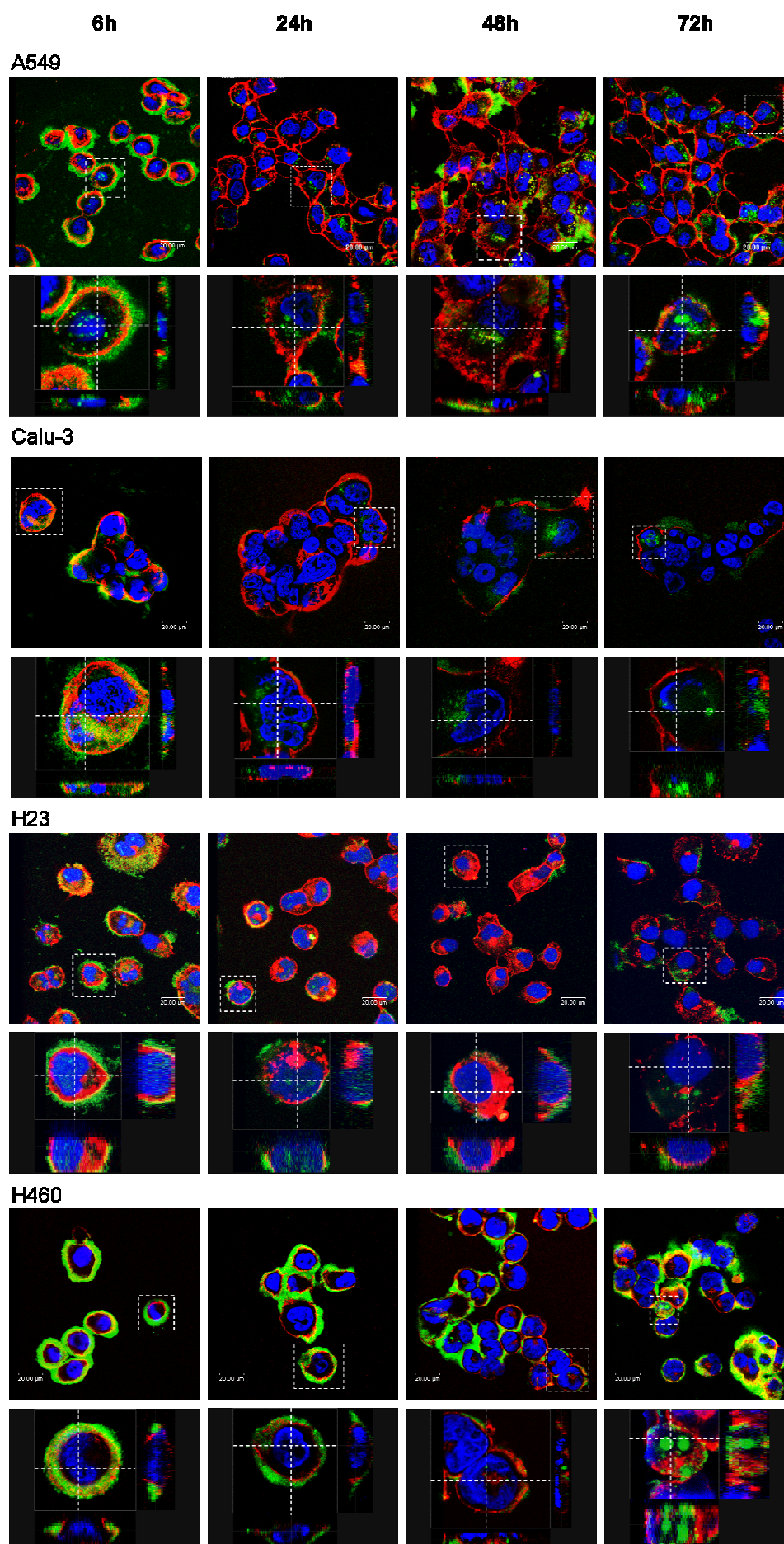


Fig. 2: Uptake of FAM-labeled OMR –nanoplexes by human lung cancer cells

Human A549, Calu-3 and H23 cells were treated with FAM-labeled OMR-nanoplexes (FAM-OMR+NP), nanoparticles (NP) or FAM-labeled OMR (FAM-OMR). The corresponding non-treated cells were used as control. Cells were analyzed by FACS 24h after treatment and the proportion of FAM positive cells was expressed as the percentage of the total population. The percentage of positive cells is indicated in each histogram.

The biological activity of OMR depends on its intracellular distribution within the cells. Therefore the intracellular localization of FAM-OMR was determined by CLSM. As shown in Fig. 3A, 6h after treated with FAM-OMR-nanoplexes, FAM-OMR was mainly accumulated in the membrane of all the tested cells (A549, Calu-3, H23 and H460). Calu-3 cells had less accumulation compared to the other cells. In some A549 and H23 cells, a clear nuclear localization of the FAM-OMR was observed. 24h after treatment, most of the FAM-OMR was present inside the cells and it was mainly located in the cytoplasm as small spots in the perinuclear area. More than 70% of A549 cells displayed positive staining for FAM-OMR. H460 cells still had a lot of dye accumulated in the cell membrane. Forty-eight hours after treatment, more FAM-OMR was delivered inside the cytoplasm of the cells. Calu-3 cells illustrated different cell morphology and less FAM-OMR uptake than the other three cell lines. After 72h following transfection, approximately 80% of A549 cells were stained with a spotted distribution within the cytoplasm but not within the nucleus. H23 cells exhibited similar results as A549. About 55% of H460 cells showed a positive fluorescent staining which was slightly lower than the other two cell lines; Calu-3 cells had only a minor fluorescent staining, but the positive Calu-3 cells showed similar distribution for the uptake of FAM-OMR (Fig. 3A).

A



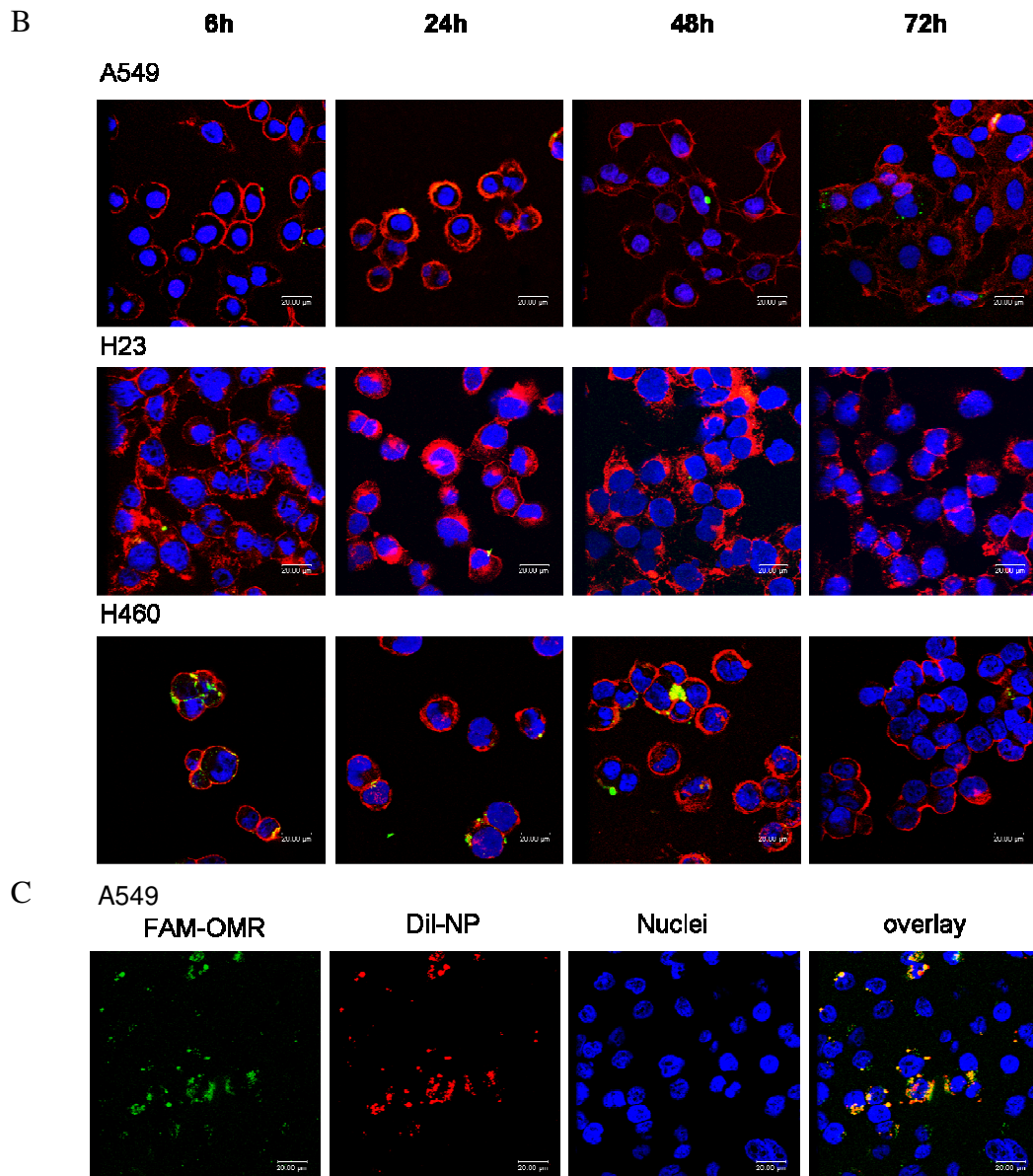


Fig. 3: Intracellular localization of FAM-labeled OMR in A549, Calu-3, H23 and H460 cells visualized by CLSM

Cells were imaged 6h, 24h, 48h and 72h after treatment with FAM-labeled OMR-nanoplexes (A), FAM-labeled OMR (B) or FAM-labeled OMR (FAM-OMR) and DiI-labeled nanoparticles (DiI-NP) formed nanoplexes (C). FAM-OMR had a green fluorescence signal. Cellular nuclei were stained with TOPRO-3 (blue). In (A) and (B), cell membranes were stained with RCA I (red). In (C) DiI-labeled nanoparticles had a red fluorescence signal. In (A) the second row of each cell line shows the transverse (XZ axis) and vertical (YZ axis) cross sections of a single zoomed cell from corresponding upper image for each time point. Images were analyzed by a 63 \times objective. Scale bars represent 20 μ m.

As shown in Fig. 3B, at all time points after treatment with FAM-OMR, only very few cells had positive staining and most of the fluorescent signal was accumulated in cell membrane or cytoplasm. No nuclear uptake of FAM-OMR was observed. DiI-NP and FAM-OMR demonstrated a co-localization in A549 cells 72h after treatment (Fig. 3C). This demonstrated that OMR uptake mediated by nanoparticles occurred as OMR-nanoplexes and kept stable for

72h after treatment. From the overlay image in Fig.3C, the green signal of OMR and the red signal of the nanoparticle are co-localized and resulted in a yellow signal surrounding the cell nuclei.

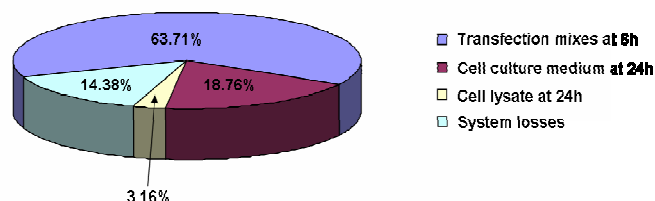


Fig. 4: Quantification of FAM-labeled OMR uptake in A549 cells

A549 cells were treated with FAM-OMR-nanoplexes. The fluorescence level of original transfection mixes at 0h was set to 100%. All the values are shown as percentage of the fluorescence level of transfection mixes at 0h.

We further quantified the nanoparticle mediated delivery of FAM-OMR in A549 cells with a microtiter plate reader. A549 cells were treated with either FAM-OMR alone or FAM-OMR-nanoplexes. As shown in Fig. 4, about 64% of FAM-OMR still remained in the transfection mixes 6h after treatment. After 24h following transfection, the cell culture medium contained about 19% of FAM-OMR indicating that about 19% of original FAM-OMR was released back to the medium from 6h to 24h after the treatment. The cell lysates at 24h demonstrated that the cells took up more than 3% of FAM-OMR during the whole experiment. About 14% of the fluorescent signals were lost during the complete experiment (Fig. 4). Combined with the CLSM results in Fig.3A, this 3% FAM-OMR was mainly taken up by about 70% of A549 cells at 24h following treatment. Compared to nanoparticle mediated delivery of FAM-OMR which had an uptake of about 3%, treatment with FAM-OMR showed only 0.55% uptake at 24h. Nanoparticle mediated delivery enhanced the OMR uptake about 5-fold.

4.4.4 Cytotoxicity of 2'-O-methyl-RNA-nanoparticle-complexes on cells

Seventy-two hours after treatment, an ATP-based luminescence assay was used to determine cell viability in short-term experiments. We tested 4 μ M OMR which was efficient for telomerase inhibition. Treatment with OMR-nanoplexes had only slight toxic effects on all tested cells. A549 cells treated with nanoparticles alone showed about 87% viability compared to untreated control A549 cells (Fig. 5). There was no difference when the antisense OMR was replaced by a mismatch oligonucleotide or nanoparticles ($p > 0.05$). This

suggests that cytotoxic effects were mainly caused by nanoparticles. Similar results were observed with Calu-3 and H23 cells. In contrast, primary lung fibroblasts isolated from different NSCLC were not affected by the different treatments.

In A549 cells apoptosis analysis by Annexin V-FITC staining showed that there was no difference for cell apoptosis among different groups 72h after treatment (Fig. 6). Untreated cells and all treated cells contained less than 10% apoptotic cells. The quantification of cell death by means of FACS analyses (Fig. 6) revealed similar results as the ATP test (Fig. 5).

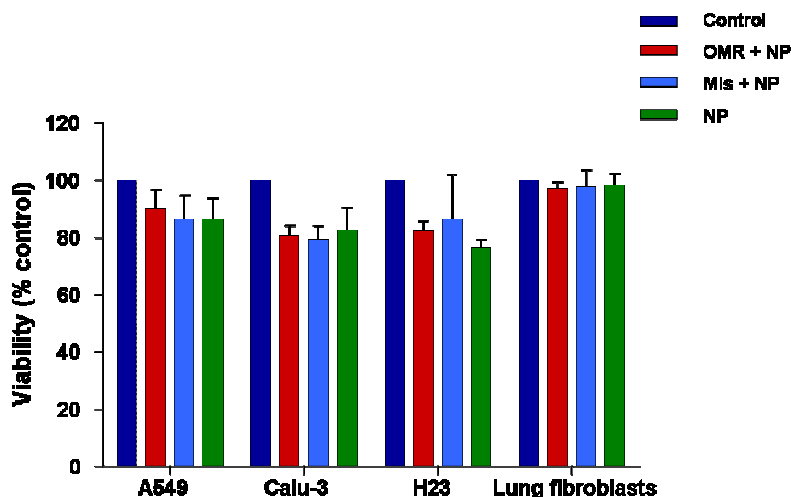


Fig. 5: Effect of OMR-nanoplexes on cell viability of human NSCLC cancer cells (A549, Calu-3 and H23) and human primary lung fibroblasts

Cells were treated with OMR-nanoplexes (OMR+NP), mismatch-nanoplexes (Mis+NP) or nanoparticles alone (NP). Cell viability was determined by the ATP test 72h after treatment. The ATP test results of untreated cells were considered as controls and set to 100%. Data represent the mean +SD from three independent experiments. In case of primary lung fibroblasts, cells were isolated from three different tumors and each one was tested at least twice.

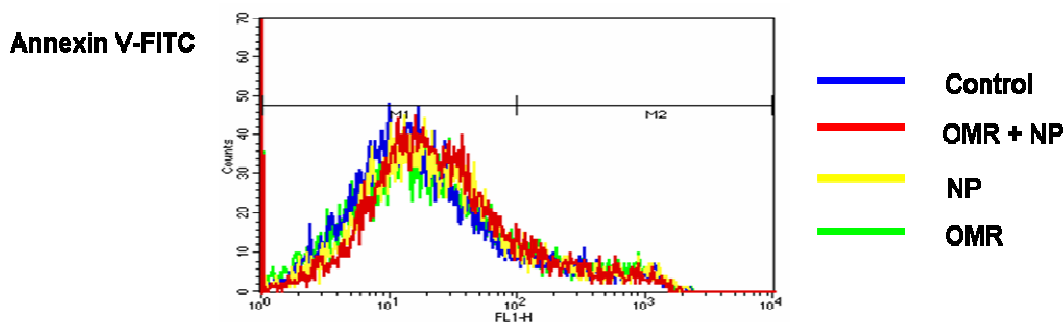


Fig. 6: Cell death indices determined by Annexin V-FITC staining with FACS analysis

A549 cells were treated with OMR-nanoplexes (OMR+NP), nanoparticles alone (NP) or OMR. Untreated A549 cells were used as control. Cells were incubated with Annexin V-FITC and analyzed by FACS 72h after treatment. Cells in M2 phase are undergoing apoptosis.

4.4.5 Telomerase inhibition by 2'-O-methyl-RNA-nanoparticle complexes

In human lung cancer cell line A549 and H23 cells the telomerase inhibitory effect of OMR delivered by chitosan-coated PLGA nanoparticles are illustrated in Fig.7. Cells were treated with complexes of 4 μ M OMR or mismatch-OMR and nanoparticles. Seventy-two hours after treatment cells were analyzed for telomerase activity using the Q-TRAP assay. Both cell lines showed comparable results for telomerase inhibition. The cells treated with OMR-nanoplexes demonstrated significant reduction of telomerase activity compared to cells treated with OMR alone or mismatch-OMR-nanoplexes (Fig.7). In A549 cells, OMR alone did not illustrate telomerase inhibition; nanoparticles delivery of OMR inhibited more than 60% of telomerase activity; mismatch-OMR-nanoplexes exhibited only 30% reduction of telomerase activity and there was a significant difference between these two treatments (Fig.7A). In H23 cells, nanoparticles delivery of OMR inhibited more than 50% of telomerase activity; mismatch-OMR-nanoplexes showed only 20% reduction of telomerase activity and a significant difference between these two treatments was also observed; OMR alone did not have telomerase inhibition (Fig.7B).

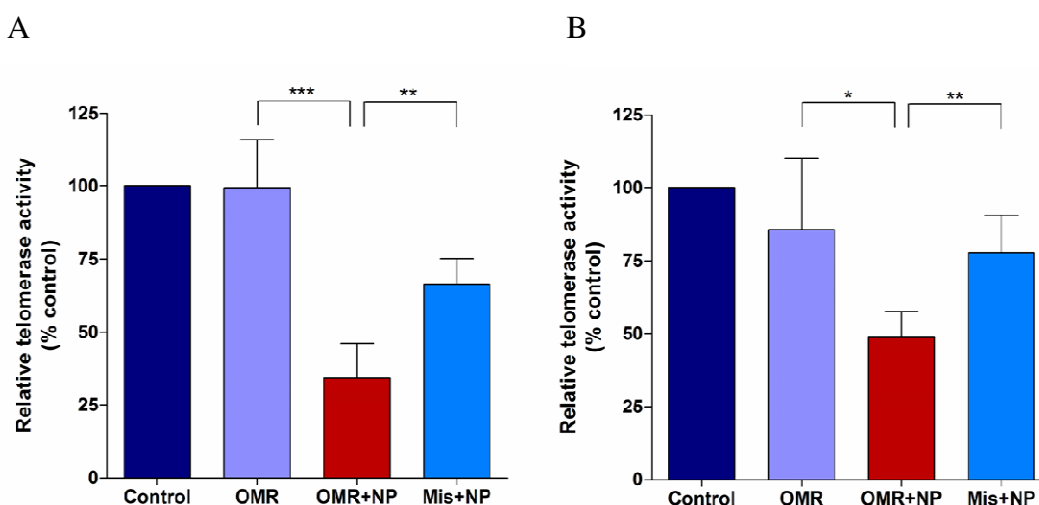


Fig. 7: Inhibition of telomerase activity after nanoparticle delivery of OMR in (A) A549 cells and (B) H23 cells

Cells were treated with OMR, OMR-nanoplexes (OMR+NP) or mismatch-OMR-nanoplexes (Mis+NP) separately. Telomerase activity was determined by Q-TRAP 72h after treatment. Telomerase activity of untreated cells was used as control and set to 100%. Data represent the mean +SD from at least three independent experiments. *t*-test: *** $p < 0.001$; ** $p < 0.01$; * $p < 0.05$.

4.4.6 Long-term treatment with 2'-O-methyl-RNA-nanoparticle complexes resulting in progressive telomere shortening

In order to investigate whether nanoparticle mediated delivery of OMR induces telomere shortening, A549 cells were treated with OMR-nanoplexes at 3 or 4 days intervals for more

than 100 days. Telomerase activity was measured at different time points by the Q-TRAP assay. OMR-nanoplexes induced a significant reduction of telomerase activity at all tested time points.

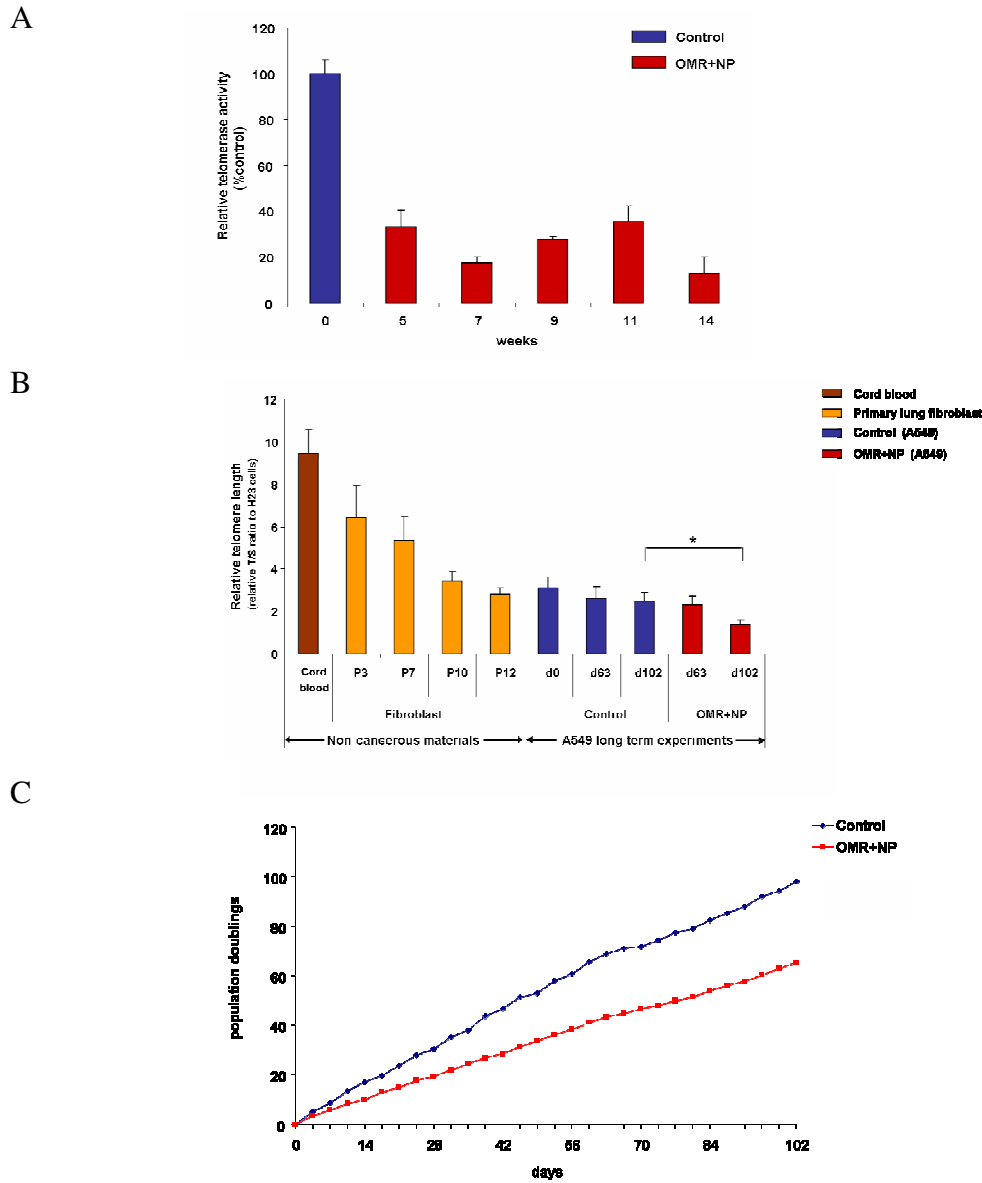


Fig. 8: Long-term effect of nanoparticle delivered OMR (OMR+NP) in A549 cells

Cells were treated every 3 or 4 days with 4 μ M OMR-nanoplexes. (A) Inhibition of telomerase activity determined by the Q-TRAP. Untreated cells at day0 was considered as control and set to 100%. (B) Telomere length shortening of primary lung fibroblast and OMR-nanoplexes treated A549 cells (OMR+NP (A549)). Untreated A549 cells during long-term culture were considered as control. Fibroblasts were analyzed at different passages (P3, P7, P10 and P12), A549 cells were analyzed at different days (d0, d63 and d102). Cord blood from a newborn baby was taken as a positive control (Cord blood). Data represent the mean +SD from 3 measurements. *t*-test: * $p < 0.05$. H23 cells were used as reference DNA sample and its T/S ratio was set as 1. All data were normalized to H23. (C) Population doubling (PD) of A549 cells at different time points during long-term treatment. Cumulative PD was plotted against time. PD was calculated using the formula $PD = \lg(n_{\text{cells harvested}} / n_{\text{cells initially seeded}}) / \lg 2$.

After 5 weeks treatment telomerase activity was reduced to approximately 30% and further reduced to about 20% after 7 weeks. This effect was relatively stable during long-term treatment (Fig.8A).

OMR-nanoplexes treatment for 102 days significantly reduced A549 cell telomere length by about 50% (Fig.8B). The telomere length of untreated control group did not change significantly during long-term culture. Because primary lung fibroblasts have relative low or no detectable telomerase activity, we used fibroblasts as a telomere shortening positive control in our experiment. As given in Fig.8B, telomere length of fibroblasts reduced according to the cell passage, it shortened about 50% at passage 12 compared to passage 3. Fibroblasts also stopped proliferating when they reached passage 12 or 13 indicating that without sufficient telomerase activity, telomere length will be shortened during each cell passage and finally cells stopped growing when the telomere length reached a critical level.

Cell growth of A549 cells was inhibited by OMR treatment leading to a reduced number of population doublings (Fig.8C). After 102 days, the control cells reached about 100 PD but the OMR-nanoplexes treated cells achieved only 65 PD.

In summary we have shown that nanoparticle mediated delivery of OMR induced a significant telomere shortening in A549 cells indicating that continuous inhibition of telomerase will cause a reduction in telomere length.

4.5 Discussion

Telomere shortening can trigger cell senescence. Tumor cells normally have short telomeres, so telomere maintenance is a key event in the immortalization and proliferation of tumor cells [Hahn *et al.*, 1999; Bodnar *et al.*, 1998]. Expression of telomerase stabilizes telomere length of most human tumors. Since telomerase activity is essential for continuous cancer cell proliferation, an efficient inhibition of telomerase offers a promising strategy for cancer therapy. We have demonstrated that in different human NSCLC cell lines chitosan-coated nanoparticles enhanced the delivery of the telomerase inhibitor OMR and telomerase was inhibited. Long-term experiments indicated that such treatment can inhibit continuously telomerase and this resulted in effective telomere shortening. Our data demonstrated that chitosan-coated nanoparticles can be used to mediate the delivery of OMR to cancer cells and they might also be used as a delivery system for gene therapy [Prabha *et al.*, 2002].

It has been shown that OMR can bind to hTR which serves as a template for the addition of telomeric repeats to the end of telomere DNA. In human prostate cancer cells and in immortalized human breast epithelial cells it can inhibit the telomerase activity [Pitts *et al.*,

1998; Folini *et al.*, 2005; Herbert *et al.*, 1999]. With the phosphorothioate modification, stability of OMR is increased and resistance to degradation by nucleases is enhanced. It can bind specifically to complementary RNA improving the selectivity of antisense effects [Pitts *et al.*, 1998; Agrawal *et al.*, 1997]. Our data have shown that in human NSCLC A549 and H23 cells nanoparticle mediated delivery of OMR inhibited more than 50% of telomerase activity 72h after treatment. Telomerase inhibition was sequence-dependent as mismatch-OMR was quite ineffective. In the cell-free TRAP assay, the EC_{50} of OMR was $1.5 \times 10^{-8} M$; different concentration of NP did not influence the results; mismatch-OMR showed less telomerase inhibitory effect at low concentration; on contrast more than 70% telomerase inhibition was observed only in concentration greater than $10^{-5} M$ indicating an unspecific inhibition. In the cell uptake experiments we used $4 \mu M$ of OMR or mismatch-OMR and only approximately 3% of oligonucleotides have been taken up into the cells. So the final amount of oligonucleotides inside the cells can not influence the TRAP assay. The lower telomerase activity of the treated cells was due to functional inhibition of telomerase and not caused by free oligonucleotides in the cells. During long-term treatment telomerase activity of A549 cells was inhibited to approximately 30% and remained stable for the tested period of 102 days. We also observed decreased cell proliferation of human lung cancer cells. These results suggest that effects on telomere length do not require complete inhibition of telomerase. Although decreased cell proliferation rate and reduced telomere length have been observed during long-term treatment, A549 cells did not reach proliferate crisis. It has been reported that human epithelial carcinoma cell A431 started crisis after 162 days treatment with the telomerase inhibitor GRN163 when telomeres had shortened from an initial length of $\sim 4.5 kb$ to an average length of $1.8 kb$ [Asai *et al.*, 2003]. The primary lung fibroblasts also stopped growing at about passage 12 to 13 when they reached a very short telomere length. In long-term experiment, 102 days after treatment in A549 cells telomere length shortened to about 50% of the original length; this suggests that longer treatment will be necessary to reach the crisis of A549 cells. The inhibitory potentials of OMR might also depend on the initial telomerase activity and telomere length of the tumor cells.

In our study, the various NSCLC cells showed different telomerase activities and telomere lengths; they also exhibited a variable response to the nanoparticle mediated delivery of OMR, e.g. Calu-3 cells had less uptake efficiency compared to the other tested cell lines according to FACS analysis (Fig. 2). This was further proved by CLSM imaging as Calu-3 cells showed much less FAM-OMR uptake (Fig. 3A). This might be explained by the cell morphology of Calu-3 cells, as these cells mainly formed colonies during proliferation which can reduce

uptake efficiency. Stronger telomerase inhibition was observed in cells with elevated telomerase activity. So such treatment will be more effective in cells with high telomerase activity and shorter telomere length. Telomere length of NSCLC tumors is relatively short and telomerase activity is high. However the individual distribution is quite broad [Hsu *et al.*, 2004; Hirashima *et al.*, 2000]. Thus pre-selection of patients will be advisable for the clinical application of telomerase inhibitors. Patients whose tumors have short telomeres might benefit more from this kind of therapy. On the other hand, for patients it might take several months to destroy the tumor cell population. Therefore, a combination with chemotherapy or radiotherapy may lead to more efficient and rapid progress in cancer treatment.

In A549 cells the quantification of OMR uptake showed that 6h after treatment with FAM-OMR-nanoplexes, more than 60% of FAM-OMR still remained in the transfection mixtures, 24h after treatment about 14% of FAM-OMR was released into the cell culture medium. This proportion might derive from the cells or the surface of the cell culture wells. Twenty-four hours after treatment, only about 3% of FAM-OMR stayed in the cell lysates. It also includes FAM-OMR attached to the cell membrane. Actually, functional OMR inside the cells was less than 3% of the original amount. About 18% FAM-OMR were lost during the complete experiment. This might be caused by the absorption to the cell culture wells, by the degradation of fluorescence dye FAM, or by the volume lost during pipetting.

ATP test and Annexin-V staining demonstrated that nanoparticle delivery of OMR had low cytotoxicity and did not induce apoptosis after short-term treatment. This might be explained by the different action mode of OMR if compared to classical antisense oligonucleotides. It was reported previously that antisense oligonucleotides directed against hTERT induced apoptosis or apoptotic cell death a few days after treatment [Folini *et al.*, 2005; Jiang *et al.*, 2003; Wang *et al.*, 2006]. In contrast, the antisense OMR caused telomerase inhibition by specific targeting the RNA template which does not interfere with the transcriptional regulation of hTR.

For *in vivo* application OMR has some limitations because of its poor uptake efficiency into the cells. Biodegradable PLGA nanoparticles have been reported as suitable drug delivery system in several areas [Costantino *et al.*, 2006; Lamprecht *et al.*, 2001; Dillen *et al.*, 2004]. But the negatively charged PLGA nanoparticles can not interact with the negatively charged OMR limiting their application. However the positively charged chitosan-coated PLGA nanoparticles with cationic surface modification can overcome this problem and serve as an efficient delivery system for antisense oligonucleotides [Nafee *et al.*, 2007]. Our results demonstrated that chitosan-coated PLGA nanoparticles have a high delivery efficiency of

OMR in human lung cancer cells. The high efficiency may provide a promising potential of cancer therapy for *in vivo* application.

Telomerase inhibitors will mainly target cancer cells which show telomerase activity, while normal cells will not be influenced because of a lack of telomerase activity. Likewise, telomerase positive human germ line cells and stem cells may not be affected by telomerase inhibitors because they have longer telomeres and they are predominantly quiescent [Zimmermann *et al.*, 2007; Shay *et al.*, 2006]. Nanoparticle delivery of the telomerase inhibitor OMR can increase its therapeutic potential. The cationic chitosan-coated PLGA nanoparticles have the advantage of being biodegradable, tailorable and exhibiting low cytotoxicity. It can be assumed that they have a great potential for *in vivo* application. More studies have to be performed to evaluate whether nanoparticle mediated delivery of telomerase inhibitors could be used for clinical applications of lung cancer therapy.

4.6 Conclusions

Our data demonstrate that in human lung cancer cell lines nanoparticle delivery of the telomerase inhibitor OMR can induce efficient telomerase inhibition and telomere shortening. The results provide evidence that telomerase inhibitors delivered by nanoparticles have a great potential for *in vivo* application of anticancer therapy.

Chapter 5

Tissue Slice Model of Human Lung Cancer to Investigate Telomerase Inhibition by Nanoparticle Delivery of Antisense 2'-O-Methyl-RNA

This chapter has been submitted for publication as an original article in *International Journal of Pharmaceutics*:

Dong M, Philippi C, Loretz B, Nafee N, Schaefer UF, Friedel G, Ammon-Treiber S, Griese EU, Lehr CM, Klotz U, Mürdter TE.

Tissue slice model of human lung cancer to investigate telomerase inhibition by nanoparticle delivery of antisense 2'-O-methyl-RNA.

*The results presented in this chapter were obtained by Meng Dong.

5.1 Abstract

Background: Telomerase activity is detected in about 80% of non-small cell lung cancers (NSCLC). The chitosan-coated poly(lactide-co-glycolide) (PLGA) nanoparticles delivery of antisense 2'-O-methyl-RNA (OMR) binding to the telomerase RNA template represents a promising approach for anticancer therapy. We used primary lung cancer cells and a tissue slice model to evaluate the effect of nanoparticle delivery of OMR in human lung cancers.

Methods: We isolated and cultured primary cells and 0.2mm thick tissue slices from freshly excised tumor samples of NSCLC patients. Oligonucleotides were complexed with chitosan-coated PLGA nanoparticles (nanoplexes) to treat primary cells and tissue slices. FACS analysis and confocal laser scanning microscopy (CLSM) were used to investigate uptake of FAM-labeled OMR. Cell viability in tissue slices was assessed by CLSM. Real-time PCR based telomeric repeat amplification protocol was used to investigate telomerase activity. Tissue structure, cell proliferation and telomerase expression were assessed by immunohistochemistry in paraffin-embedded tissues.

Results: In both cells and tissue slices, OMR cellular uptake was strongly enhanced by nanoplexes delivery. More than 80% of human primary lung cancer cells showed uptake of OMR-nanoplexes 72h after treatment. Telomerase activity was inhibited by approximately 45% in cancer cells and by about 40% in tissue slices. In tissue slices treatment with OMR-nanoplexes did not exhibit acute cytotoxicity. Tissue architecture, cell proliferation and telomerase expression were also not influenced.

Conclusion: Nanoparticle mediated delivery of OMR can inhibit telomerase in primary cancer cells isolated from NSCLC. Further, we could prove that OMR-nanoplexes penetrate into tissue and the delivered antisense OMR is able to inhibit telomerase activity in tumor tissue slices.

5.2 Introduction

Antisense oligonucleotides have great potential for cancer treatment. However, the poor cellular uptake is a limiting factor that may contribute to the lack of functional efficacy in anticancer therapy [Akhtar *et al.*, 1992; Fattal *et al.*, 2009]. Biodegradable nanoparticles have shown to be a promising drug delivery system. The cationic chitosan-coated poly(lactide-co-glycolide) (PLGA) nanoparticles are able to interact with oligonucleotides through electrostatic interaction to form naoplexes that show relatively low cytotoxicity on the cells [Bersner *et al.*, 2010; Nafee *et al.*, 2007; Katas *et al.*, 2008]. Delivery of oligonucleotides, including tissue disposition, degradation and elimination are important factors for their efficacy *in vivo* [Agrawal, 1999]. A solid tumor has a complex structure consisting of tumor cells, stromal cells and associated extracellular matrix [Tredan *et al.*, 2007]. The tumor microenvironment plays a role in drug resistance in tumor tissues [Morin, 2003] and may influence the efficient delivery of oligonucleotides to the tumor cells. Therefore, it is important to understand the effect of nanoparticle delivery of antisense oligonucleotides on tumor response in the intact tumor microenvironment of individual tumors.

The *ex vivo* tissue slice culture model as a three dimensional system has been used to investigate pharmacological properties of anticancer drugs [Sonnenberg *et al.*, 2008; Umachandran *et al.*, 2006; Vaira *et al.*, 2010; van der Kuip *et al.*, 2006]. This model could maintain both organ and cellular architecture, keep the original cancer microenvironment and preserve the integrity of the tumor-stroma interaction [Umachandran *et al.*, 2006; Vaira *et al.*, 2010]. The thin tissue slice (200 μ m thickness) allows a smooth diffusion of oxygen, nutrients and antibodies. The viability in tissue slices can be maintained for at least 4 days in normal culture condition [van der Kuip *et al.*, 2006]. This three dimensional model provides a tool that fills the gap between the current results based on monolayer culture of cancer cell lines and the reality in human solid tumors.

Lung cancer is the leading cause of cancer death worldwide in both men and women [Jemal *et al.*, 2010]. Non-small cell lung cancer (NSCLC) is the main type and constitutes about 80% of all lung cancers. One promising approach to treat NSCLC is based on the inhibition of telomerase activity in cancer cells [Dong *et al.*, 2010]. Telomerase is an enzyme that adds telomeric repeats to the end of linear eukaryotic chromosomes. The human telomerase consists of a telomerase RNA (hTR), a telomerase reverse transcriptase (hTERT) and other associated proteins. The catalytic protein subunit hTERT uses hTR as a template for adding telomeric repeats to the telomere DNA strand [Blackburn, 1991]. Telomerase is not active in

most somatic cells but is expressed in human germ line cells, stem cells and many cancer cells. As a consequence of telomerase activity the cells can become immortal and keep dividing [Kim *et al.*, 1994; Wright *et al.*, 1996]. Telomerase activity is detected in about 80% of NSCLC and is correlated with a poor prognosis [Hiyama *et al.*, 1995; Taga *et al.*, 1999]. The telomerase RNA template hTR is an ideal target for inhibition by oligonucleotides [Harley, 2008; Philippi *et al.*, 2010]. The antisense oligonucleotide 2'-O-methyl-RNA (OMR) with a phosphorothioate backbone can specifically inhibit hTR leading to progressive telomere shortening [Herbert *et al.*, 1999; Pitts *et al.*, 1998].

Previously, we have demonstrated that delivery of antisense OMR with chitosan-coated PLGA nanoparticles induced efficient telomerase inhibition in human NSCLC cells [Beisner *et al.*, 2010] and has a potential to be used as inhalation therapy. However, these results were based on established lung cancer cell lines and therefore may not totally reflect the behavior of tumor cells in original tumor tissues. In contrast, freshly isolated primary lung cancer cells in short-term culture retain many characteristics of cancer cells in primary tumors and show biological properties more closely related to the original tumors than cancer cell lines. But it is still a two dimensional culture system and can not reflect the solid tumor architecture as the tissue slice that can be used to study the tumor response to nanoparticle delivery systems in the complex environment of a primary cancer tissue. In the present study, we used freshly isolated human tumor tissue slices and primary lung cancer cells from NSCLC patients to evaluate the nanoparticle delivery of OMR and its biological effect on telomerase inhibition.

5.3 Material and methods

5.3.1 Lung tumor materials

Fresh tissues of primary lung tumors were obtained as surgical waste from patients newly diagnosed for lung cancer at the Klinik Schillerhöhe. Immediately after surgical resection, tumor tissues were maintained on ice until further processing. Fifteen tumor tissues were used for tissue slice preparations and 33 tumor tissues were used for isolation of primary lung cancer cells. The investigation was approved by the local ethics committee (#396/2005V) and informed consent was obtained from all patients.

5.3.2 Primary cells isolation, cultivation and characterization

The minced NSCLC tissue was enzymatically digested using a tissue disaggregation buffer (1mM NaH₂PO₄, 5.4mM KCl, 120mM NaCl, 5.6mM glucose, 2.5mM MgCl₂×6H₂O, 20mM

HEPES, pH7.2) supplemented with 167U/ml collagenase, 250U/ml DNase and 0.25mg/ml protease for 90min at 37°C [Sonnenberg *et al.*, 2008]. Digested tissue suspension was passed through a 70µm mesh nylon filter (BD Falcon) to remove cell clumps. Primary lung cancer cells were isolated from cell suspension using the magnetic-activated cell sorting (MACS) system. Cells were incubated with monoclonal CD326 (EpCAM) antibody conjugated to microbeads (human Anti-HEA (Ep-CAM) Microbeads, Miltenyi Biotec, Bergisch Gladbach, Germany) for 30min at 4°C and passed through a positive selection column (MACS[®] Cell Separation Column, Miltenyi Biotec, Bergisch Gladbach, Germany). The CD326 positive cell populations were selected as primary lung cancer cells and cultivated with Airway Epithelial Cell Growth Medium with SupplementMix (PromoCell, Heidelberg, Germany), 50µg/ml gentamicin (PromoCell, Heidelberg, Germany) and 0.05µg/ml amphotericin B (PromoCell, Heidelberg, Germany) in Collagen IV 24-well plates (BD Biosciences, Bedford, USA). CD326 negative cells were cultured as primary lung fibroblasts in RPMI1640 medium supplemented with 20% heat inactivated fetal calf serum (FCS), 1mM sodium pyruvate, 2mM L-glutamine, 10mM HEPES, 1% 2-mercaptoethanol, 0.5% non-essential amino acids (NEA, BioChromag, Berlin, Germany), 0.02mg/ml asparagin, 50U/ml penicillin and 50µg/ml streptomycin. Cell viability was assessed by trypan blue exclusion test. Primary cells were further identified by fluorescence-activated cell sorting (FACS) for epithelial specific antigen (ESA) expression.

5.3.3 Tissue slice preparation and cultivation

Preparation of tissue slices was performed as described previously [van der Kuip *et al.*, 2006]. Briefly, tissue slices (thickness: 200µm, diameter: 5mm) were cut by a Krumdieck microtome. Slices were individually submerged in the same medium used for primary lung cancer cell culture in 24-well plates. Each well contained one slice. Incubation was performed at 37°C in a constant atmosphere of 5% CO₂. Treatment started 24 hours after the slice preparation.

5.3.4 Oligonucleotides

The telomerase inhibitor is an antisense 2'-O-methyl-RNA(OMR) with a phosphorothioate(ps) backbone 5'-2'-O-methyl [C(ps)A(ps)GUUAGGGUU(ps)A(ps)G]-3'. The mismatch OMR is 5'-2'-O-methyl [C(ps)A(ps)GUUAGAAUU(ps)A(ps)G]-3'. The fluorescence-labeled OMR (FAM-OMR) is 5'-FAM-2'-O-methyl [C(ps)A(ps)GUUAGGGUU (ps)A(ps)G]-3' and the digoxigenin-labeled OMR (Digo-OMR) is 5'-2'-O-methyl [C(ps)A(ps)GUUAGGGUU(ps)A(ps)G]-digoxigenin-3'. All oligonucleotides were synthesized by Biomers (Ulm, Germany).

To ensure the stability and biological activity of the oligonucleotides, small aliquots were tested in the cell-free TRAP assay prior to use.

5.3.5 Preparation and characterization of chitosan-coated PLGA nanoparticles

Chitosan-coated PLGA nanoparticles were prepared by an emulsion-diffusion-evaporation method described previously [Kumar *et al.*, 2004; Nafee *et al.*, 2007]. In brief, 5ml of 2% PLGA (Polysciences Inc, Warrington, USA) were dissolved in ethyl acetate. The organic phase was added dropwise to 5ml of an aqueous solution of 2.5% (w/v) stabilizer polyvinyl alcohol (PVA) (Sigma Chemical Co., St. Louis, USA) and 0.3% (w/v) cationic polymer chitosan (NovaMatrix, Drammen, Norway) under stirring and was further stirred for 1h. The emulsion was homogenized using an UltraTurrax T25 (Janke & Kunkel GmbH & Co-KG, Staufen, Germany) for 10min. MilliQ-water was added up to 50ml to the homogenized emulsion. Organic solvent was removed by continuous stirring overnight at room temperature to obtain a suspension of nanoparticles.

Size, polydispersity index (PDI) and Zeta potential of nanoparticles were measured directly after preparation. Size of nanoparticles was in the range of 228–235nm with a mean size (\pm SD) of 230nm (\pm 4nm). The surface charge of nanoparticles measured as zeta potential was +32mV (\pm 6mV). The PDI was 0.13 (\pm 0.054). Nanoparticle concentration was determined gravimetrically after lyophilization to be 4.8mg/ml (\pm 0.79mg/ml). Particles were further confirmed by atomic force microscopy (AFM) as spherical with a monomodal size distribution.

5.3.6 Preparation of oligonucleotide-nanoparticle-complexes (nanoplexes) for transfection

Certain amounts of oligonucleotides were dissolved in cell culture medium to a final concentration of 4 μ M. A suspension of nanoparticles was added and mixed. Then the mixture was incubated for 15min at 37°C to form oligonucleotide-nanoparticle-complexes (nanoplexes). The content ratio of nanoplexes was 1:50 ($\text{weight}_{\text{oligonucleotide}}/\text{weight}_{\text{nanoparticles}}$) for primary cells treatment and 1:100 ($\text{weight}_{\text{oligonucleotide}}/\text{weight}_{\text{nanoparticles}}$) for treatment of tissue slices. Primary cells and tissue slices were treated with OMR-nanoparticle-complexes (OMR-nanoplexes), OMR alone or mismatch-OMR-nanoplexes; either FAM-OMR alone or FAM-OMR-nanoparticle-complexes (FAM-OMR-nanoplexes); either Digo-OMR alone or Digo-OMR-nanoparticle-complexes (Digo-OMR-nanoplexes), separately. Six hours after treatment the mixture was replaced by cell culture medium. Tissue slices or primary cells were further cultured for 24h or 72h.

5.3.7 Fluorescence-activated cell sorting (FACS) analysis

For characterization, primary cells were incubated with anti-ESA-FITC (1:20; Biomeda, Foster City, CA) at room temperature for 20min in the dark. For binding and/or uptake analysis, primary cells were collected and washed twice with PBS after treatment. The resuspended cell pellets were analyzed by FACScan fluorescence-activated cell sorter (Becton-Dickinson, Heidelberg, Germany) and 10,000 events were counted for each sample. Data were analyzed using CellQuest software (Becton-Dickinson, Heidelberg, Germany).

5.3.8 Confocal laser scanning microscopy analysis

One day after cells were seeded in Lab-Tek[®] chamber slides (Nalge Nunc International, Naperville, USA) primary cells were treated either with FAM-OMR alone or FAM-OMR-nanoplexes. Cells were observed at 6h, 24h and 72h after treatment, respectively. After washing with PBS, cell membranes were stained with 25 μ g/ml Rhodamine-labeled Ricinus Communis Agglutinin I (RCA I, Vector Laboratories, Burlingame, CA, USA) for 15min at 37°C. The cells were fixed with 100% ethanol at -20°C for 10min. The cell nuclei were stained with 1 μ M TO-PRO[®]-3 iodide (Molecular Probes Invitrogen, Eugene, OR, USA) for 10min at room temperature in the dark. Sections were mounted with mounting medium (Vectashield[®] Mounting Medium, Vector Laboratories, Burlingame, CA) for analyzing by CLSM.

One day after tissue slices were prepared, they were treated with either FAM-OMR alone or FAM-OMR-nanoplexes. Twenty-four hours and 72h after treatment, tissue slices were washed with PBS and incubated with 25 μ g/ml RCA I for 15min at 37°C. After washing with PBS, they were incubated with 6.25 μ M DRAQ5[™] (Biostatus Limited, Lörrach, Germany) for 10min at room temperature in the dark and immediately examined by CLSM. Images were taken randomly from different areas. For every taken image the efficiency of uptake in percent was calculated by dividing the number of positive cells by the total cell number. A mean value of each sample was calculated from 12 images.

To identify cytotoxicity within the non-fixed tissue slices, we used a three-color fluorescent viability assay as described previously [van der Kuip *et al.*, 2006]. Briefly, tumor tissue slices were incubated simultaneously with 0.5 μ M tetramethylrhodamine methyl ester perchlorate (TMRM, Sigma-Aldrich, Deisenhofen, Germany) and 5 μ M DRAQ5[™] for 20min at 37°C, followed by Picogreen in DMSO (Molecular Probes, Invitrogen) for additional 10min at 37°C and analyzed immediately without further washing steps using CLSM. Images were taken randomly from different areas. Cells which showed signals from Picogreen in the nuclei were

considered as dead cells. For each image the viability was calculated by dividing the number of living cells by the total cell number. A mean value was calculated from 12 images. Experiments were repeated with tumor tissue slices from different patients.

CLSM was performed with a Leica LCS (Leica Lasertechnik, Heidelberg, Germany) instrument based on a Leica DM IRBE microscope equipped with argon and helium/neon lasers. The excitation (Ex.) and emission (Em.) wavelengths were as follows: Picogreen and FAM (Ex. 488nm, Em. 500-540nm); TMRM and RCAI (Ex. 543nm, Em. 560-610nm); TO-PRO[®]-3 and DRAQ5[™] (Ex. 563nm, Em. 650-700nm).

5.3.9 Telomerase activity assay using real-time quantitative PCR

Primary cells were harvested and counted. 500,000 cells were further pelleted and washed with PBS. The cell pellets were either stored at -80°C or immediately resuspended in 100µl ice-cold 3-[(3-cholamidopropyl)dimethyl-ammonio]-1-propanesulfonate (CHAPS) lysis buffer and incubated on ice for 30min. Tissue slices were isolated using the FastPrep system: 300 µl CHAPS buffer with 200 U Recombinant Ribonuclease Inhibitor (RNaseOUT[™], Invitrogen, Carlsbad, CA) were added into a Lysing Matrix D tube with spheres (MP Biomedical, Solon, OH). Two frozen tissue slices were transferred into the tube and homogenized by a FastPrep[®] FP120 cell disrupter (Thermo Savant Bio101, Cedex, France) for 20sec at speed setting of 6.0 at 4°C. After short centrifugation the tubes were left on ice for 30 min. The upper phase was transferred to a new tube and centrifuged at 12,000×g for 20min at 4°C. The supernatants were aliquoted, snap-frozen and stored at -80°C.

Telomerase activity was measured using an optimization of the modified real-time quantitative PCR based telomeric repeat amplification protocol (Q-TRAP) assay described by Herbert *et al.* [Herbert *et al.*, 2006]. The details of the process are described in *Chapter 2: Part2: Materials and methods: Telomere measurement by real-time quantitative PCR.*

5.3.10 Immunohistochemical staining

After treatment, tissue slices were fixed in 4% buffered formalin and embedded in paraffin for further investigation. The fixed tissue slices were cut in 3µm serial sections by Rotary Microtome (Leica RM2255, Germany). Paraffin sections were stained with hematoxylin and eosin (HE) for histopathological examination. Immunohistochemical staining for KI67 (1:75, Monoclonal Mouse Anti-human KI67 Antigen, Clone MIB-1, Dakocytomation, Glostrup, Denmark) and hTERT (30µg/ml, Rabbit Anti-hEst2 IgG, Alpha Diagnostic International, San Antonio, USA) were performed using the Dako Envision Kit according to the manufacturer's

manual. Immunohistochemical staining for Digo-OMR was performed using Mouse-anti-DIG antibody (ZytoVision, Bremerhaven, Germany). Epitope retrieval was achieved as follows: prior to staining with KI67 and mouse-anti-DIG, sections were treated for 30min with citric acid buffer pH6.0 (Dako, Glostrup, Denmark) in a steam heater. For hTERT staining, sections were treated for 15min with Tris/EDTA buffer pH9.0 (Dako, Glostrup, Denmark) in a pressure cooker. Counterstaining was performed with hematoxylin. Images were taken by a DigitalMicroscope (Leica DM 4000B) and analyzed by Leica Application SuiteV3. Immunohistochemical assessments were performed independently by two observers (MD, TM). The percentage of positive KI67 was calculated by relating the number of positive cells to the total cell number.

5.3.11 Statistical analysis

Different groups were compared by Wilcoxon signed rank test or Wilcoxon matched pairs test. Results were considered statistically significant if $p < 0.05$. All data were analyzed by Graphpad Prism version 4.0 (GraphPad Software Incorp., San Diego, CA).

5.4 Results

5.4.1 Cultivation and characterization of primary cells

The isolated cells were put into culture in an attempt to get primary lung cancer cells. The mean cell viability after isolation was $81.4\% \pm 11\%$ (mean \pm SD). From 9 out of the isolated 33 tissue samples, primary lung cancer cells proliferated and enough cells were obtained for further experiments after 3 to 5 passages. Telomerase activity was detected in 29 out of these 33 NSCLC specimens. Before treatment, cells were tested for the expression of epithelial specific antigen (ESA) by FACS analysis (Fig.1A). At least 75% of cells showed positive expression for ESA in these tested primary cells. The ESA positive cells were used for further studies.

5.4.2 Preparation and cultivation of tissue slices

Different numbers of viable tissue slices were obtained from 14 out of 15 telomerase positive primary lung cancer samples. In one case the tissue was contaminated with bacteria. Tissue slices from 8 telomerase positive samples were used for evaluating inhibition by the Q-TRAP assay. Six samples were applied for FAM-OMR uptake efficiency tests, 3 samples for Digo-OMR uptake efficiency tests, 6 samples for viability tests, 8 samples for immunohistochemical staining.

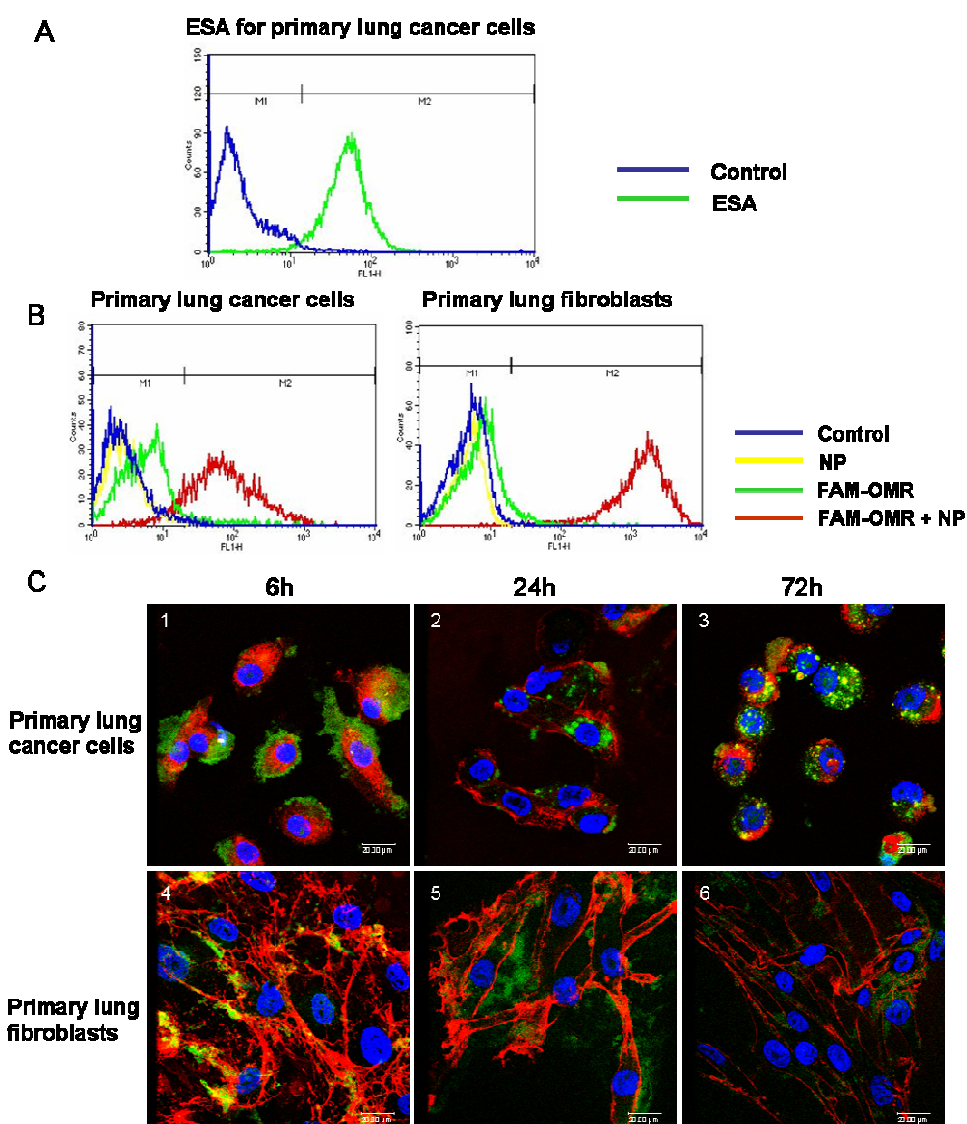


Fig. 1: (A) Characterization of primary lung cancer cells

FACS analysis of human lung cancer cells for ESA expression. The control histogram represents negative control antibodies. Experiments were performed for each cultured primary lung cancer cells and a representative experiment is shown.

(B) Uptake of OMR-nanoplexes in primary lung cancer cells and primary lung fibroblasts

Human primary lung cells were treated with FAM-OMR-nanoplexes (FAM-OMR+NP), nanoparticles (NP) or FAM-OMR were analyzed by FACS 24h after treatment. The corresponding non-treated primary cells were used as control. Figures show the histographic results of primary lung cancer cells (left panel) and primary lung fibroblasts (right panel). Experiments were repeated 3 times with different primary cells and a representative experiment is shown.

(C) Localization of nanoparticles delivered FAM-OMR in primary lung cancer cells and fibroblasts visualized by CLSM

Images were taken 6h, 24h and 72h after treated with FAM-OMR-nanoplexes. FAM-OMR has a fluorescence signal shown in green. Fig. 1, 2 and 3 display the images of primary lung cancer cells. Figures 4, 5 and 6 show the images of primary lung fibroblasts. Cells were stained with RCA I (red) and TO-PRO[®]-3 (blue) before microscopic observation (63× objectives). Scale bars represent 20µm.

Experiments were performed for each cultured primary lung cancer cells and a representative experiment is shown.

5.4.3 Nanoparticle delivery of 2'-O-methyl-RNA in primary lung cancer cells and tissue slices

FACS was used to quantify the binding and/or uptake of nanoplexes prepared with FAM-OMR in human primary lung cancer cells and fibroblasts 24h after treatment. The treatment of cells with FAM-OMR-nanoplexes revealed a markedly stronger shift in the fluorescence profile of the cell population reflecting a higher cell binding and/or uptake compared to OMR alone in both primary lung cancer cells and fibroblasts (Fig.1B). The percentage of cells above the fluorescence threshold was $99.1\% \pm 1.13\%$ (mean \pm SD, n=3) for fibroblasts and $90.9\% \pm 2.77\%$ (mean \pm SD, n=3) for primary lung cancer cells. The cell population showed a slight shift to higher fluorescence with FAM-OMR in the absence of nanoparticles in both cell types, the population shift was more pronounced in primary lung cancer cells compared to fibroblasts. But compared to the dramatic shift after FAM-OMR-nanoplexes treatment, the shift was negligible and might be caused by unspecific binding. As expected, treatment with nanoparticles alone did not show any effects.

The localization of FAM-OMR in primary cells and tissue slices was determined by CLSM. The uptake of nanoplexes into cells appeared to be a stepwise process. In primary lung cancer cells, the FAM-OMR was accumulated on the membrane of cells after 6h of incubation (Fig.1C-1). Only few cells showed an uptake of FAM-OMR, less than 5% of cells exhibited fluorescence in nuclei. An uptake into the primary cells was observed 24h after treatment; the FAM-OMR appeared inside the cells and was mainly located in the cytoplasm as small spots in the perinuclear area (Fig.1C-2). More than 80% of cells displayed fluorescence signals within the cells and approximately 20% of those cells within the nuclei 72h after treatment (Fig.1C-3). CLSM proved that the high fluorescence intensities in FAM-OMR-nanoplexes treated primary lung cancer cells as observed by FACS is due to an intracellular uptake rather than an adsorption of nanoplexes to the cell surface. In primary lung fibroblasts, the FAM-OMR accumulated mostly on the cell membranes during the whole observation time. The fluorescence signal localization showed almost no difference 6h, 24h and 72h after transfection (Fig.1C-4 to Fig.1C-6). Although primary lung fibroblasts treated with FAM-OMR-nanoplexes demonstrated high fluorescence intensities by FACS analysis, the cells did not take up the nanoplexes; thus the fluorescence signal is due to an adsorption of nanoplexes to the cell surface.

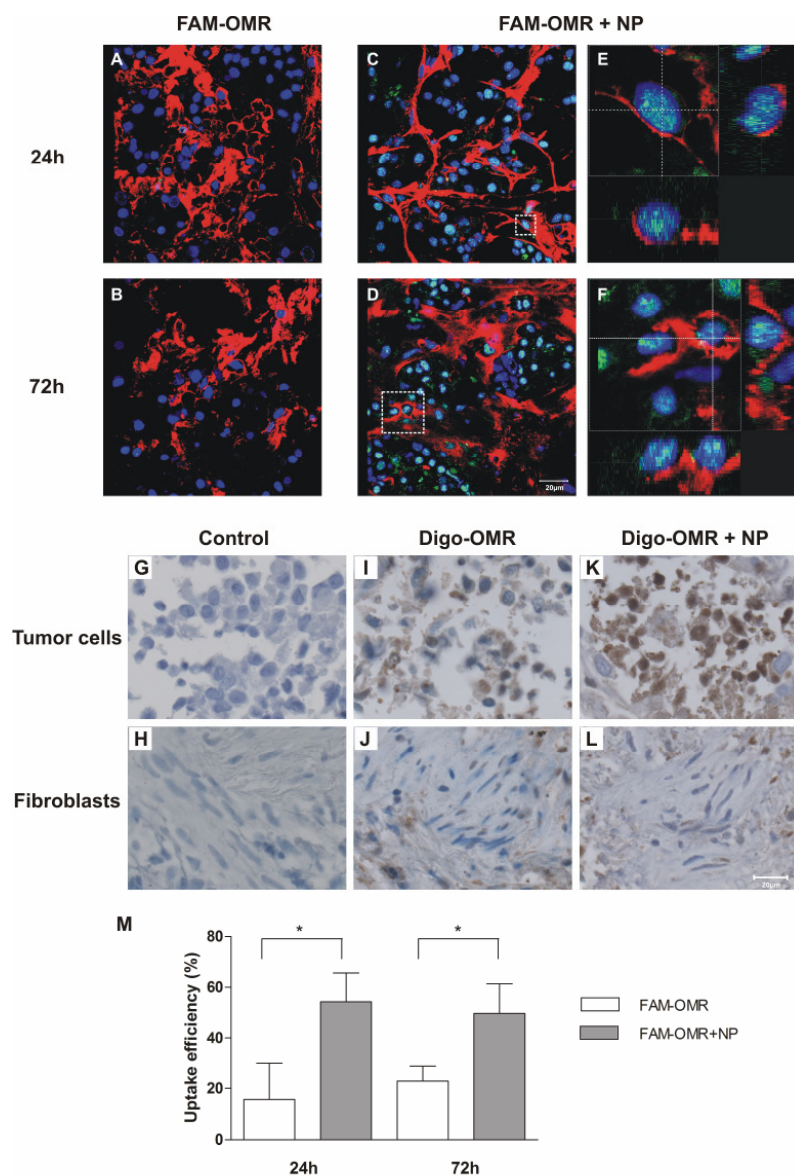


Fig. 2: (A to F) Localization of nanoparticles delivered FAM-OMR in cells of tissue slices visualized by CLSM

Fig. A and B show tissue slices treated with FAM-OMR alone (FAM-OMR). Fig. C and D show tissue slices treated with FAM-OMR-nanoplexes (FAM-OMR+NP). Fig. E and F illustrate the transverse and vertical sections of a single zoomed cell from C and D respectively. FAM-OMR has a fluorescence signal shown in green. Cells were stained with RCA I (red) and DRAQ5TM (blue) before microscopic observation (63× objective). Scale bars represent 20μm.

(G to L) Localization of nanoparticles delivered digoxigenin-labeled OMR in cells of tissue slices visualized by immunohistochemistry

Fig. I and J show tissue slices treated with digoxigenin-OMR (Digo-OMR). Fig. K and L show tissue slices treated with Digo-OMR-nanoplexes (Digo-OMR+NP). Fig. G and H show control tissue slices without treatment. Fig. G, I and K are areas mainly contain tumor cells. Fig. H, J and L are areas mainly contain fibroblasts. Scale bar represents 20μm (100× objectives).

(M) Uptake efficiency of nanoparticles delivery of FAM-OMR in human lung tissue slices

For each tissue slice, images were taken from 12 different areas and with each area at least 20 cells were counted. Uptake efficiency is given as % positive cells of total number of cells. Data represent the mean +SD from 6 independent experiments (*, $p < 0.05$).

In tumor tissue slices, the uptake of nanoplexes started after 6h of incubation (data not shown), more than 50% of cells showed uptake in the following incubation time (Fig.2C to F). The FAM-OMR-nanoplexes were able to penetrate the whole tissue slice and showed equally distribution. Interestingly, the uptake of FAM-OMR nanoplexes showed a spotted distribution within the nucleus, which is different to the uptake into primary lung cancer cells. Nanoplexes significantly enhanced efficiency of uptake: Compared to FAM-OMR-nanoplexes, uptake of FAM-OMR alone was only minor and did not improve over time (Fig. 2A to B). There was a significant difference for the uptake efficiency between FAM-OMR alone and FAM-OMR-nanoplexes treatment both, 24h and 72h after treatment (Fig.2M). The results were further confirmed by immunohistochemical staining for Digo-OMR uptake into tissue slices following treatment with Digo-OMR-nanoplexes. The digoxigenin signal mainly present in the tumor cells but not in stromal cells indicated that tumor cells showed nanoparticle mediated uptake of Digo-OMR (Fig.2G to L).

5.4.4 Cytotoxicity of nanoparticles delivery of 2'-O-methyl-RNA

After treatment with nanoplexes, viability of primary lung cancer cells was reduced by 30 ± 12% if compared to untreated controls. There was no difference in cytotoxicity among the OMR-nanoplexes, mismatch-OMR-nanoplexes and nanoparticles alone. Compared to established cancer cell lines, primary lung cancer cells were more sensitive to the culture condition and the treatment. The slight cytotoxic effects were mainly caused by the treatment with nanoparticles not by the oligonucleotide transfection. To limit this effect, we decided to use a nanoplexes ratio of 1:50 instead of 1:100 ($\text{weight}_{\text{oligonucleotide}}/\text{weight}_{\text{nanoparticles}}$) for primary cells. As all experiments were carried out with 4μM OMR, the amount of nanoparticles used was halved.

In Fig.3A and B viable cells displayed red fluorescence of TMRM which bounds to active mitochondrial membranes, whereas nuclei of dead cells showed green fluorescence from Picogreen. Nuclei of cells were stained with DRAQ5TM, which is a cell membrane permeable DNA-interactive agent. A high percentage of living cells was identified in tissue slices 72h after treatment and no difference was found between nanoplexes treated specimens and the untreated controls. This was confirmed by quantification of Picogreen negative cells in relation to total cells in 6 different tumor samples. The mean ratio of living cells was more than 80% and no significant difference was seen for viability between both groups (Fig.3C) indicating that treatment with nanoplexes did not have an acute cytotoxic effect on the tissue slices.

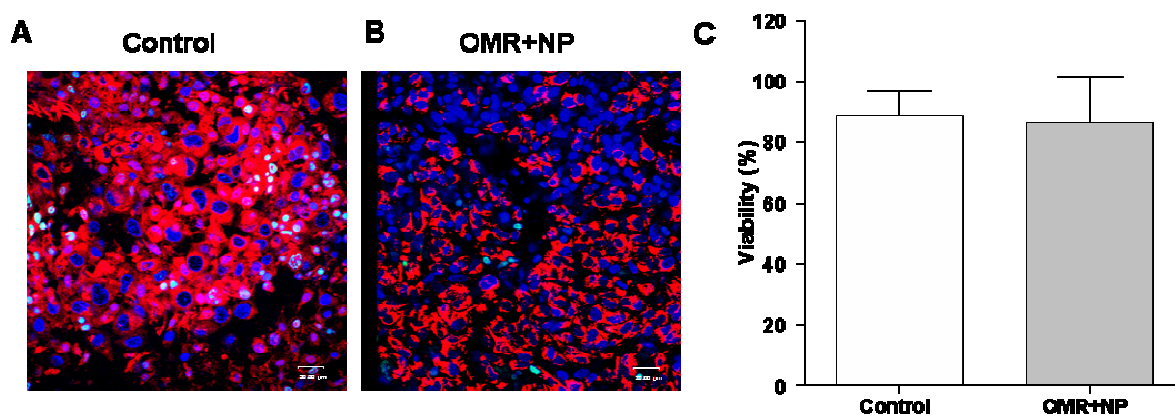


Fig. 3: Cytotoxicity of nanoparticles delivery of OMR in tissue slices determined by CLSM

Fig.A shows control tissue slices without treatment (control). B shows tissue slices treated with OMR-nanoplexes (OMR+NP). Living cells were stained with TMRM (red) and dead cells were stained with Picogreen (green), all cells nuclei were stained with DRAQ5TM (blue) before microscopic observation (40×objectives). Experiments were performed with 6 tissue slices from different patients and a representative experiment is shown. C exhibits the quantification of cell viability in tissue slices from CLSM images. For each tissue slice, images were taken from 12 different areas and with each area at least 20 cells were counted. Cell viability is given as % Picogreen negative cells of total number of cells. Data represent the means +SD from 6 independent experiments.

5.4.5 Impact of 2'-O-methyl-RNA-nanoparticle-complexes on cell proliferation and telomerase expression in tissue slices

Hematoxylin and eosin (HE) histological examination of paraffin embedded tissue slices showed that there was no obvious difference in the morphology between the nanoplexes treated and the untreated tissue slices 72h after treatment (Fig.4A and B). Nuclear hTERT expression was detected by immunohistochemistry in tissue slices with or without nanoplexes treatment using an affinity purified antibody which binds to a 16 amino acid peptide sequence within hTERT. After 72h of cultivation, immunohistochemical staining indicated positive hTERT expression in tissue slices (Fig.4C and D). The cell proliferation in tissue slices was analyzed using proliferation marker KI67 (Fig. 4E and F). The morphology from HE staining and the hTERT expression did not show any difference between nanoplexes treated and control tissue slices. However, there was a slight decrease of Ki67-positive tumor cells following treatment with nanoplexes.

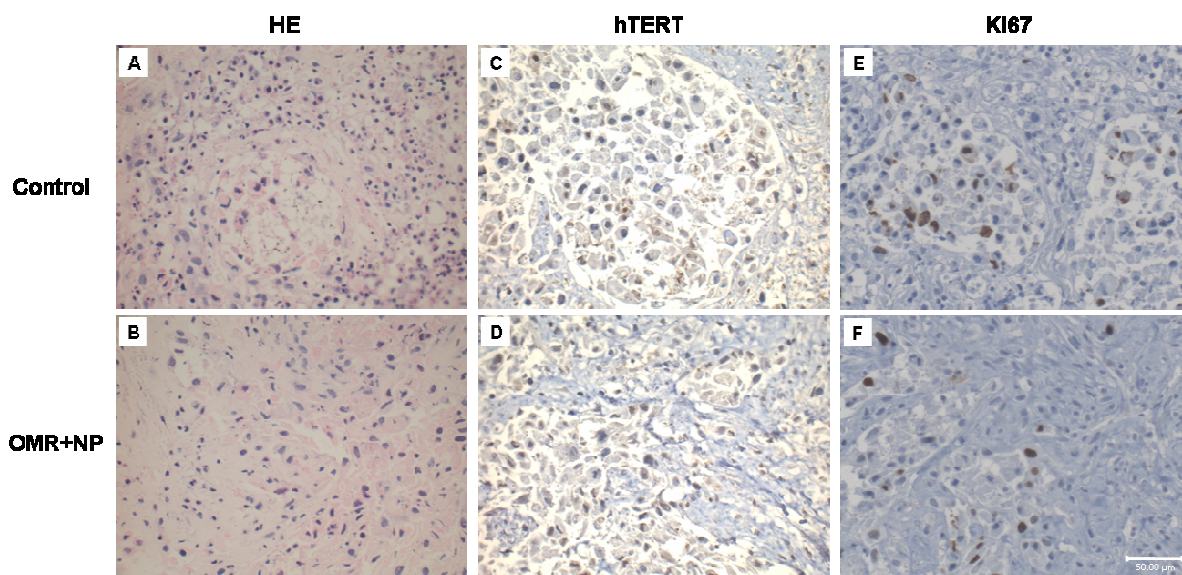


Fig. 4: Evaluation of nanoparticles delivery of OMR on morphology, proliferation and telomerase expression in human tissue slices

Images of paraffin embedded tissue slices were taken 72h after treated with OMR-nanoplexes (OMR+NP). Untreated tissue slices were used as control. A and B show representative example of Hematoxylin and eosin (HE) staining of sections from control and OMR+NP treated tissue slices. C and D exhibit representative examples of hTERT expression stained with Anti-hEst2 IgG antibody. E and F show representative examples of cell proliferation with KI67 staining in control and OMR+NP treated tissue slices (40× objectives). Scale bar represents 50μm.

5.4.6 Inhibition of telomerase activity by 2'-O-methyl-RNA-nanoparticle-complexes in primary lung cancer cells and tissue slices

The real-time quantitative PCR based TRAP assay allows a more rapid and quantitative determination of telomerase activity in cells or tissue extracts compared to assays based on electrophoresis. We modified this method to be of low-cost and high-throughput using 384-well reaction plates with only 12μl total PCR reaction volume.

We analyzed the functional effect of OMR delivered by chitosan-coated PLGA nanoparticles on telomerase activity in primary lung cancer cells from passage 3 to 5. Primary cells were treated with OMR-nanoplexes or mismatch-OMR-nanoplexes for 6h and telomerase activity was measured 72h after treatment. Following treatment with OMR-nanoplexes telomerase activity was inhibited by approximately 45% ($p=0.0313$). Primary cells treated with mismatch-OMR-nanoplexes showed only a slight reduction (~15%) of telomerase activity indicating a specific inhibition of telomerase by the OMR-nanoplexes (Fig.5A).

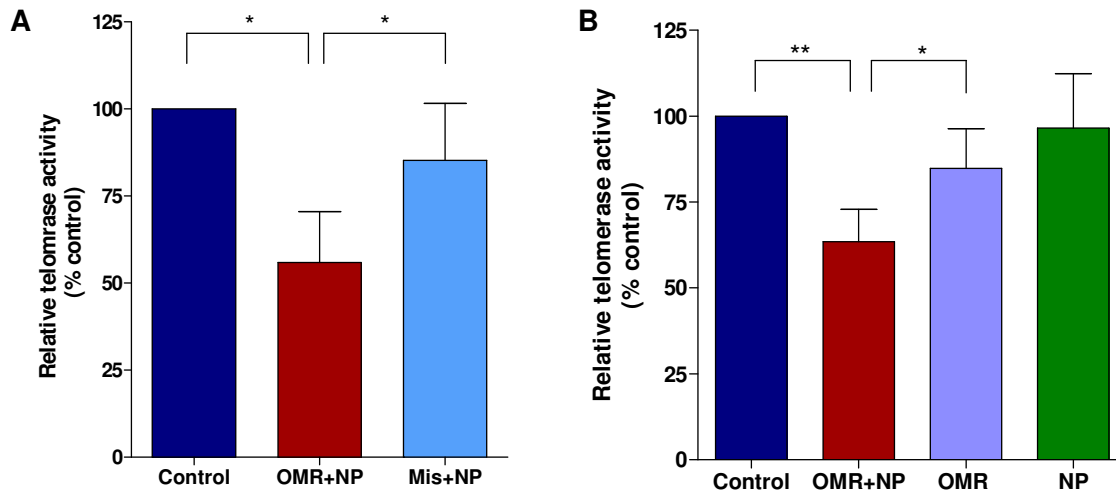


Fig. 5: (A) Telomerase inhibition by nanoparticle delivery of OMR in primary lung cancer cells Cells were treated with either OMR-nanoplexes (OMR+NP) or mismatch-OMR-nanoplexes (Mis+NP). Telomerase activity was measured by Q-TRAP 72h after treatment. Telomerase activity of untreated cells (control) was set to 100%. Telomerase activity of treated cells were normalized by corresponding control cells and shown as percentage. Data represent the mean +SD from 6 independent experiments (* $p < 0.05$).

(B) Inhibition of telomerase activity by nanoparticle delivery of OMR in lung tissue slices

Tumor tissue slices were treated with OMR-nanoplexes (OMR+NP), OMR (OMR) or nanoparticles (NP). The telomerase activity was measured by Q-TRAP 24h after treatment. Telomerase activity of untreated tissue slices (control) was set to 100%. Telomerase activity of treated tissue slices were normalized by corresponding control tissue slices and shown as percentage. Data represent the mean + SD from 8 independent experiments with different patients (** $p < 0.01$; * $p < 0.05$, n=5 for NP treated group, n=8 for all the other groups).

We further analyzed the effect of OMR delivered by chitosan-coated PLGA nanoparticles on telomerase activity in the tissue slices. Tissue slices from 8 different telomerase positive tumor samples were treated for 6h with $4\mu\text{M}$ of OMR alone or OMR-nanoplexes. 24h after treatment, OMR-nanoplexes treatment reduced telomerase activity by about 40% ($p = 0.0078$) in tumor tissue slices. The group treated with OMR alone only showed a slight of about 15% inhibition of telomerase activity ($p = 0.0156$) (Fig.5B). Treatment with nanoparticles alone did not show significant telomerase inhibition effect on tumor tissue slice.

5.5 Discussion

In contrast to normal cells, tumor cells have relatively short telomeres but often an increased telomerase activity [Zimmermann *et al.*, 2007]. This makes the inhibition of telomerase an interesting option for anticancer therapy. When the telomere length is reduced to a certain critical value, cells go to apoptosis and eventually die. However, tumor cells normally have

high telomerase activities which can maintain telomere length during proliferation [Harley *et al.*, 2008; Kim *et al.*, 1994]. The efficient inhibition of telomerase can drive tumor cells into apoptosis, while telomerase negative normal somatic cells are not targeted and affected. Other telomerase positive cells, such as germ line cells and stem cells, also remain unaffected because of their longer telomere lengths and slower cell division rates compared to tumor cells [Zimmermann *et al.*, 2007; Shay *et al.*, 2006]. Previously we have demonstrated that 2'-O-methyl-RNA (OMR) acts as a specific telomerase inhibitor and chitosan-coated PLGA nanoparticles enhance the delivery of OMR inducing telomerase inhibition and telomere length shortening in human NSCLC cells [Beisner *et al.*, 2009; Beisner *et al.*, 2010]. All these results have been based on human lung cancer cell lines which do not reflect perfectly the original tumor *in vivo*. Therefore we used primary lung cancer cells and tumor tissue slices to evaluate the telomerase inhibition by nanoparticle delivery of antisense OMR.

Primary lung cancer cells were directly isolated from the tumor lesion. During short-term culture, they undergo less transformation and show biological properties related more closely to the original tumor [Burdall *et al.*, 2003]. But it is quite difficult to establish a primary lung cancer cell culture which is suitable for *in vitro* experiments. In order to improve attachment and growth, we used collagen IV coated wells. A special airway epithelial cell culture medium was used to keep their characteristics and to avoid contamination with fibroblasts. Nevertheless, cells within this culture system have only a limited lifespan. The primary cancer cells have longer population doubling times compared to established cancer cell lines; most of the cells proliferated even more slowly after 5 passages. In addition, these primary cancer cells were more sensitive to the condition of culture and environmental changes. Especially during the transfection procedure when cells were treated with nanoplexes but also nanoparticles alone, we observed decreased cell viability. We therefore decided to reduce the amount of nanoparticles during treatments and increased the content of nanoplexes ratio from 1:100 to 1:50 ($\text{weight}_{\text{oligonucleotide}} / \text{weight}_{\text{nanoparticles}}$). Under these conditions, we were able to perform the experiments without a remarkable decrease of cell viability. Telomerase activity of primary cancer cells was inhibited by about 40% with OMR-nanoplexes prepared in a ratio of 1:50, which was similar to A549 cells treated with OMR-nanoplexes of a ratio of 1:100 as reported previously [Beisner *et al.*, 2010]. The original telomerase activities of these primary cells were highly variable within specimens from different patients. Cells which expressed high telomerase activity had longer lifespan (Spearman test, $r=0.428$, $p=0.037$).

Cell morphology, cell-cell, cell-matrix and tumor-stroma interactions in cell culture models are different compared to the ones in tumor tissue [van der Kuip *et al.*, 2006] and these

interactions are also specific for each individual tumors *in vivo* [Morin, 2003]. Although more closely related to the original tumor tissue than cell lines, primary cancer cell culture is still a two dimensional culture system and lacks most of these interactions. Compared to monolayer culture, the multicellular tumor spheroids were more resistant to anticancer drugs [Morin, 2003]. Moreover, the extracellular matrix forms a tight network that can prevent the penetration of drugs into the tumor [Morin, 2003; Tannock *et al.*, 2002; Fattal *et al.*, 2009] or affect the sensitivity of the tumor cells to these drugs [Morin, 2003; Dalton, 1999]. Therefore, the *ex vivo* tissue slice model is a suitable system to evaluate drug response and actual efficacy in human tumors.

Previous studies have shown that tumor tissue slices recover from the preparation process within 24h and are fully viable for at least 4 days. Therefore, treatment with nanoplexes was commenced after 24h and viability was evaluated up to 72h post treatment. We could show that both, small molecules and antibodies can freely penetrate the slices with 200 μm thickness [van der Kuip *et al.*, 2006]. However, no data were available on larger particles. For a successful *in vivo* treatment of solid tumors, nanoplexes have to penetrate the tumor tissue to affect all tumor cells. The results achieved with viable tumor tissue slices showed that nanoplexes were able to permeate through the whole tumor tissue slice which has a thickness of about 200 μm . Taking into account the architecture of solid tumors with its vascularization this distance should exceed to the nearest blood vessel.

In our study, a comparison of the morphology of the original tumor tissue with tissue slices by HE staining showed that neither the slicing procedure nor the treatment with nanoplexes changed the architecture of the tissue. In concordance, proliferation marker KI67 staining demonstrated no decrease in the fraction of proliferating tumor cells over 72h of incubation time. In addition, there was only a slight difference in KI67 positive cells between the treated and control groups after 72h. This is in agreement with the lack of acute toxicity of nanoplexes in lung cancer cell lines [Beisner *et al.*, 2010]. In long-term experiments, the population doublings of A549 cells reduced about 40% after 2 weeks treatment, but no obvious difference could be observed at the first 3 days [Beisner *et al.*, 2010]. This was expected as shortening of telomeres is a stepwise process needing several cell cycles to affect proliferation rate. The antisense 2'-O-methyl-RNA targeting only the telomerase RNA template does not interfere with transcriptional regulation of hTR [Pitts *et al.*, 1998]. It inhibits telomerase activity by competing with the telomeres but does not influence the hTERT expression. Accordingly, we also observed that hTERT staining did not change in tissue slices during treatment. Previously, we have demonstrated that different treatments

such as OMR-nanoplexes, mismatch-OMR-nanoplexes or nanoparticles alone had no influence on cell viability of A549, Calu-3 cells and primary lung fibroblasts [Beisner *et al.*, 2010]. In contrast to primary lung cancer cells the cell viability in the tissue slice model was not affected by OMR-nanoplexes.

Although primary lung fibroblasts showed high fluorescence intensities by FACS analysis after treatment with FAM-OMR-nanoplexes, the results of CLSM proved that these signals came from the adsorption of nanoplexes to the cell surface. The results of immunohistochemical staining for tissue slices following treatment with Digo-OMR-nanoplexes also showed that the digoxigenin signal was mainly present in the tumor cells not in the stroma cells. This indicated that stromal cells did not reveal a very good uptake of nanoplexes. This might explain that viability of primary lung fibroblasts was not affected by the treatment of nanoplexes [Beisner *et al.*, 2010] and proves that fibroblasts were not influenced by this kind of treatment.

Tissue slices from different NSCLC patients showed a broad distribution of telomerase activities. But the inhibition ratio of OMR-nanoplexes treatment did not demonstrate significant differences. The averaged telomerase inhibition was $36.5\% \pm 9.4\%$ (\pm SD) indicating that the treatment works successfully on different levels of telomerase activity. Tumor tissue consists of different kinds of cells, such as cancer cells, fibroblasts, lymphoblasts, lymphocytes, endothelial cells and extracellular matrix. Among these components, only tumor cells exhibit high telomerase activity. When comparing telomerase activity of freshly isolated cancer cells and tumor tissue homogenate, the isolated cancer cells showed higher telomerase activity. This is explained by the fact that telomerase activity determined in tumor tissue slices was the average of tumor cells with high telomerase activity and stromal cells which do not express telomerase.

5.6 Conclusion

Inhibition of telomerase in tumor cells is a promising approach in the treatment of solid tumors. The antisense OMR directed against the RNA template is a potent inhibitor of telomerase. In the primary cancer cells isolated from NSCLC we could show that nanoparticle delivery of antisense OMR can inhibit telomerase activity. Using the tissue culture model we could prove that (1) OMR-nanoplexes penetrate into tumor tissue, (2) transfect tumor cells in their “natural” environment to deliver OMR and (3) that telomerase activities of these cells are inhibited by this OMR. Therefore the tissue slice model of human lung cancer appears to

be a useful tool for translating nanotechnology based delivery of telomerase inhibitor antisense oligonucleotides into more complex *in vivo* experiments.

Chapter 6

Inhalation of Nanoplexes for the Delivery of 2'-O-Methyl-RNA in An Isolated Perfused Rat Lung Model

This chapter is prepared for publication as an original article in the journal of *Aerosol Medicine and Pulmonary Drug Delivery*:

Dong M, Ammon-Treiber S, Philippi C, Loretz B, Schaefer UF, Lehr CM, Klotz U, Mürdter TE.

Inhalation of nanoplexes for the delivery of 2'-O-methyl-RNA in an isolated perfused rat lung model.

6.1 Abstract

Background: The respiratory delivery of drugs to the lungs by inhalation has been investigated extensively and employed to treat diseases primarily localized in the lung, e.g. asthma. The respiratory tract might also be used as a route for administration of aerosolized targeted drugs in lung cancer therapy.

Methods: An isolated perfused rat lung (IPL) was used as a model to investigate in pilot trials the uptake efficiency and distribution in the lung of a complex formed from digoxigenin labeled oligonucleotides and chitosan-coated poly(lactide-co-glycolide) (PLGA) nanoparticles (nanoplexes) following inhalation. The aerosol of nanoplexes was produced and applied to the rat lung through a microsyringe needle directly placed into the bronchus of the lung. The rat lung was ventilated by negative pressure and perfused for about one hour at constant recirculating flow rate with a modified Krebs-Henseleit buffer supplemented with 2% bovine serum albumin. Perfusion parameters such as pulmonary artery pressure, pH of perfusion buffer, tidal volume, resistance and compliance were monitored continuously. Distribution of nanoplexes in the lung was assessed with a Mouse-anti-DIG antibody by immunohistochemical staining.

Results: Following the inhalation of the aerosol of nanoplexes digoxigenin labeled oligonucleotides could be detected in all different parts of the lung. However, the distribution was heterogeneous and exhibited local differences. During the preparation of the IPL and the inhalation experiment, rat lung structure and cells in the lung did not show any changes in their anatomical and physiological properties. The biological function of the lung was not altered.

Conclusion: An isolated perfused rat lung model was successfully applied to investigate the inhalative delivery of nanoplexes to the lung. Oligonucleotides transported by these nanoplexes could be localized throughout the complete lung. The inhalation of nanoplexes did not alter lung physiology.

6.2 Introduction

The respiratory delivery of drugs to the lungs by inhalation has been investigated extensively and employed to treat diseases primarily localized in the lung. The respiratory tract can be used for the direct delivery of drugs to the diseased area and the inhalation of a drug will result in a quick onset of action. It allows topical effects for the aerosolized administration of targeted drugs in lung cancer therapy.

Previously we have proved that delivery of an antisense oligonucleotide 2'-O-methyl-RNA (OMR) with chitosan-coated poly(lactide-co-glycolide) (PLGA) nanoparticles can induce efficient telomerase inhibition and telomere shortening in human non-small cell lung cancer (NSCLC) cells [Beisner *et al.*, 2010]. Nanoparticles mediated delivery of OMR by inhalation might offer a new mode for drug delivery in lung cancer therapy.

The present study was designed to use the isolated perfused rat lung (IPL) as a model to investigate the pulmonary delivery and distribution of nanoplexes consisting of oligonucleotides (OMR) and chitosan-coated PLGA nanoparticles after inhalative application of an aerosol. The aerosol was formed with a microsyringe needle connected to a high pressure syringe. The IPL model was modified from the method described by Uhlig *et al.* [Uhlig *et al.*, 1994]. The isolated lung was ventilated by negative pressure and was perfused at constant flow rate with recirculating buffer. Compared to other *in vitro* models, cells in the IPL are maintained in their "normal" anatomical and physiological environment and are not fragmented or dispersed. Therefore, transcellular transport and diffusion of agents are probably not altered [Niemeier, 1984]. This technique offers a versatile experimental system which supplements isolated organelle preparation [Rhoades, 1984] and allows the continuous assessment of lung mechanics [Uhlig *et al.*, 1994]. Using the microsyringe device to generate a homogenous aerosol with particle sizes of 16 to 22 μm the inhalative application of nanoplexes can be studied with this model.

6.3 Material and methods

6.3.1 Animals

Two male Wistar rats (Harlan, Horst, Netherlands) of 290g and 310g weight were used for the experiments. The rats were housed under controlled conditions with temperature 20-21°C, humidity 50-60%, light (12:12 light-dark rhythm) and free access to standard food (pellets) and tap water. The experiments were approved by the local authorities (Regierungspräsidium Tübingen, Germany).

6.3.2 Isolated perfused rat lung (IPL) preparation

Rats were anesthetized with ketamine (Ketavet[®], 100mg/kg body weight) and xylazine (Rompun[®], 10mg/kg body weight) by intraperitoneal (i.p.) administration. Heparin-sodium (500IE/100g) was injected i.p. to avoid blood clotting during the preparation.

After incision of the trachea and insertion of a tracheal cannula, positive pressure ventilation was started. Rats were exsanguinated by cutting the renal artery. Following cannulation of the pulmonary artery and the pulmonary vein, perfusion was started and the lung with trachea was carefully dissected together with the heart and suspended in a humidified glass chamber maintained at 37°C. Thereafter, perfusion was switched to recirculation (total recirculating volume: 270ml) with a flow rate of 20ml/min and ventilation was switched to negative pressure ventilation (70breaths/min, end-expiratory pressure: -2cm H₂O, end-inspiratory pressure -8 cm H₂O) with a deep insufflation (-20cm H₂O) every five minutes to avoid atelectasis of the peripheral airways.

The lungs were perfused through the pulmonary artery with filtered Krebs-Henseleit buffer at 37°C consisting of 118mM NaCl, 4.7mM KCl, 1.2mM KH₂PO₄, 1.2mM MgSO₄ (x 7 H₂O), 2.5mM CaCl₂ (x 2H₂O), 24.9mM NaHCO₃, 2% (w/v) albumin, 0.1% (w/v) glucose and 0.3% (w/v) HEPES. The pH of the perfusate was maintained between 7.3-7.4 by adding CO₂. Data on lung mechanics (breath rate, tidal volume, end-inspiratory pressure, end-expiratory pressure, compliance, resistance, flow rate and pH of the perfusate, pulmonary artery pressure) were monitored continuously. Signs of edema formation were checked by visual inspections. Perfusion apparatus and the electronic equipment were purchased from Hugo Sachs Elektronik-Havard Apparatus GmbH (March-Hugstetten, Germany).

6.3.3 Inhalation of nanoplexes

A digoxigenin-labeled antisense oligonucleotide OMR (Digo-OMR) with a phosphorothioate (ps) backbone 5'-2'-O-methyl [C(ps)A(ps) GUUAGGGUU(ps)A(ps)G]-digoxigenin-3' was used in this experiment (Biomers, Ulm, Germany). Certain amount of OMR was mixed with nanoparticles at ratio of 1:50 (weight _{oligonucleotide} / weight _{nanoparticles}) and incubated for 15min at 37°C to form Digo-OMR-nanoplexes. The process is described in detail in *Chapter 5: Materials and methods*.

Automatic breath was turned off after 15min equilibration. Respiratory rate was decreased to 30breaths/min for a short-term. A deep breath was activated manually; 100μl 0.9% NaCl solution was instilled through a microsyringe (Model IA-1C, with high pressure syringe model FMJ-250, PennCentury, INC., P.A., USA) during inspiration. Another deep breath was

initiated manually. Subsequently automatic breath was turned on and the respiratory rate was set back to 70 breaths/min. Ten minutes after NaCl application inhalation was repeated with 100 μ L of nanoplexes solution. The lung was perfused continuously for another 30min. At the end 4% buffered formalin was perfused into the lung for fixation and the lung was embedded in paraffin for the preparation of histological sections. Fig. 1 shows the schematic diagram of the IPL inhalation experiment.

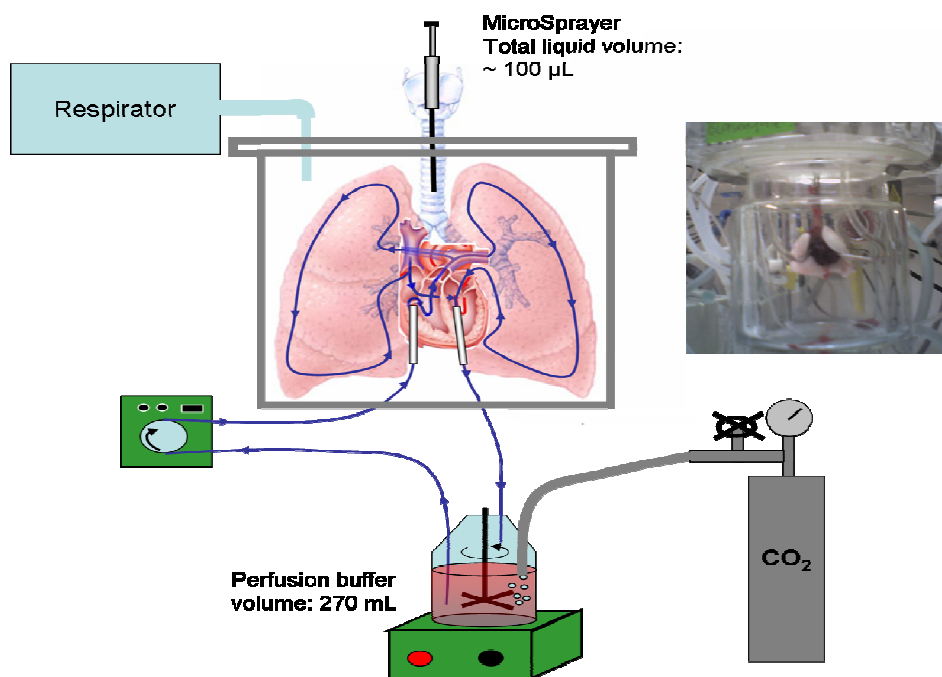


Fig.1: Schematic diagram of IPL inhalation

Arrows give the flow direction of perfusion buffer. The photo exhibits the rat lung with the trachea and the heart in a humidified glass apparatus.

6.3.4 Immunohistochemical staining

The paraffin fixed perfused lung tissues were cut in 3 μ m serial sections by Rotary Microtome (Leica RM2255, Germany) and epitope retrieval pretreatment was achieved by heating in epitope retrieval solution (ZytoVision, Bremerhaven, Germany). Immunohistochemical staining for Digo-OMR was performed using Mouse-anti-DIG antibody (ZytoVision, Bremerhaven, Germany) according to the manufacture's instructions. The images were taken by a DigitalMicroscope (Leica DM 4000B) and analyzed by Leica Application Suite V3 software. The details of the process are described in *Chapter 5: Materials and methods: Immunohistochemical staining*.

6.4 Results and discussion

Following the inhalation of an aerosol of nanoplexes rat lung structure and cells in the lung did not show changes in their anatomical and physiological properties. As the cover of the

perfusion cask was adapted for inhalation no continuous measurement of lung weight for the sensitive detection of oedema was feasible. However, the surface of the lung was uniformly white and no oedema formation was observed during the complete experiment.

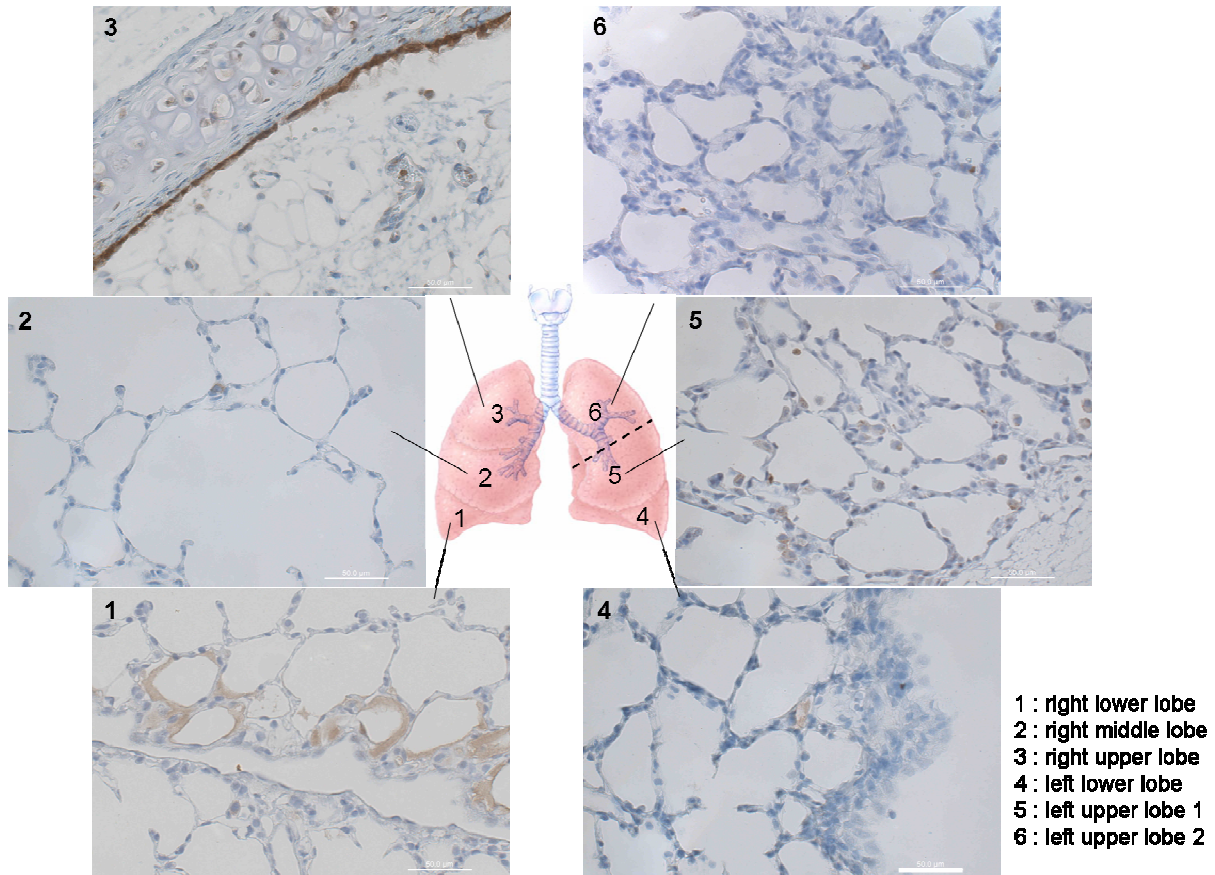


Fig.2: Localization of Digo-OMR-nanoplexes in rat lung visualized by immunohistochemistry (40× objectives)

Rat lung was divided into 6 parts according to the lobes and labelled from 1 to 6. The left upper lobe was cut into two parts (5 and 6) because of the large size. Images were marked with the corresponding numbers. Paraffin sections were stained with Mouse-anti-DIG antibody. Counterstaining was performed with hematoxylin. Scale bar represents 50 µm.

After inhalation Digo-OMR-nanoplexes (in brown colour) were observed in both parts of the rat lungs. However, the two parts did not exhibit similar localizations of Digo-OMR indicating that the distribution of nanoplexes following inhalation showed some differences. Fig.2 illustrates the detailed distribution of Digo-OMR-nanoplexes. Most of the nanoplexes were attached in form of a layer to the surface of bronchus, as shown in Fig.2-3. In the left upper lobe (Fig.2-5) numerous cells with positive signals can be seen. In the right lower lobe (Fig.2-1) positive signals can be observed on the inner surface of alveoli. This might be caused by the interaction of Digo-OMR-nanoplexes with the surfactant on the alveolar surface. Few signals were also found in other lobes indicating that the nanoplexes can reach almost the entire lung but with heterogeneous distribution. According to their morphology, cells

demonstrating an uptake of Digo-OMR-nanoplexes could be either macrophages or alveolar type II cells, but not alveolar type I cells. To identify exactly the cell type further immunohistochemical experiments are necessary.

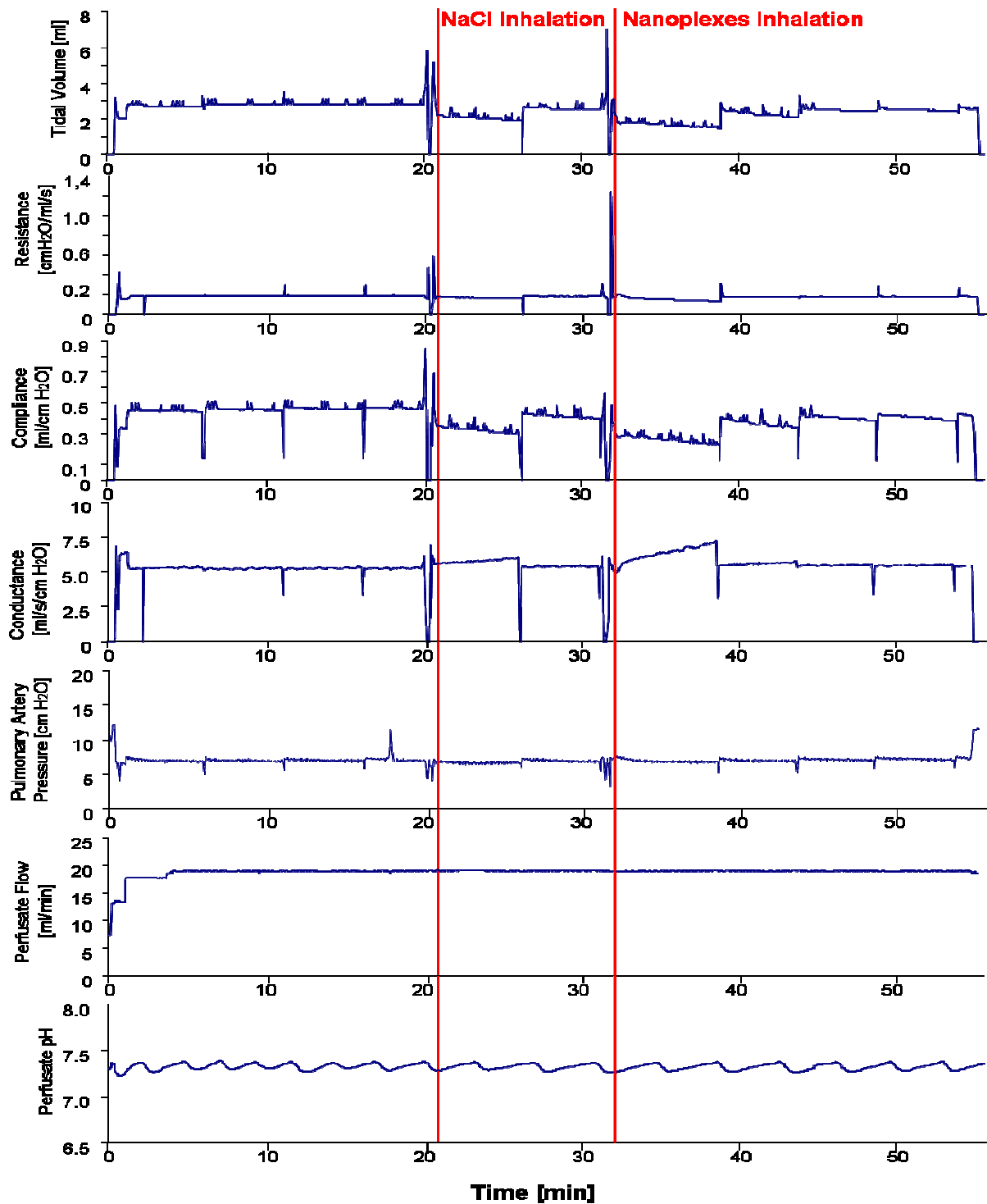


Fig.3: Time course of lung functions during perfusion of the IPL with inhalation of nanoplexes Red lines indicate the time when inhalation was applied. Aerosol of Digo-OMR-nanoplexes was administered for inhalation. The same amount of 0.9% NaCl solution was used as control for inhalation experiment.

The effects of the inhalation of nanoplexes on the physiology of the IPL are summarized in Fig.3. Lung perfusion requires a continuous exchange of medium within the vascular bed. As a marker of gas exchange, the biological function of the lung and pH changes were monitored continuously. Following the inhalation of 100µl of physiological saline the rate of pH increase was slightly decreased. This indicated a decreased capability of the lung to exhale carbon dioxide. Following the application of nanoplexes no further alteration of the pH profile was observed. Immediately after the inhalation of both, saline and nanoplexes, there was some decrease in tidal volume and compliance. However, both parameters recovered after subsequent deep breaths (Fig.3). Flow rate of the perfusion buffer was kept constant during the perfusion experiment. Constant pulmonary artery pressure indicated that there was no change in the vascular structure during IPL.

Proper ventilation is very critical in the perfused lung; it provides the physiologic route for oxygenation. After the lung and heart was suspended in a sealed glass chamber negative pressure ventilation was applied. Positive pressure ventilation may cause destruction of lung architecture by overinflation followed by oedema formation and progressive atelectasis. Negative pressure ventilation is preferable since it can mimic more closely the *in vivo* situation [Uhlig *et al.*, 1994].

The changes of the functional parameters around the time of inhalation (peaks next to the red lines in Fig.3) are caused by the two manually activated deep breaths before and after the inhalation in combination with the manipulations at the air inlet to introduce the microprayer needle. More experiments are needed to confirm the results of the pilot trials and to further investigate the biological function of the telomerase inhibitor OMR delivered by nanoparticles through inhalation in lung cancer patients.

6.5 Conclusion

An isolated perfused rat lung model was successfully used to investigate the inhalative delivery of nanoplexes to the lung. Topical uptake of oligonucleotides transported by these nanoplexes could be localized throughout the complete lung. The inhalation of nanoplexes did not impair pulmonary physiology.

Chapter 7

Proliferation Marker KI67, Human Telomerase Reverse Transcriptase (hTERT), Stem Cell Marker CD133 Expression and Telomerase Activity in Non-Small Cell Lung Cancers

7.1 Abstract

Background: Previous studies have shown that telomerase activity is detected in about 80% of non-small cell lung cancers (NSCLC) and correlated with a poor prognosis. Cancer stem cells should have telomere-lengthening mechanisms to maintain their replicative ability. Therefore tumors may arise from telomerase-positive stem cells. It is still not known if CD133 is an appropriate marker of organ-specific cancer stem cells or not. The telomerase dynamics in cancer stem cells also remain unclear. The aim of this study was to determine whether in NSCLC relationships exist between telomerase activity, tumor proliferation (KI67 expression), cellular expression of hTERT, and cancer stem cell population (CD133 expression).

Methods: Thirty one primary NSCLC and 9 lung metastases from 40 patients (27 males, 13 females) were analyzed. Telomerase activity of fresh tumor tissue was measured with a real time PCR based telomeric repeat amplification protocol (Q-TRAP). Paraffin sections were stained for hTERT, proliferation marker KI67 and stem cell marker CD133, and their interrelations were analyzed.

Results: Telomerase activity was present in 29 (93.5%) of the 31 primary NSCLC and 8 (89%) of the 9 lung metastases. Similar telomerase activity levels were detected between lung metastases and primary lung cancers. Metastases showed a trend of higher KI67 expression. No significant correlations were found in the expression of KI67, hTERT and CD133. There was a tendency that CD133 expression was correlated inversely with telomerase activity.

Conclusion: The CD133 positive cells may show downregulation of telomerase activity. Significant correlations were not found in the expression of KI67, hTERT and CD133. Larger sample sizes and further research are required to identify cancer stem cells and to understand better the relationship between cancer stem cells and telomerase activity.

7.2 Introduction

Lung cancer is the most common cause of cancer-related mortality all over the world. Non-small cell lung cancer (NSCLC) is the most frequent form and constitutes approximately 80% of all lung cancers. The NSCLC includes adenocarcinoma, squamous cell carcinoma, adeno-squamous carcinoma and large cell carcinoma.

Previous studies have shown that telomerase activity was detected in more than 80% of NSCLC and correlated with a poor prognosis [Taga *et al.*, 1999]. Human telomerase contains two major components: the catalytic protein subunit human telomerase reverse transcriptase (hTERT) replicating the ends of linear DNA, and the human telomerase RNA (hTR) that provides the template for the synthesis of human telomeric repeats [Feng *et al.*, 1995; Nakamura *et al.*, 1997]. It has been reported that hTERT and functional telomerase are both located primarily in the nucleolus [Smith *et al.*, 2004]. Kyo S *et al.* found that functional hTERT was expressed in both the nucleus and cytoplasm of cancer cells and hTERT expression did not strictly reflect telomerase activity [Kyo *et al.*, 2003]. Therefore we analyzed hTERT expression at the cellular level in lung cancer specimens by immunohistochemistry and compared it to telomerase activity from the same sample by a modified TRAP assay using real-time quantitative PCR. KI67 is a marker for cell proliferation which is present in the nucleus of proliferating cells [Cattoretti *et al.*, 1992]. KI67 was demonstrated to have a weak correlation with hTERT expression [Smith *et al.*, 2004] and telomerase activity [Albanell *et al.*, 1997].

Cancer stem cells have been isolated from various tissues and cell lines [Singh *et al.*, 2003; Al-Hajj *et al.*, 2003; Tirino *et al.*, 2009]. The cancer stem cell theory suggests that a rare fraction of cells with stem cell properties can drive tumorigenesis [Reya *et al.*, 2001]. The failure of current cancer therapies may be due to the inefficacy of drugs on cancer stem cells [Dean *et al.*, 2005]. Therefore the identification of cancer stem cells is very important for targeted cancer therapy. A variety of stem cell markers have been applied to differentiate cancer stem cells from solid tumors. These markers include CD34, CD133 and CD24 coupled with migration molecules such as CD29, CD44, integrin $\alpha_2\beta_1$ and CD31 [Collins *et al.*, 2001; Tirino *et al.*, 2009]. Hoechst 33342 dye was also used to isolate side population cells which have distinguishing biological characteristics from the main population as a different approach [Brown *et al.*, 2007]. CD133 is a membrane glycoprotein with unknown biological function. It is suggested to be a stem cell marker for normal and cancer tissues [Shmelkov *et al.*, 2008]. It has been used for the identification and isolation of cancer stem cell populations

from malignant tumors of liver [Suetsugu *et al.*, 2006], brain [Singh *et al.*, 2003; Singh *et al.*, 2004], prostate [Collins *et al.*, 2005], pancreas [Hermann *et al.*, 2007], colon [O'Brien *et al.*, 2007] and lung [Eramo *et al.*, 2008]. Cancer stem cells should have telomere-lengthening mechanisms to maintain their replicative ability. However, the identification and purification of cancer stem cells are difficult in most solid tumors. In addition, telomere and telomerase dynamics in cancer stem cells remain unclear [Hiyama *et al.*, 2007]. Armanios M *et al.* suggested that tumors may arise from telomerase positive stem cells [Armanios *et al.*, 2005]. However it was reported that CD133 was not a selective marker of organ-specific stem and progenitor cells [Shmelkov *et al.*, 2008]. Shervington A *et al.* found that telomerase activity is downregulated in cancer brain stem cells which express CD133. Therefore to identify cancer stem cells and to understand their relationships with telomerase activity are crucial for a more effective anti-cancer therapy.

The aim of this study was to determine in NSCLC whether relationships exist between telomerase activity, tumor proliferation (KI67 expression), cellular expression of hTERT, and cancer stem cell populations (CD133 expression).

7.3 Material and methods

7.3.1 Tissues collection

Fresh lung tumor tissues were obtained at the time of surgery from 40 patients (27 males, 13 females; age range 36-88 years) newly diagnosed for lung cancer at the Klinik Schillerhöhe. Immediately after surgical resection, the main portion of tumor tissues were fixed in formalin and sent to pathology for further diagnosis. The remaining parts were snap-frozen with liquid nitrogen and stored at -80°C for analysis. The investigation was approved by the local ethics committee (# 396/2005V) and informed consent was obtained from the patients.

7.3.2 Telomerase activity measurement of lung cancer tissues

For each tissue specimen, one piece (50 to 100mg) was taken for determination of telomerase activity. Tissue pieces were isolated by FastPrep methods as described in *Chapter 2: Part1: Materials and methods: Preparation of tumor tissue extracts*. Telomerase activity was measured using a modified real-time quantitative PCR based telomeric repeat amplification protocol (Q-TRAP) assay as described previously [Herbert *et al.*, 2006]. The detailed process is described in *Chapter 2: Part1: Materials and methods: Telomerase activity assay using real-time quantitative PCR*. The cutoff value for Q-TRAP assay was set as 0.01 (compared to

the activity of 1µg protein from NSCLC cell line A549 cells). The Q-TRAP result was considered as telomerase positive if the value was greater than 0.01.

7.3.3 Immunohistochemical staining

The paraffin fixed tissues were cut in 3 µm serial sections by Rotary Microtome (Leica RM2255, Germany) and stained with hematoxylin and eosin (HE) for histopathological examination. Immunostaining for KI67 (1:75, Monoclonal Mouse Anti-human KI67 Antigen, Clone MIB-1, Dakocytomation, Glostrup, Denmark), human telomerase reverse transcriptase (hTERT, 30µg/ml, Rabbit Anti-hEst2 IgG, Alpha Diagnostic International, San Antonio, TX) and CD133 (1:10, Monoclonal Mouse Anti-human CD133/1 (AC133) pure antibodies, Miltenyi Biotec, Bergisch Gladbach, Germany) were performed using the Dako REAL™ Envision™ Kit (EnVision, Dako, Glostrup, Denmark) according to the manufacturer's manual. A heat-induced epitope retrieval technique was employed as following: prior to staining for KI67 and CD133, sections were treated in a steam heater for 30 min with pH6.0 citric acid buffer (Dako, Glostrup, Denmark). For hTERT staining, sections were treated in a pressure cooker for 15 min with pH 9.0 Tris/EDTA buffer (Dako, Glostrup, Denmark). The detailed process of immunohistochemical staining is described in *Chapter 5: Part1: Materials and methods: Telomerase activity assay using real-time quantitative PCR*.

7.3.4 Scoring methods

Images of immunohistochemical staining were taken by a 40× objective with Digital Microscope (Leica DM 4000B) and analyzed by Leica Application Suite V3. For each sample, cells were counted from at least 4 randomly selected fields. The ratio of positive cells was calculated as the percentage of positively stained cells related to total cells.

7.3.5 Statistical analysis

GraphPad Prism Software Version 4.0 (GraphPad Prism Incorp., San Diego, CA, USA) was used for statistic analysis. The Spearman correlation test was applied to measure associations between telomerase activity and expressions of KI67, hTERT, CD133.

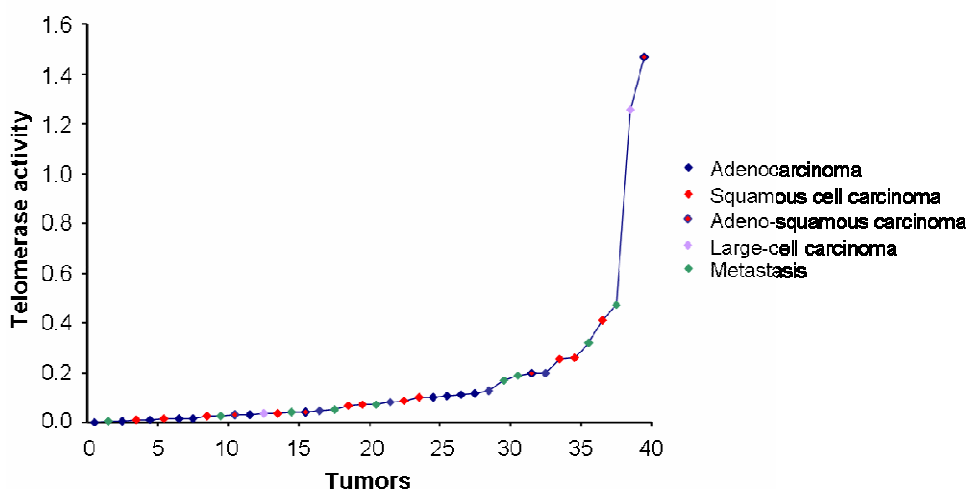
7.4 Results

7.4.1 Telomerase activity and histopathology of lung tumors

In 40 specimens, there were 31 primary NSCLC and 9 lung metastases from different origins. Telomerase activity was detected in 29 (93.5%) of the 31 primary NSCLC and in 8 (89%) of the 9 lung metastases. Some details are summarized in Table1.

Table 1. Comparison of tumor histology with telomerase activity in primary NSCLC and lung metastasis

Histology	Tumors numbers	Telomerase activity		
		Negative	Positive	% positive
Adenocarcinoma	14	2	12	85.7
Squamous cell carcinoma	11	1	10	90.9
Adeno-squamous carcinoma	4	0	4	100
Large-cell carcinoma	2	0	2	100
Metastasis	9	1	8	88.9

**Fig. 1: Telomerase activity of primary NSCLC (Adenocarcinoma, Squamous cell carcinoma, Adeno-squamous carcinoma and Large-cell carcinoma) and lung metastasis**

(Each point represents an individual tumor sample)

Telomerase activities of all 40 analyzed lung tumor specimens are illustrated in Fig.1. The level of telomerase activity was in the range of 0.001 to 1.469 with an average value of 0.166 (compared to the activity of 1 μ g protein of A549 cells). There was no significant difference among different lung tumor types. The telomerase activity of metastasis exhibited a similar distribution as primary lung cancers as shown in Fig.1. and Fig.3 (A).

7.4.2 Relationships between telomerase activity and expressions of KI67, hTERT and CD133

Fig. 2 illustrates the histological examination of paraffin embedded lung cancers of different tumor types and the cell proliferation in lung tumors analyzed as KI67 expression. Nuclear hTERT expression was detected by immunohistochemistry using an affinity purified antibody which binds to a 16 amino acid peptide sequence within hTERT. Although cancer stem cell marker CD133 is a 120kDa membrane glycoprotein, positive staining was not only observed on the cell membrane but also in both nucleus and cytoplasm (see Fig. 2-CD133).

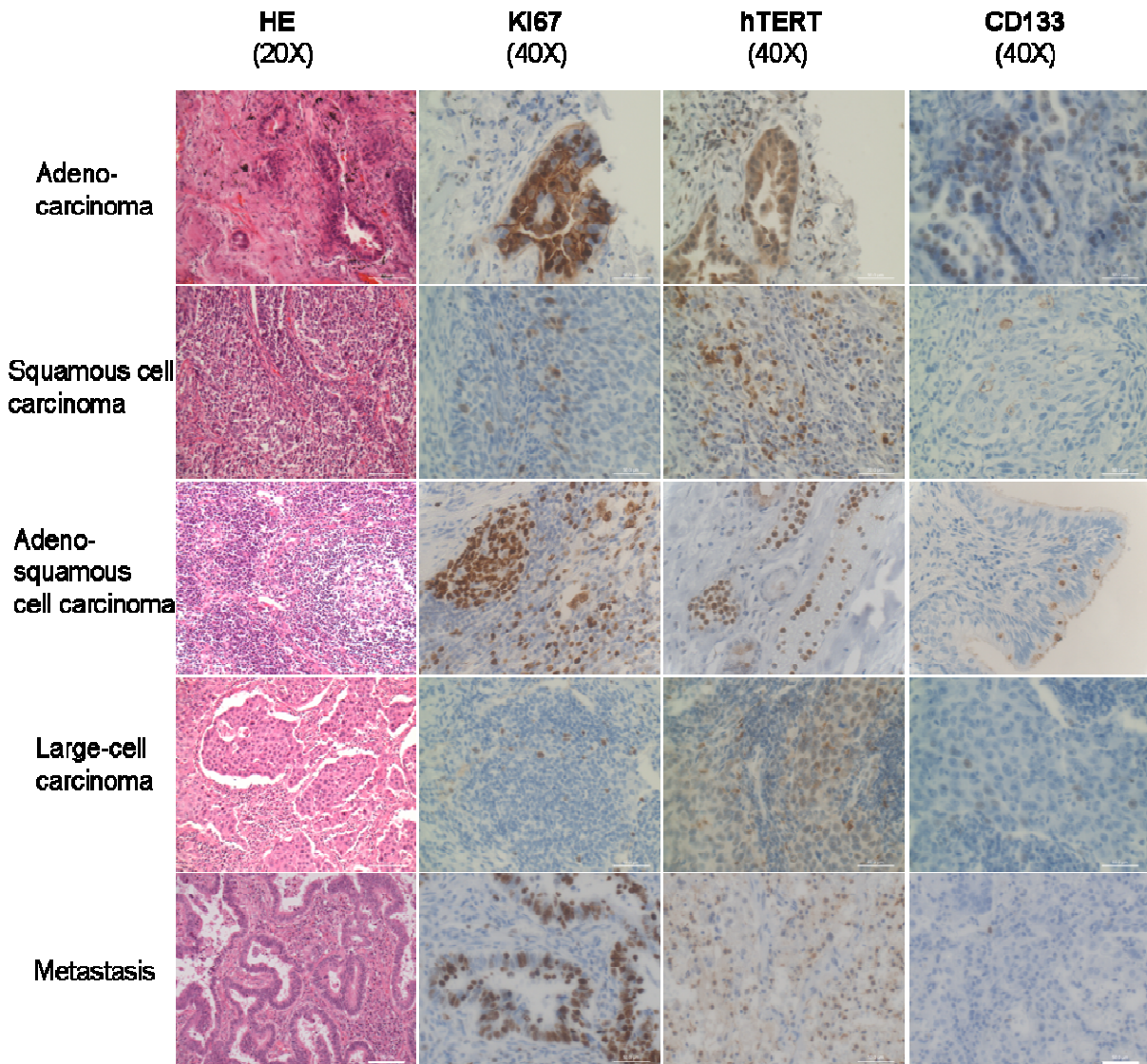


Fig. 2: HE staining (20× objectives) and immunohistochemistry (40× objectives) of KI67, hTERT and CD133 expression in NSCLC

Scale bars represent 100µm in 20× objectives and 50µm in 40× objectives.

Positive KI67 expression with nucleus localization was found in all tumors with a range of 2.4% to 49.6% (Fig. 3B). Metastasis showed a trend of higher KI67 expression but no significant differences were observed. In primary NSCLC cells and lung metastasis cells hTERT immunostaining was clearly visualized in both nucleus and cytoplasm (range: 4.5% - 36.2%). Expressions of KI67 and hTERT were not related to tumor types. Only 35% of primary lung cancers (range: 0.12%-34.7%) and 33% of lung metastases (range: 1.3% - 12.3%) showed positive immunostaining of CD133. As shown in Fig. 3D, CD133 exhibited a trend of lower expression in lung metastasis but this did not reach statistical significance.

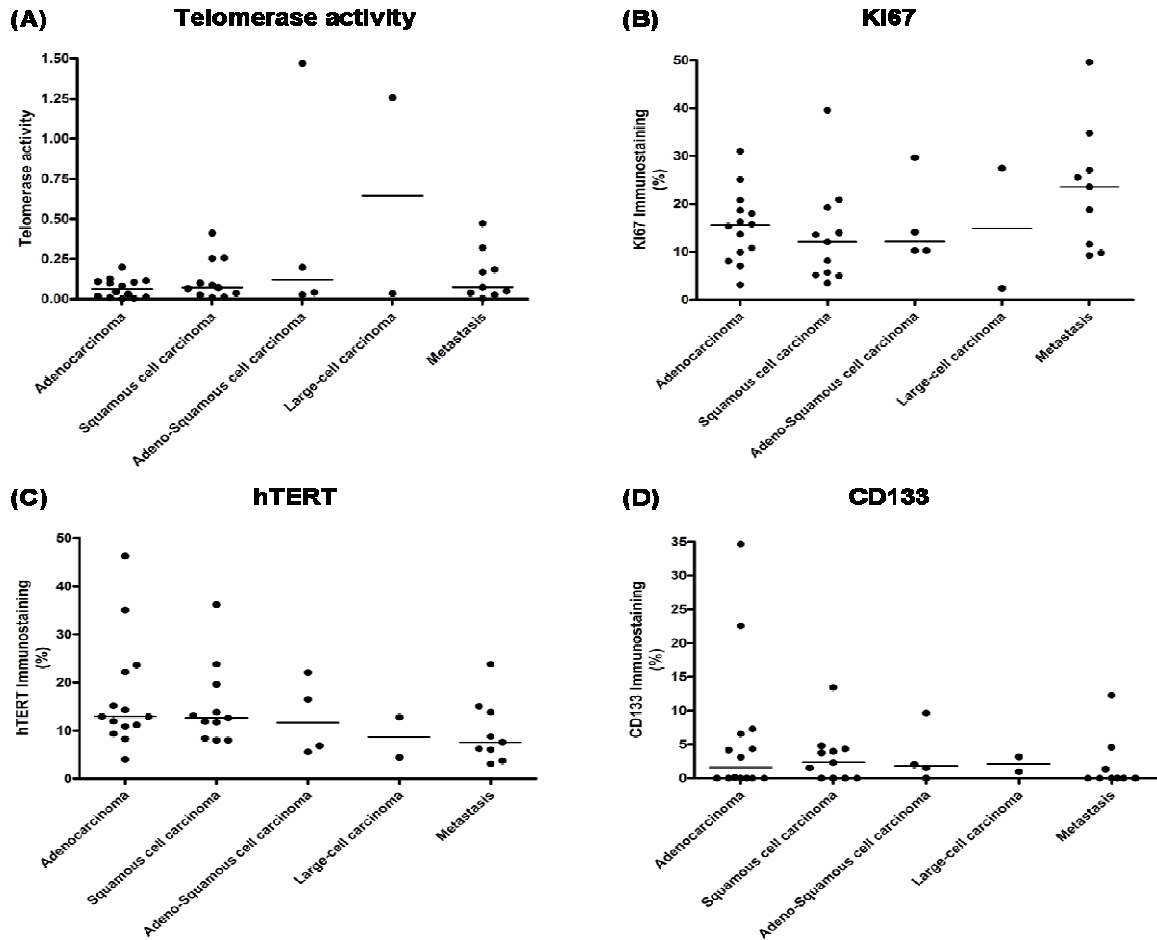


Fig. 3: Telomerase activity (A) and KI67 (B), hTERT (C), CD133 (D) immunostaining quantification in NSCLC and metastasis (The horizontal lines indicate the medians of the samples)

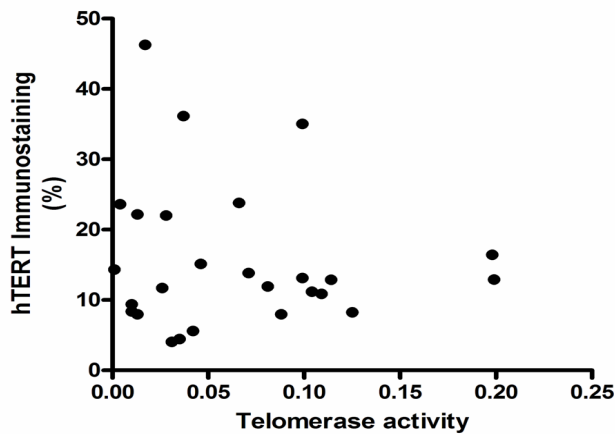


Fig. 4: Relationship between hTERT immunostaining and telomerase activity in primary NSCLC

No significant correlation was found between hTERT expression and telomerase activity in 31 primary NSCLC specimens (Fig.4), indicating that hTERT expression assessed by immunostaining may not represent telomerase activity. Likewise, no significant correlations could be found between the expression of KI67, hTERT or CD133; telomerase activity and KI67 staining also did not show a significant correlation.

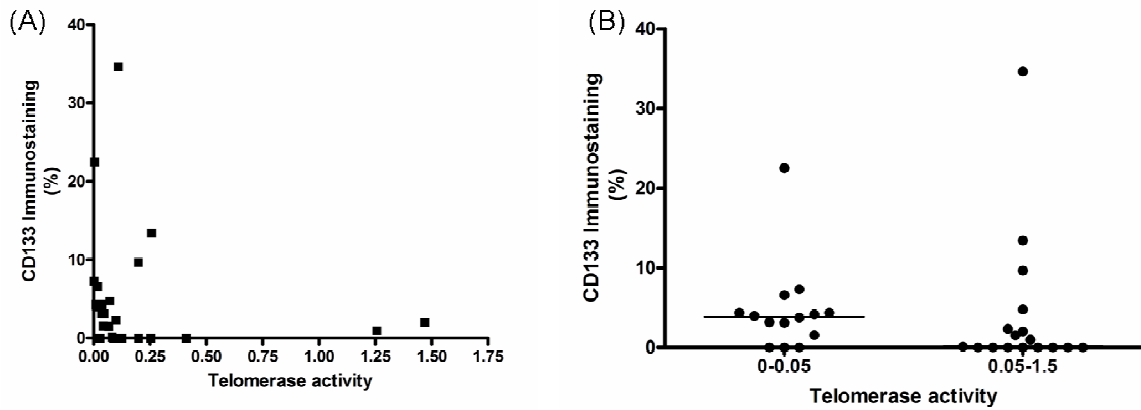


Fig. 5: Relationship between CD133 immunostaining and telomerase activity (A); distribution of CD133 immunostaining according to levels of telomerase activity (B) in primary NSCLC
(The horizontal lines indicate the medians of the samples)

An inverse trend ($r = -0.32$, $p = 0.079$) was detected between CD133 expression and telomerase activity (Fig. 5A). This finding was supported by separating CD133 expression into two groups according to low (0-0.05) and high (0.05-1.5) levels of telomerase activities. The group with high telomerase activity level showed lower CD133 expression (median: 0.12%) if compared to the group (median: 3.86%) with low telomerase activity level (Fig. 5B). Positive CD133 expression was found in 79% of tumors of the low telomerase activity level group and in 53% of the high telomerase activity level group. This might indicate if CD133 is the appropriate marker for cancer stem cells, these cells would have lower telomerase activity.

7.5 Discussion

Telomerase activity is detected in most tumor tissues and has been considered as a potentially diagnostic marker for tumor progress. Albanell J *et al.* reported that telomerase activity was detected in 84.8% of primary NSCLC [Albanell *et al.*, 1997]. In our study, telomerase activity was detected in 93.5% of the primary NSCLC specimens. This higher value can be explained by the modified Q-TRAP assay which we used for measurements of telomerase activity. The highly sensitive and specific new method can avoid end-point PCR problems and provides linear telomerase detection down to much lower levels than with the old assays. Specimens with lower than 0.010 (compared to the activity of 1 μ g protein of A549 cells) telomerase activity were defined as telomerase negative. Therefore the percentage of positive telomerase activity of NSCLC has been increased.

KI67 is a proliferation associated antigen that is present only in proliferating cells. Immunological detection of KI67 is a useful method for detecting cellular proliferation in tissue samples [Cattoretti *et al.*, 1992]. Telomerase activity was significantly associated with

KI67 expression in breast cancer [Mokbel *et al.*, 1999], psoriasis lesional skin [Jang *et al.*, 2001], malignant melanomas [Miracco *et al.*, 2000] and primary NSCLC [Albanell *et al.*, 1997]. In our study we did not observe a statistically significant correlation between telomerase activity and KI67 expression. This could be due to the small sample size or the heterogeneous nature of tumor samples.

hTERT represents the catalytic subunit of telomerase. The expression of hTERT has important implications in cancer diagnostics and prognostics [Hiyama *et al.*, 2001] and in human cancer tissues it correlated with telomerase activity [Hiyama *et al.*, 2001]. A weak association between hTERT and KI67 expression was found in patients with curative resection of hepatic colorectal metastases [Smith *et al.*, 2004]. In our study, no significant correlation was detected between hTERT expression and telomerase activity, or between the expressions of hTERT and KI67 in 31 primary NSCLC specimens. These negative findings might be due to the small sample size. Smith DL *et al.* suggested that nucleolar hTERT expression was a good reflection of functional telomerase activity. On the contrary, Kyo S *et al.* reported that functional hTERT was expressed in both the nucleus and cytoplasm of cancer cells and hTERT expression did not always reflect telomerase activity. Our results demonstrated that both nucleus and cytoplasm had strong hTERT expression in lung cancer specimens. Therefore our results confirm the theory of Kyo S *et al.* that hTERT expression does not always reflect telomerase activity.

Recently, several studies indicated that a small population of cancer stem cells in tumors were responsible for tumor maintenance and spreading [Eramo *et al.*, 2008; Singh *et al.*, 2004]. CD133 antibody has been used for the identification and isolation of cancer stem cell population from malignant tumors. We found that only about 30% of lung tumor specimens showed a CD133 positive staining. This result is in agreement with the general concept that cancer stem cells are expressed in a very small percentage of the total tumor cell population [Tirino *et al.*, 2009].

It has been reported that cancer stem cells express high telomerase activity [Hiyama *et al.*, 2007]. According to our initial hypothesis we tried to identify in lung cancer specimens a correlation between CD133 and telomerase activity. However, we could only find a trend for an inverse correlation between CD133 expression and telomerase activity which most likely can be explained by the small sample size. Telomerase activity was downregulated in cancer brain stem cells which express CD133 [Shervington *et al.*, 2009]. During differentiation cells proliferate and telomerase activity is upregulated. So non-differentiated CD133 positive

(CD133+) cells exhibit low telomerase activity. This might explain our results that the specimens with high telomerase activity exhibited low CD133 expression. Shmelkov SV *et al.* suggested that CD133 is not a specific marker of organ-specific stem and progenitor cells as both CD133+ and CD133- metastatic colon cancer cells initiate tumors. Meng X *et al.* reported both, CD133+ and CD133- subpopulations of lung cancer cell lines A549 and H446 cells contain cancer-initiating cells. Therefore CD133 may not be a reliable marker for cancer stem cells in lung tumor specimens. Consequently, either CD133 is not the perfect marker for cancer stem cells or cancer stem cells have very low telomerase activity.

High telomerase activity was correlated with poor prognosis in gastric cancer [Hiyama *et al.*, 1995], breast cancer [Kim *et al.*, 1996] and neuroblastoma [Hiyama *et al.*, 1995]. In NSCLC high telomerase activity was associated with increased cell proliferation and advanced pathologic stage [Albanell *et al.*, 1997]. More investigations are needed to clarify the relationship between telomerase activity and prognosis in NSCLC. In such studies lymph node metastasis and survival data should be also considered.

7.6 Conclusion

In 40 lung tumor specimens no significant correlations were found between the expression of KI67, hTERT and CD133. Lung tumor metastasis showed a trend of higher KI67 expression. The weak inverse relation between CD133 expression and telomerase activity suggests that CD133 positive cells are associated with low telomerase activity. Larger sample sizes and further research are required to better understand the relationships between different markers of cancer stem cells and telomerase biology.

Chapter 8

Summary and Outlook

The experiments presented in this thesis focus on the inhibition of telomerase to provide data whether this approach is suitable for non-small cell lung cancer (NSCLC) therapy. An antisense oligonucleotide 2'-O-methyl-RNA (OMR) was used as a specific telomerase inhibitor. Several strategies were tested to deliver OMR to its target site in different models based on cell cultures, tissue slices and an isolated perfused rat lung.

Telomerase activity and telomere length are the two biomarkers to evaluate the therapeutic potential of telomerase inhibitors. The real-time quantitative PCR based assays for measuring these two parameters were optimized to provide specific and quantitative data of various biological materials. Compared to current techniques, the new methods permit rapid and accurate analysis for large sample sets.

In NSCLC A549 cells, five commercial available transfection reagents (DOTAP, MegaFectin 60, SuperFect, FuGENE 6 and MATra-A) were tested for cellular uptake of OMR and telomerase inhibition. The cationic lipid DOTAP displayed a relatively higher transfection efficiency, a lower cytotoxicity and stronger telomerase inhibition if compared to the other four reagents. Furthermore, biodegradable and chitosan-coated poly(lactide-co-glycolide) (PLGA) nanoparticles were applied for delivering OMR into human lung cancer cells. Positively charged nanoparticles can form nanoplexes with the negatively charged OMR and can be taken up by cells. In the cells OMR was released and specifically blocked the telomerase RNA template region. In human NSCLC cell lines the nanoparticle delivery of OMR induced efficient telomerase inhibition. Telomerase activity was continuously reduced by approximately 80% and telomeres were shortened about 50% during long-term (102 days) treatment. Nanoplexes did not exhibit acute cytotoxicity in NSCLC cell lines and had almost no influence in primary lung fibroblasts.

Freshly isolated primary lung cancer cells represent much better biological model related to the original tumors. However, they are very sensitive to culture conditions and environmental changes. Therefore these cells need to be treated with a reduced amount of nanoparticles to avoid toxicity. Telomerase activity was inhibited by about 40% 72h after treatment. Cell morphology, cell-cell or cell matrix interactions are different in isolated cells compared to tissues and therefore experiments with isolated cells have several limitations if used as models

for *in vivo* tumors. The *ex vivo* tissue slice model can overcome these problems presenting a suitable system to evaluate drug response in tumors.

In tissue slice model, tumor microenvironment and integrity of the tumor-stroma interaction will be preserved. In this model 0.2 mm thick tissue slices were freshly excised from tumor samples of NSCLC patients. We could prove that OMR-nanoplexes can penetrate into tumor tissue, transfected tumor cells in their natural environment, and delivered the telomerase inhibitor OMR to its target. Furthermore, the released OMR could inhibit telomerase activity by about 40%. Tissue architecture, cell proliferation and telomerase expression were not influenced. However, due to the short survival time of tissue slices (about 4 days) no biological response can be expected. A long-term *in vivo* experiment using a tumor xenograft model is recommended to investigate such effects.

An isolated perfused rat lung (IPL) model is one step closer to the *in vivo* situation especially for the inhalative delivery of nanoplexes. An IPL was used to investigate the delivery and distribution of an inhaled aerosol of OMR-nanoplexes. The aerosol was produced and applied through a microsyringe needle directly connected to the bronchus of the lung. Following the inhalation OMR-nanoplexes could be detected within the entire lung. The nanoplexes did not alter lung physiology.

The cancer stem cells theories suggest that cancers may arise from a rare subpopulation of stem cell-like tumor cells and they are responsible for the failure of current cancer therapies. Cancer stem cells present a novel target for anticancer therapy. Therefore, it was tested whether in NSCLC relationships exist between telomerase, and markers of tumor proliferation or for cancer stem cell populations. In 40 tumor samples of patients with NSCLC no significant correlations between these factors could be found. Only stem cell marker CD133 positive tumor cells showed a trend for downregulation of telomerase activity. Large samples sizes or more reliable stem cell markers are probably required to identify cancer stem cells and to better understand their relationship to telomerase activity.

This thesis provides evidence that telomerase inhibitors delivered by nanoparticles have a considerable potential for *in vivo* application of anticancer therapy. Inhaled nanoplexes might be suitable agents for the topical treatment of lung cancer.

Chapter 9

Zusammenfassung und Ausblick

Die in dieser Arbeit vorgestellten Experimente konzentrierten sich auf die Hemmung der Telomeraseaktivität für die Therapie des nichtkleinzellig Lungenkarzinoms (NSCLC). Als spezifischer Telomeraseinhibitor wurde ein Antisense Oligonukleotid 2'-O-methyl-RNA (OMR) eingesetzt. Verschiedene Strategien wurden getestet, um OMR an seinen Wirkort zu bringen. Dazu wurden Modelle eingesetzt, die auf immortalisierten Zelllinien, viablen Gewebeschnitten und isoliert perfundierten und ventilierten Rattenlungen basieren.

Telomerase-Aktivität und Telomerlänge sind die beiden Biomarker zur Bewertung des therapeutischen Potenzials. Die auf Echtzeit-quantitativer Polymerase-Kettenreaktionen basierten Methoden zur Messung dieser zwei Parameter wurden optimiert, um spezifische und quantitative Daten von verschiedenen biologischen Materialien zu liefern. Im Vergleich zu den Standardtechniken ermöglichen diese neuen Methoden schnellere und genauere Analysen für große Stichprobenmengen.

In NSCLC-Zellen A549 wurden fünf Transfektionsreagenzien (DOTAP, MegaFectin 60, SuperFect, FuGENE 6 und Matra-A) für die zelluläre Aufnahme der OMR und die Auswirkungen auf Hemmung der Telomerase getestet. Das kationische Lipid DOTAP zeigte die höchste Transfektionseffizienz, niedrigere Zytotoxizität und stärkere Telomeraseinhibition im Vergleich zu den anderen vier Reagenzien. Außerdem wurden die biologisch abbaubaren, mit Chitosan beschichteten Polylaktat-coglykolat- (PLGA) Nanopartikel für die Aufnahme von OMR in humane Lungenkarzinomzellen untersucht. Die positiv geladenen Nanopartikel können mit der negativ geladenen OMR Komplexe (Nanoplexe) bilden, die von Zellen aufgenommen werden. OMR werden in den Zellen aus den Nanoplexen freigegeben und binden an die RNA-Untereinheit der Telomerase. Durch Nanopartikel in die Tumorzellen eingeschleuste OMR hemmte die Telomerase effizient. Wiederholte Behandlung mit Nanoplexen über 102 Tage reduzierte die Telomerase-Aktivität in A549 Zellen kontinuierlich um 80% und verkürzte die Länge der Telomere auf etwa 50%. Nanoplexe zeigten eine nur sehr geringe akute Cytotoxizität. Darüber hinaus hatte diese Behandlung auf die Viabilität von primären Fibroblasten, die aus humanen Lungengewebe isoliert wurden, keinen Einfluss.

Im Vergleich zu Zelllinien repräsentieren frisch isolierte primäre Lungenkrebszellen besser die biologischen Eigenschaften der ursprünglichen Tumoren. Allerdings sind sie schwierig zu kultivieren und reagieren empfindlich auf die Kulturbedingungen und Veränderungen der Umwelt. Deshalb wurden diese Zellen mit einer verringerten Menge an Nanopartikeln behandelt (Gewicht Oligonukleotid / Gewicht Nanopartikel 1:50). 72 Stunden nach dem Experiment war die Telomerase-Aktivität im Mittel zu 60% gehemmt. Zellmorphologie, Zell-Zell und Zell-Matrix-Interaktionen sind in den isolierten Zellen unterschiedlich im Vergleich zum ursprünglichen Gewebe. Deshalb ist die Übertragbarkeit von Experimenten mit isolierten Zellen auf *in vivo* Tumoren limitiert. Die *ex vivo*

Kultivierung viabler Schnitte von Tumorgewebe kann solche Probleme überwinden und ist ein geeignetes System, die Reaktion von Tumorzellen auf eine medikamentöse Behandlung im Gewebeverband zu evaluieren.

Im Gewebeschnittmodell werden Tumor-Mikroumgebung und die Integrität der Tumor-Stroma Interaktion bewahrt. Hierfür wurden 0,2 mm dicke Gewebeschnitte frisch aus Tumorproben von NSCLC-Patienten hergestellt. Wir konnten weisen, dass OMR-Nanoplexe in das Tumorgewebe vordringen, Tumorzellen in ihrer "natürlichen" Umgebung transfizieren und die Telomerase um ca. 40% hemmen können. Architektur des Gewebes, Zellproliferation und Expression der Telomerase wurden nicht beeinflusst. Aufgrund der kurzen Beobachtungszeit von 4 Tagen sind bei der Gewebekultur jedoch keine biologische Reaktion zu erwarten. Um diese zu untersuchen, werden *in vivo* Experimente mit einem Tumor Xenograft Modell empfohlen.

Insbesondere für die Untersuchung einer inhalativen Applikation ist das Modell der isoliert perfundierten und beatmeten Rattenlunge einen Schritt näher an der *in vivo* Situation. Dieses Modell wurde erfolgreich eingesetzt, um die Aufnahme und Verteilung des inhalativen Aerosols von OMR-Nanoplexen zu untersuchen. Das Aerosol wurde mittels einer direkt in die Bronchien der Lunge eingeführten Microsprayer-Nadel erzeugt. Nach der Inhalation konnten OMR-Nanoplexe in der gesamten Lunge detektiert werden. Die Inhalation von Nanoplexen beeinflusste die Lungenphysiologie nicht.

Die Stammzellen-Theorien besagen, dass Krebserkrankungen aus einer seltenen Subpopulation von stammzellartigen Tumorzellen entstehen können und diese für das Versagen der gegenwärtigen Krebstherapien verantwortlich sind. Daher kommen Krebsstammzellen in den Fokus für neue Therapiestrategien. Deswegen wurde getestet, ob in NSCLC eine Beziehung zwischen Telomerase, und Markern der Tumorphiliferation oder Markern für Tumor-Stammzellen bestehen. In 41 Tumorproben von Patienten mit NSCLC wurde keine signifikante Korrelation zwischen diesen Faktoren gefunden. Tumorzellen, die positiv für den Stammzellmarker CD133 waren, zeigten eine Tendenz zur geringeren Expression von Telomerase. Es sind wahrscheinlich große Probenmengen oder besser Stammzellmarker erforderlich, um Krebsstammzellen zu identifizieren und die Beziehung zwischen Krebsstammzellen und Telomeraseaktivität besser zu verstehen.

Die hier beschriebenen Experimente geben klare Hinweise darauf, dass die durch Nanopartikel unterstützte Behandlungsverfahren mit Telomeraseinhibitoren auf Oligonukleotid-Basis ein großes Potenzial für die *in vivo* Anwendung in der Krebstherapie haben. Inhalative verabreichte Nanoplexe könnten ein geeignetes Mittel zur topischen Behandlung von Lungenkrebs werden.

Abbreviations

AFM	atomic force microscopy
ATCC	American Type Culture Collection
BCA assay	bicinchoninic acid assay
BSA	bovine serum albumin
CHAPS	3-[(3-cholamidopropyl)dimethyl-ammonio]-1-propanesulfonate
CLSM	Confocal Laser Scanning Microscopy
Digo-OMR	Digoxigenin-labeled 2'-O-Methyl-RNA
Digo-OMR-nanoplexes	Digo-OMR-nanoparticle-complexes
DiI	1,1'-Dioctadecyl-3,3,3',3'-tetramethylindocarbocyanine perchlorate
DiI-NP	DiI-labeled nanoparticle
Em.	emission
ESA	epithelial specific antigen
Ex.	excitation
FACS	Fluorescence-activated cell sorting
FAM	6-carboxy-fluorescein
FAM-OMR	FAM-labeled 2'-O-Methyl-RNA
FAM-OMR-nanoplexes	FAM-OMR-nanoparticle-complexes
FCS	fetal calf serum
FISH	fluorescence in situ hybridization
h	hours
H23	NCI-H23
H460	NCI-H460
HE	hematoxylin and eosin
hTERT	human telomerase reverse transcriptase
hTR	human telomerase RNA
IPL	isolated perfused rat lung
ITAS	internal telomerase assay standard
MEM	Minimum Essential Medium
min	minutes
Mismatch-OMR-nanoplexes	Mismatch 2'-O-Methyl-RNA-nanoparticle-complexes
nanoplexes	oligonucleotide-nanoparticle-complexes
NSCLC	Non-small cell lung cancer
OMR	2'-O-Methyl-RNA
OMR-nanoplexes	2'-O-Methyl-RNA-nanoparticle-complexes

Abbreviations

PD	population doubling
PdI	polydispersity index
PI	Propidium Iodide
PLGA	poly(lactide-co-glycolide)
ps	phosphorothioate
PVA	polyvinyl alcohol
Q-PCR	real-time quantitative PCR
Q-TRAP	Real-time quantitative PCR based telomeric repeat amplification protocol
RCA I	Rhodamine-labeled Ricinus Communis Agglutinin I
RPMI	Roswell Park Memorial Institute
RTA	relative telomerase activity
SCLC	Small cell lung cancer
SD	standard deviations
SDS	sodium dodecyl sulfate buffer
sec	seconds
SSC	sodium chloride-sodium citrate buffer
TA	telomerase activity
TMRM	tetramethylrhodamine methyl ester perchlorate
TNM system	Tumor node metastasis system
TRAP	telomeric repeat amplification protocol
TRAP-CE	Telomeric repeat amplification protocol using capillary electrophoresis
TRF	terminal restriction fragment
$\Delta\Delta C_t$	delta-delta C_t method

References

- Agrawal S, Jiang Z, Zhao Q, Shaw D, Cai Q, Roskey A, Channavajjala L, Saxinger C, Zhang R. Mixed-backbone oligonucleotides as second generation antisense oligonucleotides: in vitro and in vivo studies. *Proc Natl Acad Sci U S A*. 1997 Mar 18;94(6):2620-5.
- Agrawal S. Importance of nucleotide sequence and chemical modifications of antisense oligonucleotides. *Biochim Biophys Acta*. 1999 Dec 10;1489(1):53-68.
- Akhtar S, Juliano RL. Cellular uptake and intracellular fate of antisense oligonucleotides. *Trends Cell Biol*. 1992 May;2(5):139-44.
- Albanell J, Lonardo F, Rusch V, Engelhardt M, Langenfeld J, Han W, Klimstra D, Venkatraman E, Moore MA, Dmitrovsky E. High telomerase activity in primary lung cancers: association with increased cell proliferation rates and advanced pathologic stage. *J Natl Cancer Inst*. 1997 Nov 5;89(21):1609-15.
- Al-Hajj M, Wicha MS, Benito-Hernandez A, Morrison SJ, Clarke MF. Prospective identification of tumorigenic breast cancer cells. *Proc Natl Acad Sci U S A*. 2003 Apr 1;100(7):3983-8.
- Allshire RC, Dempster M, Hastie ND. Human telomeres contain at least three types of G-rich repeat distributed non-randomly. *Nucleic Acids Res*. 1989 Jun 26;17(12):4611-27.
- Anabousi S. Liposomal Drug Carrier Systems for Inhalation Treatment of Lung Cancer. Dissertation 2006.
- Anwer K, Meaney C, Kao G, Hussain N, Shelvin R, Earls RM, Leonard P, Quezada A, Rolland AP, Sullivan SM. Cationic lipid-based delivery system for systemic cancer gene therapy. *Cancer Gene Ther*. 2000 Aug;7(8):1156-64.
- Armanios M, Greider CW. Telomerase and cancer stem cells. *Cold Spring Harb Symp Quant Biol*. 2005;70:205-8.
- Asai A, Oshima Y, Yamamoto Y, Uochi TA, Kusaka H, Akinaga S, Yamashita Y, Pongracz K, Pruzan R, Wunder E, Piatyszek M, Li S, Chin AC, Harley CB, Gryaznov S. A novel telomerase template antagonist (GRN163) as a potential anticancer agent. *Cancer Res*. 2003 Jul 15;63(14):3931-9.
- Atha DH, Miller K, Sanow AD, Xu J, Hess JL, Wu OC, Wang W, Srivastava S, Highsmith WE. High-throughput analysis of telomerase by capillary electrophoresis. *Electrophoresis*. 2003 Jan;24(1-2):109-14.
- Barbone F, Bovenzi M, Cavallieri F, Stanta G. Cigarette smoking and histologic type of lung cancer in men. *Chest*. 1997 Dec;112(6):1474-9.
- Beisner J, Dong M, Taetz S, Piotrowska K, Kleideiter E, Friedel G, Schaefer U, Lehr CM, Klotz U, Mürdter TE. Efficient telomerase inhibition in human non-small cell lung cancer cells by liposomal delivery of 2'-O-methyl-RNA. *J Pharm Sci*. 2009 May;98(5):1765-74.
- Beisner J, Dong M, Taetz S, Nafee N, Griese EU, Schaefer U, Lehr CM, Klotz U, Mürdter TE. Nanoparticle mediated delivery of 2'-O-methyl-RNA leads to efficient telomerase inhibition and telomere shortening in human lung cancer cells. *Lung Cancer* 2010 Jun. 68 (3): 346-54.

- Bennett CF, Chiang MY, Chan H, Shoemaker JE, Mirabelli CK. Cationic lipids enhance cellular uptake and activity of phosphorothioate antisense oligonucleotides. *Mol Pharmacol*. 1992 Jun;41(6):1023-33.
- Bielinska A, Kukowska-Latallo JF, Johnson J, Tomalia DA, Baker JR Jr. Regulation of in vitro gene expression using antisense oligonucleotides or antisense expression plasmids transfected using starburst PAMAM dendrimers. *Nucleic Acids Res*. 1996 Jun 1;24(11):2176-82.
- Blackburn EH. Structure and function of telomeres. *Nature*. 1991 Apr 18; 350 (63 19) :569-73.
- Blackburn EH. Telomeres. *Trends Biochem Sci*. 1991 Oct;16(10):378-81.
- Blasco MA. Telomeres and human disease: ageing, cancer and beyond. *Nat Rev Genet*. 2005 Aug;6(8):611-22.
- Bodnar AG, Ouellette M, Frolkis M, Holt SE, Chiu CP, Morin GB, Harley CB, Shay JW, Lichtsteiner S, Wright WE. Extension of life-span by introduction of telomerase into normal human cells. *Science*. 1998 Jan 16;279(5349):349-52.
- Boulay JL, Reuter J, Ritschard R, Terracciano L, Herrmann R, Rochlitz C. Gene dosage by quantitative real-time PCR. *Biotechniques*. 1999 Aug;27(2):228-30, 232.
- Brambilla E, Travis WD, Colby TV, Corrin B, Shimosato Y. The new World Health Organization classification of lung tumours. *Eur Respir J*. 2001 Dec;18(6):1059-68.
- Brigger I, Dubernet C, Couvreur P. Nanoparticles in cancer therapy and diagnosis. *Adv Drug Deliv Rev*. 2002 Sep 13;54(5):631-51.
- Brown MD, Gilmore PE, Hart CA, Samuel JD, Ramani VA, George NJ, Clarke NW. Characterization of benign and malignant prostate epithelial Hoechst 33342 side populations. *Prostate*. 2007 Sep 15;67(13):1384-96.
- Burdall SE, Hanby AM, Lansdown MR, Speirs V. Breast cancer cell lines: friend or foe? *Breast Cancer Res*. 2003;5(2):89-95.
- Buzea C, Pacheco II, Robbie K. Nanomaterials and nanoparticles: sources and toxicity. *Biointerphases*. 2007 Dec;2(4):MR17-71.
- Capaccioli S, Di Pasquale G, Mini E, Mazzei T, Quattrone A. Cationic lipids improve antisense oligonucleotide uptake and prevent degradation in cultured cells and in human serum. *Biochem Biophys Res Commun*. 1993 Dec 15;197(2):818-25.
- Cattoretti G, Becker MH, Key G, Duchrow M, Schlüter C, Galle J, Gerdes J. Monoclonal antibodies against recombinant parts of the Ki-67 antigen (MIB 1 and MIB 3) detect proliferating cells in microwave-processed formalin-fixed paraffin sections. *J Pathol*. 1992 Dec;168(4):357-63.
- Cawthon RM. Telomere measurement by quantitative PCR. *Nucleic Acids Res*. 2002 May 15;30(10):e47.
- Chemotherapy in non-small cell lung cancer: a meta-analysis using updated data on individual patients from 52 randomised clinical trials. Non-small Cell Lung Cancer Collaborative Group. *BMJ*. 1995 Oct 7;311(7010):899-909.

- Chen H, Li Y, Tollefsbol TO. Strategies targeting telomerase inhibition. *Mol Biotechnol.* 2009 Feb;41(2):194-9.
- Cho K, Wang X, Nie S, Chen ZG, Shin DM. Therapeutic nanoparticles for drug delivery in cancer. *Clin Cancer Res.* 2008 Mar 1;14(5):1310-6.
- Collins AT, Berry PA, Hyde C, Stower MJ, Maitland NJ. Prospective identification of tumorigenic prostate cancer stem cells. *Cancer Res.* 2005 Dec 1;65(23):10946-51.
- Collins AT, Habib FK, Maitland NJ, Neal DE. Identification and isolation of human prostate epithelial stem cells based on alpha(2)beta(1)-integrin expression. *J Cell Sci.* 2001 Nov;114(Pt 21):3865-72.
- Collins LG, Haines C, Perkel R, Enck RE. Lung cancer: diagnosis and management. *Am Fam Physician.* 2007 Jan 1;75(1):56-63.
- Costantino L, Gandolfi F, Bossy-Nobs L, Tosi G, Gurny R, Rivasi F, Vandelli MA, Forni F. Nanoparticulate drug carriers based on hybrid poly(D,L-lactide-co-glycolide)-dendron structures. *Biomaterials.* 2006 Sep;27(26):4635-45.
- Crapo JD, Barry BE, Gehr P, Bachofen M, Weibel ER. Cell number and cell characteristics of the normal human lung. *Am Rev Respir Dis.* 1982 Aug;126(2):332-7.
- Crook K, Stevenson BJ, Dubouchet M, Porteous DJ. Inclusion of cholesterol in DOTAP transfection complexes increases the delivery of DNA to cells in vitro in the presence of serum. *Gene Ther.* 1998 Jan;5(1):137-43.
- Dalton WS. The tumor microenvironment as a determinant of drug response and resistance. *Drug Resist Updat.* 1999 Oct;2(5):285-288.
- de Lange T. T-loops and the origin of telomeres. *Nat Rev Mol Cell Biol.* 2004 Apr;5(4):323-9.
- Dean M, Fojo T, Bates S. Tumour stem cells and drug resistance. *Nat Rev Cancer.* 2005 Apr;5(4):275-84.
- Dikmen ZG, Gellert GC, Jackson S, Gryaznov S, Tressler R, Dogan P, Wright WE, Shay JW. In vivo inhibition of lung cancer by GRN163L: a novel human telomerase inhibitor. *Cancer Res.* 2005 Sep 1;65(17):7866-73.
- Dillen K, Weyenberg W, Vandervoort J, Ludwig A. The influence of the use of viscosifying agents as dispersion media on the drug release properties from PLGA nanoparticles. *Eur J Pharm Biopharm.* 2004 Nov;58(3):539-49.
- Dong M, Mürdter TE, Klotz U. Telomeres and telomerase as novel drug targets: reflections on the 2009 Nobel Prize in Physiology or Medicine. *Eur J Clin Pharmacol.* 2010 Jan;66(1):1-3.
- Eldridge L. Chemotherapy for lung cancer. 2010 Sep. <http://lungcancer.about.com/od/treatmentoflungcancer/a/chemolungrx.htm>
- Eramo A, Lotti F, Sette G, Piloizzi E, Biffoni M, Di Virgilio A, Conticello C, Ruco L, Peschle C, De Maria R. Identification and expansion of the tumorigenic lung cancer stem cell population. *Cell Death Differ.* 2008 Mar;15(3):504-14.
- Effros Richard M. Anatomy, development, and physiology of the lungs. *GI Motility online.* 2006 May; doi:10.1038/gimo73

- Fattal E, Barratt G. Nanotechnologies and controlled release systems for the delivery of antisense oligonucleotides and small interfering RNA. *Br J Pharmacol*. 2009 May;157(2):179-94.
- Feng J, Funk WD, Wang SS, Weinrich SL, Avilion AA, Chiu CP, Adams RR, Chang E, Allsopp RC, Yu J, et al. The RNA component of human telomerase. *Science*. 1995 Sep 1;269(5228):1236-41.
- Folini M, Brambilla C, Villa R, Gandellini P, Vignati S, Paduano F, Daidone MG, Zaffaroni N. Antisense oligonucleotide-mediated inhibition of hTERT, but not hTERC, induces rapid cell growth decline and apoptosis in the absence of telomere shortening in human prostate cancer cells. *Eur J Cancer*. 2005 Mar; 41(4):624-34.
- Gagnadoux F, Hureauux J, Vecellio L, Urban T, Le Pape A, Valo I, Montharu J, Leblond V, Boisdrion-Celle M, Lerondel S, Majoral C, Diot P, Racineux JL, Lemarie E. Aerosolized chemotherapy. *J Aerosol Med Pulm Drug Deliv*. 2008 Mar;21(1):61-70.
- Gavory G, Balasubramanian S. PNA and oligonucleotide inhibitors of human telomerase. *Telomerases, Telomeres and Cancer*.2002. ISBN: 0-306-47437-9.
- Gersting SW, Schillinger U, Lausier J, Nicklaus P, Rudolph C, Plank C, Reinhardt D, Rosenecker J. Gene delivery to respiratory epithelial cells by magnetofection. *J Gene Med*. 2004 Aug;6(8):913-22.
- González-Quevedo R, Iniesta P, Morán A, de Juan C, Sánchez-Pernaute A, Fernández C, Torres A, Díaz-Rubio E, Balibrea JL, Benito M. Cooperative role of telomerase activity and p16 expression in the prognosis of non-small-cell lung cancer. *J Clin Oncol*. 2002 Jan 1;20(1):254-62.
- Gorlova OY, Weng SF, Zhang Y, Amos CI, Spitz MR. Aggregation of cancer among relatives of never-smoking lung cancer patients. *Int J Cancer*. 2007 Jul 1;121(1):111-8.
- Gradishar WJ, Tjulandin S, Davidson N, Shaw H, Desai N, Bhar P, Hawkins M, O'Shaughnessy J. Phase III trial of nanoparticle albumin-bound paclitaxel compared with polyethylated castor oil-based paclitaxel in women with breast cancer. *J Clin Oncol*. 2005 Nov 1;23(31):7794-803.
- Griffith JD, Comeau L, Rosenfield S, Stansel RM, Bianchi A, Moss H, de Lange T. Mammalian telomeres end in a large duplex loop. *Cell*. 1999 May 14;97(4):503-14.
- Hahn WC, Stewart SA, Brooks MW, York SG, Eaton E, Kurachi A, Beijersbergen RL, Knoll JH, Meyerson M, Weinberg RA. Inhibition of telomerase limits the growth of human cancer cells. *Nat Med*. 1999 Oct;5(10):1164-70.
- Harley CB. Telomerase and cancer therapeutics. *Nat Rev Cancer*. 2008 Mar;8(3):167-79.
- Herbert B, Pitts AE, Baker SI, Hamilton SE, Wright WE, Shay JW, Corey DR. Inhibition of human telomerase in immortal human cells leads to progressive telomere shortening and cell death. *Proc Natl Acad Sci USA*.1999 Dec 7; 96 (25):14276-81.
- Herbert BS, Gellert GC, Hochreiter A, Pongracz K, Wright WE, Zielinska D, Chin AC, Harley CB, Shay JW, Gryaznov SM. Lipid modification of GRN163, an N3'-->P5' thio-phosphoramidate oligonucleotide, enhances the potency of telomerase inhibition. *Oncogene*. 2005 Aug 4;24(33):5262-8.

- Herbert BS, Hochreiter AE, Wright WE, Shay JW. Nonradioactive detection of telomerase activity using the telomeric repeat amplification protocol. *Nat Protoc.* 2006;1(3):1583-90.
- Hermann PC, Huber SL, Herrler T, Aicher A, Ellwart JW, Guba M, Bruns CJ, Heeschen C. Distinct populations of cancer stem cells determine tumor growth and metastatic activity in human pancreatic cancer. *Cell Stem Cell.* 2007 Sep 13;1(3):313-23.
- Hirashima T, Komiya T, Nitta T, Takada Y, Kobayashi M, Masuda N, Matui K, Takada M, Kikui M, Yasumitsu T, Ohno A, Nakagawa K, Fukuoka M, Kawase I. Prognostic significance of telomeric repeat length alterations in pathological stage I-IIIa non-small cell lung cancer. *Anticancer Res.* 2000 May-Jun;20(3B):2181-7.
- Hiyama E, Hiyama K, Yokoyama T, Matsuura Y, Piatyszek MA, Shay JW. Correlating telomerase activity levels with human neuroblastoma outcomes. *Nat Med.* 1995 Mar;1(3):249-55.
- Hiyama E, Hiyama K, Yokoyama T, Shay JW. Immunohistochemical detection of telomerase (hTERT) protein in human cancer tissues and a subset of cells in normal tissues. *Neoplasia.* 2001 Jan-Feb;3(1):17-26.
- Hiyama E, Hiyama K. Clinical utility of telomerase in cancer. *Oncogene.* 2002 Jan 21;21(4):643-9.
- Hiyama E, Hiyama K. Telomere and telomerase in stem cells. *Br J Cancer.* 2007 Apr 10;96(7):1020-4.
- Hiyama E, Yokoyama T, Tatsumoto N, Hiyama K, Imamura Y, Murakami Y, Kodama T, Piatyszek MA, Shay JW, Matsuura Y. Telomerase activity in gastric cancer. *Cancer Res.* 1995 Aug 1;55(15):3258-62.
- Hiyama K, Hiyama E, Ishioka S, Yamakido M, Inai K, Gazdar AF, Piatyszek MA, Shay JW. Telomerase activity in small-cell and non-small-cell lung cancers. *J Natl Cancer Inst.* 1995 Jun 21;87(12):895-902.
- Hollins AJ, Benboubetra M, Omid Y, Zinselmeyer BH, Schatzlein AG, Uchegbu IF, Akhtar S. Evaluation of generation 2 and 3 poly(propyleneimine) dendrimers for the potential cellular delivery of antisense oligonucleotides targeting the epidermal growth factor receptor. *Pharm Res.* 2004 Mar;21(3):458-66.
- Holt SE, Wright WE, Shay JW. Regulation of telomerase activity in immortal cell lines. *Mol Cell Biol.* 1996 Jun;16(6):2932-9.
- Hou M, Xu D, Björkholm M, Gruber A. Real-time quantitative telomeric repeat amplification protocol assay for the detection of telomerase activity. *Clin Chem.* 2001 Mar;47(3):519-524.
- Hsu CP, Miaw J, Shai SE, Chen CY. Correlation between telomerase expression and terminal restriction fragment length ratio in non-small cell lung cancer--an adjusted measurement and its clinical significance. *Eur J Cardiothorac Surg.* 2004 Aug;26(2):425-31.
- Hultdin M, Grönlund E, Norrback K, Eriksson-Lindström E, Just T, Roos G. Telomere analysis by fluorescence in situ hybridization and flow cytometry. *Nucleic Acids Res.* 1998 Aug 15;26(16):3651-6.

- Jacobsen LB, Calvin SA, Colvin KE, Wright M. FuGENE 6 Transfection Reagent: the gentle power. *Methods*. 2004 Jun;33(2):104-12.
- Jang HS, Oh CK, Jo JH, Kim YS, Kwon KS. Detection of telomerase activity in psoriasis lesional skin and correlation with Ki-67 expression and suppression by retinoic acid. *J Korean Med Sci*. 2001 Oct;16(5):623-9.
- Jemal A, Siegel R, Xu J, Ward E. Cancer statistics, 2010. *CA Cancer J.Clin* 2010;60: 277-300.
- Jemal A, Siegel R, Ward E, Murray T, Xu J, Thun MJ. Cancer statistics, 2007. *CA Cancer J.Clin.*, 2007; 57 (1):43-66.
- Jiang YA, Luo HS, Zhang YY, Fan LF, Jiang CQ, Chen WJ. Telomerase activity and cell apoptosis in colon cancer cell by human telomerase reverse transcriptase gene antisense oligodeoxynucleotide. *World J Gastroenterol*. 2003 Sep;9(9):1981-4.
- Kabir Z, Bennett K, Clancy L. Lung cancer and urban air-pollution in Dublin: a temporal association? *Ir Med J*. 2007 Feb;100(2):367-9.
- Kakiuchi Y, Sasaki N, Satoh-Masuoka M, Murofushi H, Murakami-Murofushi K. A novel pyrazolone, 4,4-dichloro-1-(2,4-dichlorophenyl)-3-methyl-5-pyrazolone, as a potent catalytic inhibitor of human telomerase. *Biochem Biophys Res Commun*. 2004 Aug 6;320(4):1351-1358.
- Katas H, Chen S, Osamuyimen AA, Cevher E, Oya Alpar H. Effect of preparative variables on small interfering RNA loaded Poly(D,L-lactide-co-glycolide)-chitosan submicron particles prepared by emulsification diffusion method. *J Microencapsul*. 2008 Dec;25(8): 541-8.
- Keith WN, Bilsland A, Evans TRJ and Glasspool RM. Schematic representation of the composition of telomeric complexes, telomerase and proteins implicated in cellular signalling from the telomere (telomere repair). *Expert reviews in molecular medicine*. 2002
- Kemp SJ, Thorley AJ, Gorelik J, Seckl MJ, O'Hare MJ, Arcaro A, Korchev Y, Goldstraw P, Tetley TD. immortalization of human alveolar epithelial cells to investigate nanoparticle uptake. *Am J Respir Cell Mol Biol*. 2008 Nov;39(5):591-7.
- Kim NW, Levitt D, Huang G, Wu F, Osborne K, Clark G. Correlation of telomerase with prognostic indicators of breast cancer. *Proc Am Assoc Cancer Res* 1996;37:561-2.
- Kim NW, Piatyszek MA, Prowse KR, Harley CB, West MD, Ho PL, Coviello GM, Wright WE, Weinrich SL, Shay JW. Specific association of human telomerase activity with immortal cells and cancer. *Science*. 1994 Dec 23;266(5193):2011-5.
- Kim NW, Wu F. Advances in quantification and characterization of telomerase activity by the telomeric repeat amplification protocol (TRAP). *Nucleic Acids Res*. 1997 Jul 1;25(13):2595-7.
- Kleideiter E, Piotrowska K, Klotz U. Screening of telomerase inhibitors. *Methods Mol Biol*. 2007;405:167-80.
- Krötz F, de Wit C, Sohn HY, Zahler S, Gloe T, Pohl U, Plank C. Magnetofection--a highly efficient tool for antisense oligonucleotide delivery in vitro and in vivo. *Mol Ther*. 2003 May;7(5 Pt 1):700-10.

- Kumar MN, Mohapatra SS, Kong X, Jena PK, Bakowsky U, Lehr CM. Cationic poly(lactide-co-glycolide) nanoparticles as efficient in vivo gene transfection agents. *J Nanosci Nanotechnol*. 2004 Nov;4(8):990-4.
- Kyo S, Masutomi K, Maida Y, Kanaya T, Yatabe N, Nakamura M, Tanaka M, Takarada M, Sugawara I, Murakami S, Taira T, Inoue M. Significance of immunological detection of human telomerase reverse transcriptase: re-evaluation of expression and localization of human telomerase reverse transcriptase. *Am J Pathol*. 2003 Sep;163(3):859-67.
- Lamprecht A, Ubrich N, Yamamoto H, Schaefer U, Takeuchi H, Maincent P, Kawashima Y, Lehr CM. Biodegradable nanoparticles for targeted drug delivery in treatment of inflammatory bowel disease. *J Pharmacol Exp Ther*. 2001 Nov;299(2):775-81.
- Larsen AK, Escargueil AE, Skladanowski A. Resistance mechanisms associated with altered intracellular distribution of anticancer agents. *Pharmacol Ther*. 2000 Mar;85(3):217-29.
- Laube BL. The expanding role of aerosols in systemic drug delivery, gene therapy, and vaccination. *Respir Care*. 2005 Sep;50(9):1161-76.
- Liu Y, Mounkes LC, Liggitt HD, Brown CS, Solodin I, Heath TD, Debs RJ. Factors influencing the efficiency of cationic liposome-mediated intravenous gene delivery. *Nat Biotechnol*. 1997 Feb;15(2):167-73.
- Loke SL, Stein CA, Zhang XH, Mori K, Nakanishi M, Subasinghe C, Cohen JS, Neckers LM. Characterization of oligonucleotide transport into living cells. *Proc Natl Acad Sci U S A*. 1989 May;86(10):3474-8.
- Maeda H. The enhanced permeability and retention (EPR) effect in tumor vasculature: the key role of tumor-selective macromolecular drug targeting. *Adv Enzyme Regul*. 2001;41:189-207.
- Marchetti A, Bertacca G, Buttitta F, Chella A, Quattrocchio G, Angeletti CA, Bevilacqua G. Telomerase activity as a prognostic indicator in stage I non-small cell lung cancer. *Clin Cancer Res*. 1999 Aug;5(8):2077-81.
- McCalden Th. A. Particulate systems for drug delivery to the lung. *Adv Drug Deliv Rev*. 1990 Jun 7; 5(3):253-263.
- Meng X, Li M, Wang X, Wang Y, Ma D. Both CD133+ and CD133- subpopulations of A549 and H446 cells contain cancer-initiating cells. *Cancer Sci*. 2009 Jun;100(6):1040-6.
- Merck Manual Profesional. The Merck Manuals Online Medical library. <http://www.merckmanuals.com/professional/sec05/ch062/ch062b.html>
- Meyerson M, Counter CM, Eaton EN, Ellisen LW, Steiner P, Caddle SD, Ziaugra L, Beijersbergen RL, Davidoff MJ, Liu Q, Bacchetti S, Haber DA, Weinberg RA. hEST2, the putative human telomerase catalytic subunit gene, is up-regulated in tumor cells and during immortalization. *Cell*. 1997 Aug 22;90(4):785-95.
- Miracco C, Pacenti L, Santopietro R, Biagioli M, Fimiani M, Perotti R, Rubegni P, Pirtoli L, Luzi P. Detection of telomerase activity and correlation with mitotic and apoptotic indices, Ki-67 and expression of cyclins D1 and A in cutaneous melanoma. *Int J Cancer*. 2000 Nov 1;88(3):411-6.

- Moghimi SM, Szebeni J. Stealth liposomes and long circulating nanoparticles: critical issues in pharmacokinetics, opsonization and protein-binding properties. *Prog Lipid Res.* 2003 Nov;42(6):463-78.
- Mokbel K, Parris CN, Ghilchik M, Williams G, Newbold RF. The association between telomerase, histopathological parameters, and KI-67 expression in breast cancer. *Am J Surg.* 1999 Jul;178(1):69-72.
- Molina JR, Yang P, Cassivi SD, Schild SE, Adjei AA. Non-small cell lung cancer: epidemiology, risk factors, treatment, and survivorship. *Mayo Clin Proc.* 2008 May;83(5):584-94.
- Morin GB. The human telomere terminal transferase enzyme is a ribonucleoprotein that synthesizes TTAGGG repeats. *Cell.* 1989 Nov 3;59(3):521-9.
- Morin PJ. Drug resistance and the microenvironment: nature and nurture. *Drug Resist Updat.* 2003 Aug;6(4):169-72.
- Mountain CF. Revisions in the International System for Staging Lung Cancer. *Chest.* 1997 Jun;111(6):1710-7.
- Mountain CF. The international system for staging lung cancer. *Semin Surg Oncol.* 2000 Mar;18(2):106-15.
- Nafee N, Taetz S, Schneider M, Schaefer UF, Lehr CM. Chitosan-coated PLGA nanoparticles for DNA/RNA delivery: effect of the formulation parameters on complexation and transfection of antisense oligonucleotides. *Nanomedicine.* 2007 Sep;3(3):173-83.
- Nafee N. Cationically-modified nanoparticles for the pulmonary delivery of the telomerase inhibitor 2'-O-methyl RNA for the treatment of lung cancer. Dissertation 2008.
- Nakamura TM, Morin GB, Chapman KB, Weinrich SL, Andrews WH, Lingner J, Harley CB, Cech TR. Telomerase catalytic subunit homologs from fission yeast and human. *Science.* 1997 Aug 15;277(5328):955-9.
- Neumann AA, Reddel RR. Telomere maintenance and cancer -- look, no telomerase. *Nat Rev Cancer.* 2002 Nov;2(11):879-84.
- Niemeier RW. The isolated perfused lung. *Environ Health Perspect.* 1984 Jun;56:35-41.
- O'Brien CA, Pollett A, Gallinger S, Dick JE. A human colon cancer cell capable of initiating tumour growth in immunodeficient mice. *Nature.* 2007 Jan 4;445(7123):106-10.
- O'Callaghan N, Dhillon V, Thomas P, Fenech M. A quantitative real-time PCR method for absolute telomere length. *Biotechniques.* 2008 May;44(6):807-9.
- Pascolo E, Wenz C, Lingner J, Huel N, Priepke H, Kauffmann I, Garin-Chesa P, Rettig WJ, Damm K, Schnapp A. Mechanism of human telomerase inhibition by BIBR1532, a synthetic, non-nucleosidic drug candidate. *J Biol Chem.* 2002 May 3;277(18):15566-72.
- Philippi C, Loretz B, Schaefer UF, Lehr CM. Telomerase as an emerging target to fight cancer--opportunities and challenges for nanomedicine. *J Control Release.* 2010 Sep 1;146(2):228-40

- Piatyszek MA, Kim NW, Weinrich SL, Hiyama K, Hiyama E, Wright WE, Shay JW. Detection of telomerase activity in human cells and tumors by a telomeric repeat amplification protocol (TRAP). *Methods in Cell Sci.* 1995 Feb; 17:1-15.
- Piotrowska K, Kleideiter E, Mürdter TE, Taetz S, Baldes C, Schaefer U, Lehr CM, Klotz U. Optimization of the TRAP assay to evaluate specificity of telomerase inhibitors. *Lab Invest.* 2005 Dec;85(12):1565-9.
- Pitts AE, Corey DR. Inhibition of human telomerase by 2'-O-methyl-RNA. *Proc Natl Acad Sci U S A.* 1998 Sep 29;95(20):11549-54.
- Prabha S, Zhou WZ, Panyam J, Labhasetwar V. Size-dependency of nanoparticle-mediated gene transfection: studies with fractionated nanoparticles. *Int J Pharm.* 2002 Sep 5;244(1-2):105-15.
- Rankin AM, Faller DV, Spanjaard RA. Telomerase inhibitors and 'T-oligo' as cancer therapeutics: contrasting molecular mechanisms of cytotoxicity. *Anticancer Drugs.* 2008 Apr;19(4):329-38.
- Reya T, Morrison SJ, Clarke MF, Weissman IL. Stem cells, cancer, and cancer stem cells. *Nature.* 2001 Nov 1;414(6859):105-11.
- Rhoades RA. Isolated perfused lung preparation for studying altered gaseous environments. *Environ Health Perspect.* 1984 Jun;56:43-50.
- Ross PC, Hui SW. Lipoplex size is a major determinant of in vitro lipofection efficiency. *Gene Ther.* 1999 Apr;6(4):651-9.
- Sabbatini P, Aghajanian C, Dizon D, Anderson S, Dupont J, Brown JV, Peters WA, Jacobs A, Mehdi A, Rivkin S, Eisenfeld AJ, Spriggs D. Phase II study of CT-2103 in patients with recurrent epithelial ovarian, fallopian tube, or primary peritoneal carcinoma. *J Clin Oncol.* 2004 Nov 15;22(22):4523-31.
- Sato N, Kobayashi H, Saga T, Nakamoto Y, Ishimori T, Togashi K, Fujibayashi Y, Konishi J, Brechbiel MW. Tumor targeting and imaging of intraperitoneal tumors by use of antisense oligo-DNA complexed with dendrimers and/or avidin in mice. *Clin Cancer Res.* 2001 Nov;7(11):3606-12.
- Shay JW, Pereira-Smith OM, Wright WE. A role for both RB and p53 in the regulation of human cellular senescence. *Exp Cell Res.* 1991 Sep;196(1):33-9.
- Shay JW, Wright WE. Telomerase therapeutics for cancer: challenges and new directions. *Nat Rev Drug Discov.* 2006 Jul;5(7):577-84.
- Shervington A, Lu C, Patel R, Shervington L. Telomerase downregulation in cancer brain stem cell. *Mol Cell Biochem.* 2009 Nov;331(1-2):153-9.
- Shmelkov SV, Butler JM, Hooper AT, Hormigo A, Kushner J, Milde T, St Clair R, Baljevic M, White I, Jin DK, Chadburn A, Murphy AJ, Valenzuela DM, Gale NW, Thurston G, Yancopoulos GD, D'Angelica M, Kemeny N, Lyden D, Rafii S. CD133 expression is not restricted to stem cells, and both CD133+ and CD133- metastatic colon cancer cells initiate tumors. *J Clin Invest.* 2008 Jun;118(6):2111-20.

- Simberg D, Weisman S, Talmon Y, Barenholz Y. DOTAP (and other cationic lipids): chemistry, biophysics, and transfection. *Crit Rev Ther Drug Carrier Syst.* 2004;21(4):257-317.
- Singh SK, Clarke ID, Terasaki M, Bonn VE, Hawkins C, Squire J, Dirks PB. Identification of a cancer stem cell in human brain tumors. *Cancer Res.* 2003 Sep 15;63(18):5821-8.
- Singh SK, Hawkins C, Clarke ID, Squire JA, Bayani J, Hide T, Henkelman RM, Cusimano MD, Dirks PB. Identification of human brain tumour initiating cells. *Nature.* 2004 Nov 18;432(7015):396-401.
- Smith DL, Soria JC, Morat L, Yang Q, Sabatier L, Liu DD, Nemr RA, Rashid A, Vauthey JN. Human telomerase reverse transcriptase (hTERT) and Ki-67 are better predictors of survival than established clinical indicators in patients undergoing curative hepatic resection for colorectal metastases. *Ann Surg Oncol.* 2004 Jan;11(1):45-51.
- Smith PK, Krohn RI, Hermanson GT, Mallia AK, Gartner FH, Provenzano MD, Fujimoto EK, Goeke NM, Olson BJ, Klenk DC. Measurement of protein using bicinchoninic acid. *Anal Biochem.* 1985 Oct;150(1):76-85.
- Sonnenberg M, van der Kuip H, Haubeis S, Fritz P, Schroth W, Friedel G, Simon W, Mürdter TE, Aulitzky WE. Highly variable response to cytotoxic chemotherapy in carcinoma-associated fibroblasts (CAFs) from lung and breast. *BMC Cancer.* 2008 Dec 11;8:364.
- Spiro SG, Tanner NT, Silvestri GA, Janes SM, Lim E, Vansteenkiste JF, Pirker R. Lung cancer: progress in diagnosis, staging and therapy. *Respirology.* 2010 Jan;15(1):44-50.
- Suetsugu A, Nagaki M, Aoki H, Motohashi T, Kunisada T, Moriwaki H. Characterization of CD133+ hepatocellular carcinoma cells as cancer stem/progenitor cells. *Biochem Biophys Res Commun.* 2006 Dec 29;351(4):820-4.
- Sun S, Schiller JH, Spinola M, Minna JD. New molecularly targeted therapies for lung cancer. *J Clin Invest.* 2007 Oct;117(10):2740-50.
- Taga S, Osaki T, Ohgami A, Imoto H, Yasumoto K. Prognostic impact of telomerase activity in non-small cell lung cancers. *Ann Surg.* 1999 Nov;230(5):715-20.
- Tamura Y, Tao M, Miyano-Kurosaki N, Takai K, Takaku H. Inhibition of human telomerase activity by antisense phosphorothioate oligonucleotides encapsulated with the transfection reagent, FuGENE6, in HeLa cells. *Antisense Nucleic Acid Drug Dev.* 2000 Apr;10(2):87-96.
- Tang MX, Redemann CT, Szoka FC Jr. In vitro gene delivery by degraded polyamidoamine dendrimers. *Bioconjug Chem.* 1996 Nov-Dec;7(6):703-14.
- Tannock IF, Lee CM, Tunggal JK, Cowan DS, Egorin MJ. Limited penetration of anticancer drugs through tumor tissue: a potential cause of resistance of solid tumors to chemotherapy. *Clin Cancer Res.* 2002 Mar;8(3):878-84.
- Tao M, Miyano-Kurosaki N, Takai K, Takaku H. Specific inhibition of human telomerase activity by transfection reagent, FuGENE6-antisense phosphorothioate oligonucleotide complex in HeLa cells. *FEBS Lett.* 1999 Jul 9;454(3):312-6.

- Tatsumura T, Koyama S, Tsujimoto M, Kitagawa M, Kagamimori S. Further study of nebulisation chemotherapy, a new chemotherapeutic method in the treatment of lung carcinomas: fundamental and clinical. *Br J Cancer*. 1993 Dec;68(6):1146-9.
- Taetz S, Mürdter TE, Zapp J, Boettcher S, Baldes C, Kleideiter E, Piotrowska K, Schaefer UF, Klotz U, Lehr CM. Decomposition of the telomere-targeting agent BRACO19 in physiological media results in products with decreased inhibitory potential. *Int J Pharm*. 2008 Jun 5;357(1-2):6-14.
- Taetz S. New therapeutic options for the treatment of lung cancer by telomerase inhibition. Dissertation 2008.
- Templeton NS, Lasic DD, Frederik PM, Strey HH, Roberts DD, Pavlakis GN. Improved DNA: liposome complexes for increased systemic delivery and gene expression. *Nat Biotechnol*. 1997 Jul;15(7):647-52.
- Tirino V, Camerlingo R, Franco R, Malanga D, La Rocca A, Viglietto G, Rocco G, Pirozzi G. The role of CD133 in the identification and characterisation of tumour-initiating cells in non-small-cell lung cancer. *Eur J Cardiothorac Surg*. 2009 Sep;36(3):446-53.
- Travis WD. Pathology of lung cancer. *Clin Chest Med*. 2002 Mar;23(1):65-81, viii.
- Tredan O, Galmarini CM, Patel K, Tannock IF. Drug resistance and the solid tumor microenvironment. *J Natl.Cancer Inst*. 2007 Oct 3; 99(19), 1441-54.
- Uhlig S, Wollin L. An improved setup for the isolated perfused rat lung. *J Pharmacol Toxicol Methods*. 1994 Apr;31(2):85-94.
- Umachandran M, Ioannides C. Stability of cytochromes P450 and phase II conjugation systems in precision-cut rat lung slices cultured up to 72 h. *Toxicology*. 2006 Jul 5;224(1-2):14-21.
- Vaira V, Fedele G, Pyne S, Fasoli E, Zadra G, Bailey D, Snyder E, Favarsani A, Coggi G, Flavin R, Bosari S, Loda M. Preclinical model of organotypic culture for pharmacodynamic profiling of human tumors. *Proc Natl Acad Sci U S A*. 2010 May 4;107(18):8352-6.
- Van der Kuip H, Mürdter TE, Sonnenberg M, McClellan M, Gutzeit S, Gerteis A, Simon W, Fritz P, Aulitzky WE. Short term culture of breast cancer tissues to study the activity of the anticancer drug taxol in an intact tumor environment. *BMC Cancer* 2006;6:86
- Vidgren M, Karkkainen A, Karjalainen P, Nuutinen J, Paronen P. In vitro and in vivo deposition of drug particles inhaled from pressurized aerosol and dry powder inhaler. *Drug Dev. Industr. Pharm*. 1988; 14: 2649-2665.
- Wang YF, Guo KJ, Huang BT, Liu Y, Tang XY, Zhang JJ, Xia Q. Inhibitory effects of antisense phosphorothioate oligodeoxynucleotides on pancreatic cancer cell Bxpc-3 telomerase activity and cell growth in vitro. *World J Gastroenterol*. 2006 Jul 7;12(25):4004-8.
- Wicha MS, Liu S, Dontu G. Cancer stem cells: an old idea--a paradigm shift. *Cancer Res*. 2006 Feb 15;66(4):1883-90; discussion 1895-6.
- Wisse E, Braet F, Luo D, De Zanger R, Jans D, Crabbé E, Vermoesen A. Structure and function of sinusoidal lining cells in the liver. *Toxicol Pathol*. 1996 Jan-Feb;24(1):100-11.

- Wright WE, Piatyszek MA, Rainey WE, Byrd W, Shay JW. Telomerase activity in human germline and embryonic tissues and cells. *Dev Genet.* 1996;18(2):173-9.
- Wu YY, Hruszkewycz AM, Delgado RM, Yang A, Vortmeyer AO, Moon YW, Weil RJ, Zhuang Z, Remaley AT. Limitations on the quantitative determination of telomerase activity by the electrophoretic and ELISA based TRAP assays. *Clin Chim Acta.* 2000 Mar;293(1-2):199-212.
- Yuan F, Dellian M, Fukumura D, Leunig M, Berk DA, Torchilin VP, Jain RK. Vascular permeability in a human tumor xenograft: molecular size dependence and cutoff size. *Cancer Res.* 1995 Sep 1;55(17):3752-6.
- Zimmermann S, Martens UM. Telomeres and telomerase as targets for cancer therapy. *Cell Mol Life Sci.* 2007 Apr;64(7-8):906-21.

Acknowledgements

I am heartily thankful to those who were involved in the process of my PhD study and made this thesis possible over the past four years.

First of all, I would like to express my sincere gratitude to **Prof. Dr. Ulrich Klotz** for accepting me to perform my PhD studies at the Dr. Margarete Fischer-Bosch-Institute of Clinical Pharmacology, for providing me with scientific guidance, for showing me the way to be not only a good scientist but also a kind person, for correcting this thesis and teaching me how to write scientific papers. His confidence, encouraging and patience have provided a good basis for this thesis.

I would like to express my deep and sincere appreciation to **Prof. Dr. Claus-Michael Lehr**, my doctor-father at the Saarland University, for offering me the chance to work under his supervision. Many thanks for his trust, his optimistic encouragement and support during my time as PhD student. His wide knowledge and valuable scientific suggestions have been of great value for me.

A lot of special thanks to my scientific supervisor **Dr. Thomas E. Mürdter** for guiding me throughout this whole PhD study, for directing all the research work, for teaching me many useful scientific techniques and precious time that he generously gave to me. Many thanks for being always supportive and the friendly and comfortable atmosphere that he created at work. He really helped me to improve my skills, broadened my knowledge and developed my growth in the scientific world.

I am grateful to the expert technician **Sabine Rekersbrink** for her excellent technical support and generous help with the lab work. Thanks for her never-ending encouragement and support. To me you are not only a nice friend but also a patient German teacher. I enjoyed the time we worked together and the conversations we had in German. Thank you and your husband for the delicious foods, the concerts and the invitation for the Zwiebelfest. Your active attitude to life is what I will always remember.

I want to express my appreciation to **Dr. Ernst-Ulrich Griese** for ideas, suggestions and support he gave to this project, for helping with the techniques especially the optimization of telomeres measurement and his supportive encouragement. Many thanks to **Dr. Julia Beisner** for all her teaching guidance at the beginning of my PhD study.

My warm and sincere gratitude also goes to the people from the Department of Biopharmaceutics and Pharmaceutical Technology, Saarland University, for their fruitful collaboration and kind supports, especially to **Prof. Dr. Ulrich F. Schäfer**, **Dr. Noha Nafee**, **Dr. Brigitta Loretz**, and **Claudia Philippi** for all the valuable meetings we had during my study, for the helpful ideas, suggestions and discussions given to this project that made this

study more productive and stimulating. **Noha** and **Claudia**, thanks for providing me the nanoparticles, sharing the happy time during the cell courses and warm welcome when I was in Saarbrücken.

My respect and thanks to **Dr. Heiko van der Kuip** for offering his knowledge about microscopy, FACS, tissue slicer and many antibodies, for his fruitful discussion, suggestions, and patience. Many thanks also to other colleagues from his group, especially **Silke Haubeiß** and **Jens Schmid** for their supports with tissue slices preparation and fibroblasts culturing. Thanks to **Jens** for creating an enjoyable atmosphere during work, for the interesting discussions, for always going together with me to the pathology and helping me with the patients' data.

A lot of thanks to **Dr. Peter Fritz** for helping with the evaluation of immunostaining; **Dr. Maike Sonnenberg** for sharing her experience of immunostaining and data analysis; **Susanne Gutzeit** for collecting the tissue blocks and guiding histology work; **Dagmar Biegger** for always being kind to answer my questions about histology; **Stefan Winter** for helping with the statistic analysis.

Many thanks to **Prof. Dr. Godehard Friedel**, **Prof. Dr. German Ott**, **Dr. Andreas Grabner** from Robert-Bosch-Krankenhaus and Klinik Schillerhöhe for providing the primary lung tumor tissue samples and paraffin blocks. I am grateful to **PD Dr. Susanne Ammon-Treiber** from University Hospital Tübingen for helping with the rat experiments.

Further, I would also like to convey my appreciation to all my colleagues for being so nice to me. Especially my friends **Rita**, **Lydia**, **Ella**, **Svetlana** and **Daniela** for all the nice time we spent together, for pleasant company, for sharing thoughts, opinions, moods, easy and hard moments.

Last but not least, I owe my deepest gratitude to my family to whom this thesis is dedicated: my **parents**, who always stand by my side, thank you for your unconditional love, understanding and supports. To my husband **Yang**, the most precious person of my life, thank you for always being there for me, for your encouragement, support, professional help and your true love.

German Cancer Aid, Robert Bosch Foundation and German Federal Ministry of Education and Research are gratefully acknowledged for the financial support.

My apologies to the people who are not mentioned here, I would like to convey my sincere appreciation to all of you!

Curriculum Vitae

Personal Information

Name: Meng DONG
Date of Birth: March 25th, 1980
Place of Birth: Shaanxi, China
Email Address: meng.dong@ikp-stuttgart.de

Education

1998-2003: Bachelor of Medical Science, Sanitary Technology, Sichuan University, China.
Bachelor Thesis: “Detection of Horse Genus-derived Ingredients in Foodstuffs with Molecular Biotechnology Method”, Chinese Academy of Inspection and Quarantine, Peking, China

2004-2006: M.Sc. of Molecular Bioengineering, International Master Program of TU-Dresden, Germany
Master Thesis: “Chondrogenic Differentiation of Chondrocytes in Three Different Three-dimensional Gels for Tissue Engineering of Cartilage”, Clinic and Polyclinic of Orthopaedics, TU-Dresden, Germany

2007-current: Ph.D. student at the Dr. Margarete Fischer-Bosch-Institute of Clinical Pharmacology, Stuttgart and University of Tübingen with cooperation of Department of Biopharmaceutics and Pharmaceutical Technology, Saarland University, Germany
Area of Research: “Telomerase inhibition for non-small cell lung cancer therapy with *in vitro* and *ex vivo* models”

Scientific Publications

Dong M, Philippi C, Loretz B, Nafee N, Schaefer UF, Friedel G, Ammon-Treiber S, Griese EU, Lehr CM, Klotz U, Mürdter TE. Tissue slice model of human lung cancer to investigate telomerase inhibition by nanoparticle delivery of antisense 2'-O-methyl-RNA. *Int J Pharm.* (submitted)

Dong M, Mürdter TE, Klotz U. Telomeres and telomerase as novel drug targets: reflections on the 2009 Nobel Prize in Physiology or Medicine. *Eur J Clin Pharmacol.* 2010 Jan; 66(1):1-3.

Beisner J, **Dong M**, Taetz S, Nafee N, Griese EU, Schaefer UF, Lehr CM, Klotz U, Mürdter TE. Nanoparticle mediated delivery of 2'-O-methyl-RNA leads to efficient telomerase

inhibition and telomere shortening in human lung cancer cells. *Lung Cancer*. 2010 Jun; 68(3):346-54.

Beisner J, **Dong M**, Taetz S, Piotrowska K, Kleideiter E, Friedel G, Schaefer UF, Lehr CM, Klotz U, Mürdter TE. Efficient telomerase inhibition in human non-small cell lung cancer cells by liposomal delivery of 2'-O-methyl-RNA. *J Pharm Sci*. 2009 May; 98(5):1765-74.

Bernstein P, **Dong M**, Graupher S, Corbeil D, Gelinsky M, Günther KP, Fickert S. Sox9 expression of alginate-encapsulated chondrocytes is stimulated by low cell density. *J Biomed Mater Res A*. 2009 Dec; 91(3):910-8.

Bernstein P, **Dong M**, Corbeil D, Gelinsky M, Günther KP, Fickert S. Pellet culture elicits superior chondrogenic redifferentiation than alginate-based systems. *Biotechnol Prog*. 2009 Jul-Aug; 25(4):1146-52.

Poster Presentations

Dong M, Beisner J, Taetz S, Piotrowska K, Mürdter TE, Schaefer UF, Lehr CM, Klotz U. "Nanoparticle mediated delivery of 2'-O-methyl-RNA induces effective telomerase inhibition and telomere shortening in human lung cancer cells". The Role of Telomeres and Telomerase in Cancer Research. American Association for Cancer Research (AACR), December 6-9, 2007, San Francisco, California, USA

Dong M, Beisner J, Nafee N, Friedel G, Grabner A, Schaefer UF, Lehr CM, Klotz U, Mürdter TE. "Effective telomerase inhibition by 2'-O-methyl-RNA nanoplexes leads to telomere shortening in human lung cancer cells". 3rd Mildred Scheel Cancer Conference, June 18-20, 2008, Königswinter near Bonn, Germany

Dong M, Nafee N, Philippi C, Loretz B, Schaefer UF, Griese U, Lehr CM, Klotz U, Mürdter TE. "Nanoparticle mediated delivery of 2'-O-methyl-RNA induces effective telomerase inhibition in cell lines and in *ex vivo* models of human lung cancer". Telomere Biology and DNA Repair, Keystone Symposia on Molecular and Cellular Biology, October 9-14, 2009, Ashmore, Queensland, Australia

Dong M, Philippi C, Loretz B, Nafee N, Schaefer UF, Griese U, Lehr CM, Klotz U, Mürdter TE. "Nanoparticle mediated delivery of 2'-O-methyl-RNA induces effective telomerase inhibition in human lung cancer". 8th International conference and workshop on Biological Barriers- *in vitro* Tools, Nanotoxicology and Nanomedicine, March 22-27, 2010, Saarbrücken, Germany